UNIVERSITY OF CALIFORNIA

Santa Barbara

Electrochemical Triggering and Optical Interrogation of Dynamic Biomolecular Systems

A dissertation submitted in partial satisfaction of the

requirements for the degree Doctor of Philosophy

in Chemistry

by

Sheng-Ping Liang

Committee in charge:

Professor Michael J. Gordon Co-Chair

Professor Lior Sepunaru, Co-Chair

Professor Daniel E. Morse

Professor Horia Metiu

Professor Mattanjah S. de Vries

December 2021

The dissertation of Sheng-Ping Liang is approved.

_____
Mattanjah S. de Vries

_____
Horia Metiu

_____
Daniel E. Morse

_____
Lior Sepunaru, Committee Co-Chair

_____
Michael J. Gordon, Committee Co-Chair

September 2021

Electrochemical Triggering and Optical Interrogation of Dynamic Biomolecular Systems

Sheng-Ping Liang

ACKNOWLEDGEMENTS

This thesis covers topics across molecular biology, biophysics, electrochemistry, optical spectroscopy, and microscopy, which would only be possible with the supports and advices from a supportive and diverse environment like University of California Santa Barbara. I would like to first acknowledge UCSB for making communication a simple and natural action for anyone, which is especially valuable for an international student without prior English communication experience like myself.

The success of my thesis research can be attributed to a fortunate combination of my personal effort and good dynamics within my research team. Mike always provides critical opinion that forces me to look at the important details that I always neglected or overlooked. Dan always shows me how methodological thinking could retain positivity in times where nothing seems to function. Lior always gives useful advices in communication which really helped me steer the discussions of all our bio-inspired photonics meeting. Rob is always open to provide his technical supports and share his experiences and opinions. Brandon always gives timely and meticulous assistance in sample preparation. Eloise, as an excellent student and teacher, always reminds me of how effective communication and organized methodologies could elevate science to levels working alone can never achieve.

Finally, I would like to specially thank the Department of Chemistry and Biochemistry at UCSB for letting me participate in such a great research community working and learning with top-of-the-line researchers from around the world.

VITA OF SHENG-PING LIANG
August 2021

EDUCATION

Bachelor of Science in Chemistry, National Taiwan University, June 2013
Doctor of Philosophy in Chemistry, University of California, Santa Barbara, August 2021 (expected)

PROFESSIONAL EMPLOYMENT

2016-2021: Graduate Student Researcher, Department of Chemical Engineering, University of California, Santa Barbara, CA, USA
2015-2016: Research Assistant, Institute of Atomic and Molecular Sciences, Academia Sinica, Taipei, Taiwan
2013-2014: Research Assistant, Department of Chemistry, National Taiwan University, Taipei, Taiwan

PUBLICATIONS

1. S.-P. Liang, R. Levenson, B. Malady, M. J. Gordon, D. E. Morse and L. Sepunaru, Electrochemistry as a Surrogate for Protein Phosphorylation: Voltage-Controlled Assembly of Reflectin A1, *J. R. Soc. Interface*, **2020**, 17, 20200774
2. S.-P. Liang, I-C. Lu, S.-T. Tsai, J.-L. Chen, Y. T. Lee, C.-K. Ni, Laser Pulse Width Dependence and Ionization Mechanism of Matrix-Assisted Laser Desorption/Ionization, *J. Am. Soc. Mass. Spectrom.*, **2017**, 10, pp 2235-2245
3. C. Lee, I-C. Lu, H. C. Hsu, H.-Y. Lin, S.-P. Liang, Y.-T. Lee, and C.-K. Ni, Formation of Metal-Related Ions in Matrix-Assisted Laser Desorption Ionization, *J. Am. Soc. Mass. Spectrom.*, **2016**, 9, pp 1491-1498
4. H.-W. Liu, S.-P. Liang, T.-J. Wu, H. Chang, P.-K. Kao, C.-C. Hsu, J.-Z. Chen, P.-T. Chou, and I-C. Cheng, Rapid Atmospheric Pressure Plasma Jet Processed Reduced Graphene Oxide Counter Electrodes for Dye-Sensitized Solar Cells, *ACS Appl. Mater. Interfaces*, **2014**, 6, pp 15105–15112

5. D.-Y. Chen, W.-H. Tseng, S.-P. Liang, C.-I Wu, C.-W. Hsu, Y. Chi, W.-Y. Hung, and P.-T. Chou, Application of F4TCNQ doped spiro-MeOTAD in high performance solid state dye sensitized solar cells, *Phys. Chem. Chem. Phys.*, **2012**, 14, pp 11689–11694

FIELDS OF STUDY

Major Field: Physical Chemistry

Studies in Biophysics and Molecular Biology with Professors Daniel E. Morse

Studies in Analytical Methods and Instrumentation with Professor Michael J. Gordon

Studies in Electrochemistry with Professor Lior Sepunaru

ABSTRACT

Electrochemical Triggering and Optical Interrogation of Dynamic Biomolecular Systems

by

Sheng-Ping Liang

The rich structure and function of many biological systems relies on the dynamic conformations and assemblies of biomolecules. These dynamic structures are often governed by inter- and intramolecular forces, such as hydrogen bonding, Van der Waals forces, and/or Coulombic interactions. Among these, Coulombic interactions that are governed by protonation level are the most tunable *in vitro*, and have been demonstrated to trigger structural evolution of biomolecules in various pH titration experiments.

This thesis presents a novel approach that leverages site-selective deprotonation electrochemistry to manipulate the dynamic structures of biomolecules. Using cyclic and differential pulse voltammetry, a linear correlation was found between proton dissociation constant (pKa) and redox potential of molecular moieties in various biomolecules, leading to the hypothesis that site-selective proton reduction could be used to manipulate the dynamic evolution of biomolecular structures. This hypothesis was tested using site-selective electrochemistry coupled with *in situ* optical spectroscopies to trigger and analyze the structural transitions of two biomolecular systems representing transitions of different hierarchical structures, namely the coil-to-helix transition of polylysine and assembly of reflectin (the unique protein that enables structural color changes in squid skin).

Evidence from voltammetry, optical spectroscopy, and microscopy indicates that site-selective deprotonation electrochemistry indeed occurred in sidechain moieties of amino acid residues of biomolecules, and could trigger structural conversion of biomolecules at multiple structural hierarchies. The methods developed in this thesis provide new ways to induce localized structural transition on demand, which, in contrast to conventional pH titration or genetic engineering, may provide unpredicted access to the kinetics and thermodynamics of biomolecules that are challenging to assess by other means. Furthermore, being able to actively actuate biomolecular structures may inspire the design and/or discovery of advanced, bio-functional materials that leverage nanoscopic mechanics to achieve unprecedented chemical and physical functions.

TABLE OF CONTENTS

LIST OF FIGURES

Chapter 1
Introduction

1.1 Protein Structure and Assembly Processes

Proteins adopt an elegant architecture that utilizes molecular codes to program dynamic functions with great complexity and flexibility[1]. These dynamic functions are derived from their conformation, assembly, and other structural transitions[2]. The dynamic structure of each protein originates from their primary structure, which ultimately determines their inter- and intramolecular interactions. In particular, Coulombic interactions governed by the protonation of sidechains of amino acid residues, as well as the surrounding chemical environments, are the most tunable, and can influence protein secondary and tertiary structures, as well as assembly dynamics[3–7].

Reflectin, a protein that regulates the dynamic color of cephalopod iridocytes, stands out as an interesting case study due to its simple molecular structure and unique assembly behavior, governed by enzymatic phosphorylation *in vivo*, and protonation level *in vitro*[6,7]. Reflectin is a His-rich protein (10% His/all AAs) found in cephalopods, and its unique reversible assembly is responsible for the dynamically tunable structural color of skin cells, enabling a recently evolved family of squids to communicate and camouflage themselves[8]. Reflectin has been triggered *in vivo* by acetylcholine (ACh)-activated phosphorylation that reduces the protein's net positive charge[9], and *in vitro* using several methods that act as surrogates for phosphorylation, including changes in solution pH[6] and ionic strength[7] to reduce the effective number or contribution of its positively charged amino acids. Assembly can also be tuned through genetic modification of the wild-type protein to alter the balance of positively and negatively charged amino acids[6]. These works clearly demonstrate that the charge states

of amino acids in a protein have far-reaching implications because they critically influence protein structure and assembly dynamics, and thus functionality. Such effects and interactions are not unique to reflectin[10–13], and developing novel methods to probe and control protein charge state, as a means to unravel protein assembly processes and machinery, are important and challenging endeavors.

Common approaches to influence the protonation-related Coulombic interactions in proteins include pH titration and/or genetic engineering of the primary structures. pH titration is the most common lab technique that allows one to probe the proton associated thermodynamics as well as the electro- or nucleophilic reactivity of a molecule. Since the higher order hierarchical structures of proteins or peptides are often dynamic and sensitive to drastic shifts in chemical environment, the window of observation in a pH titration experiment for biological system is often very narrow, compare to the entire pH scale. Genetic engineering may act as a complementary approach to pH titration, where, instead of eliminating the protons in amino acid residues, protonation is investigated via replacing specific protonatable amino acid residues with non-protonatable residues with compatible physical or chemical properties. However, subtle changes in local chemical environments in a protein may alter the entire structure and function, so extensive characterization and control experiments are required to understand the effects of genetic modification.

Due to the limitations of the aforementioned methods, novel approaches are needed to modulate the protonation level of biomolecules for the investigation of a wider collection of biomolecular processes, and is the core motivation of this thesis. The work herein aims to develop an electrochemical methodology to selectively influence the protonation level of a selected set of molecular moieties and further affect their structures. Being able to electrochemically trigger dynamic structural transitions of a biomolecule may enable a novel way to investigate dynamic biomolecular structures and functions that are otherwise not accessible. Moreover, this methodology may further act as an interfacing mechanism that allows the communications between electronics and biomolecular systems.

1.2 Probing Dynamic Structural Biophysics of Proteins via Spectroelectrochemistry

Although there exist many optical methods to analyze the structural behavior of a biomolecule, the investigation of kinetics is limited by the approaches available to trigger structural transitions. Traditionally, static methods such as genetic engineering, pH or salt titration are used to convert biomolecules between states that represents "snapshots" of the overall dynamic process. However, as mentioned in Section 1.1, these approaches are often limited to biomolecules with large tolerance to changes in chemical environment, and requires extensive preliminary studies to create chemical environments that mimic physiological conditions. Recent developments in laser technology and science enable *in situ* approaches, such as temperature jump experiments using pulsed lasers to induce sudden shifts in equilibrium constants between different conformation of biomolecules[14,15]. Though this method provides promising results to study the kinetics of many biomolecular systems in great detail, the technique is limited to systems where light absorbing amino acid residues (tyrosine

or tryptophan) are present. This is not always the case, and thus alternative approaches are needed to expand the toolbox to investigate various biomolecular processes.

As will be explained in detailed in the following chapters, a combined electrochemical and optical method was developed in this work, and found to be an effective way to trigger and monitor structural biophysics related to protonation level. Traditionally, these studies rely on pH titration to gradually tune protonation level, or careful genetic engineering to add or eliminate protonatable groups. Both of these approaches alter the micro- and/or macro-level chemical environment, and thus require careful control experiments that may add extra challenges. With electrochemistry, however, one can tune the protonation level of biomolecule without altering the chemical environment, which maintains the integrity of the primary structure of proteins and allows one to analyze proteins with low tolerance toward shifts in chemical environments. Moreover, the heterogeneous nature of electrochemistry provides temporal and spatial resolution, which allows real-time kinetic studies when combined with optical spectroscopies.

1.3 Thesis Overview

The purpose of this thesis is to develop and use electrochemical methods to modify the charge state of amino acid residues in proteins, and demonstrates that protein conformational changes and assembly processes can be manipulated and controlled on-demand using electrochemistry. The first part (Chapters 2 and 3) of this work focuses on the fundamental methods and theory that enables the triggering and monitoring of structural transition in biomolecules. Chapter 2 aims to cover fundamental knowledge associated with and required for the research presented herein, which includes the introduction of protein structures, electrochemistry, optical spectroscopies, and pH titration. Chapter 3 introduces the novel site-selective electrochemistry of freely diffusing charged amino acids or charged amino acid residues in peptides and proteins. Chapter 3 also covers the diagnostic function of site-selective electrochemical deprotonation, which is shown to be useful to probe and understand the thermodynamics of electrochemical reduction of dissociable protons in amino acids, as well as how the local chemical environments may affect the redox behavior of these residues.

The second part of the thesis introduces the evidence and discoveries of electrochemically triggered structural transition in two biomolecular hierarchical systems that represents the intra- and intermolecular interactions governed by protonation. Chapter 4 details the electrochemical reduction of polylysines as a function of chain length (10-mer, 20-mer, and 50-mer) with *in situ* circular dichroism to detect and understand their electrochemically triggered structural evolution. In Chapter 5, the amassed knowledge is then applied to demonstrate that direct electrochemical deprotonation of charged amino acid residues in the more complex protein reflectin is indeed possible, and results in triggered assembly of the respective monomers at specific electrochemical potentials. The importance of pH-controlled

(de)protonation vs. direct electroreduction, as it relates to AA thermodynamics and reflectin assembly, was carefully studied over a wide range of chemical (e.g., pH, salt conc.) and electrochemical potential conditions. The results in both Chapters 4 and 5 demonstrate how the methods presented herein apply not only to the proteins studied, but can be used more generally to probe protein thermodynamics as well as unravel and even control protein conformations and assembly. Chapter 6 summarizes and concludes the discovery in this thesis research and provides perspectives for future developments of the science and technology developed in this thesis.

1.4 References

[1] Y. Bai, J. S. Milne, L. Mayne, S. W. Englander, *Proteins Struct. Funct. Genet.* **1993**, *17*, 75–86.

[2] A. Thomas, S. Deshayes, M. Decaffmeyer, M. H. Van Eyck, B. Charloteaux, R. Brasseur, *Proteins Struct. Funct. Bioinforma.* **2006**, *65*, 889–897.

[3] W. Dzwolak, V. Smirnovas, *Biophys. Chem.* **2005**, *115*, 49–54.

[4] G. M. Ullmann, E. Bombarda, *Biol. Chem.* **2013**, *394*, 611–619.

[5] K. Rosenheck, P. Doty, *Proc. Natl. Acad. Sci.* **1961**, *47*, 1775–1785.

[6] R. Levenson, C. Bracken, N. Bush, D. E. Morse, *J. Biol. Chem.* **2016**, *291*, 4058–4068.

[7] R. Levenson, C. Bracken, C. Sharma, J. Santos, C. Arata, B. Malady, D. E. Morse1, *J. Biol. Chem.* **2019**, *294*, 16804–16815.

[8] Z. Guan, T. Cai, Z. Liu, Y. Dou, X. Hu, P. Zhang, X. Sun, H. Li, Y. Kuang, Q. Zhai, H. Ruan, X. Li, Z. Li, Q. Zhu, J. Mai, Q. Wang, L. Lai, J. Ji, H. Liu, B. Xia, T. Jiang, S.-J. Luo, H.-W. Wang, C. Xie, *Curr. Biol.* **2017**, *27*, 2833-2842.e6.

[9] M. Izumi, A. M. Sweeney, D. DeMartini, J. C. Weaver, M. L. Powers, A. Tao, T. V. Silvas, R. M. Kramer, W. J. Crookes-Goodson, L. M. Mäthger, R. R. Naik, R. T. Hanlon, D. E. Morse, *J. R. Soc. Interface* **2010**, *7*, 549–560.

[10] S. Törnroth-Horsefield, Y. Wang, K. Hedfalk, U. Johanson, M. Karlsson, E. Tajkhorshid, R. Neutze, P. Kjellbom, *Nature* **2006**, *439*, 688–694.

[11] C. M. Mair, T. Meyer, K. Schneider, Q. Huang, M. Veit, A. Herrmann, *J. Virol.* **2014**, *88*, 13189–13200.

[12] B. R. Branchini, R. A. Magyar, M. H. Murtiashaw, S. M. Anderson, M. Zimmer, *Biochemistry* **1998**, *37*, 15311–15319.

[13] G. Dodson, *Trends Biochem. Sci.* **1998**, *23*, 347–352.

[14] B. Fierz, T. Kiefhaber, *J. Am. Chem. Soc.* **2007**, *129*, 672–679.

[15] B. Fierz, A. Reiner, T. Kiefhaber, *Proc. Natl. Acad. Sci.* **2009**, *106*, 1057–1062.

Chapter 2 Methods and the Associated Theories

2.1 *Structures of Proteins and Peptides*

Proteins and peptides are polymers of amino acids connected via peptide bonds (Figure 2.1a), which manifest various functions via adopting various hierarchical structures. In principle, there are four hierarchies to the structure for a protein (see Figure 2.1a and b), i.e., from simple to complex, namely primary, secondary, tertiary, and quaternary structures. Primary structure refers to the collection and arrangement of amino acids that constitute the protein. Besides the primary structure, higher order hierarchical structures are formed via inter- and intramolecular interactions programmed by the primary structure and are thus dynamic, meaning that the structures are mostly flexible and can often only be determined when both the environment and the primary structures are taken into consideration.

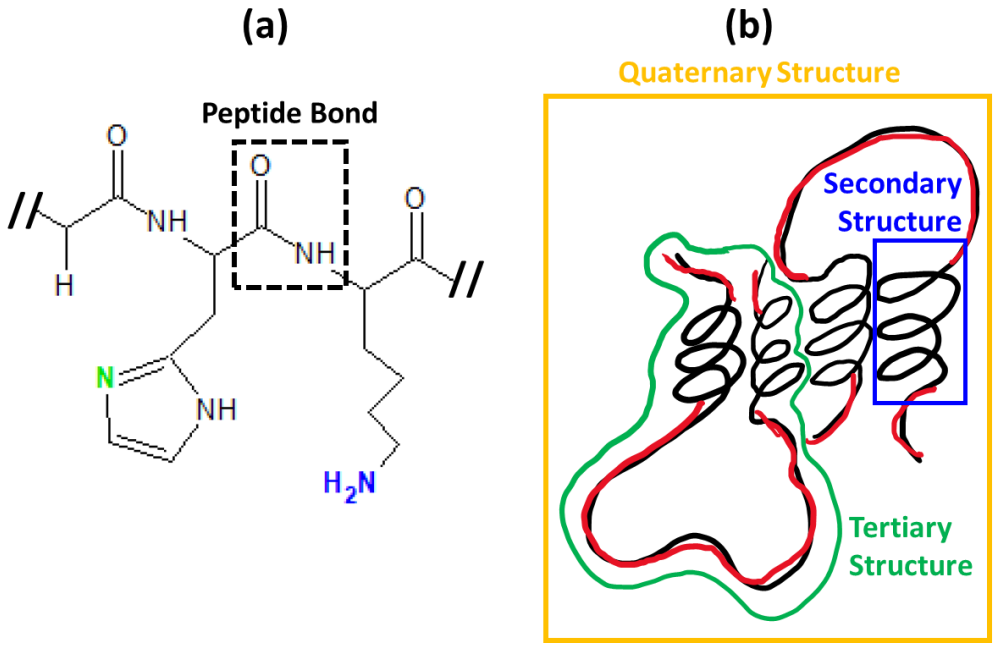

Figure 2.1. The illustrations of (a) part of the primary structure of and (b) higher order hierarchical structures of a protein

Higher order hierarchical structures are the foundation of the complexity and flexibility of proteins. Secondary structure refers to the local assembly that occurs nearby amino acid residues. Secondary structure is the fundamental building block that determines the local physical and chemical environments (such as flexibility or hydrophobicity). Tertiary structure is the result of intrachain folding via covalent or non-covalent interactions. These are formed via non-covalent interactions and are extremely dynamic; however, covalent interactions such as disulfide linkage, results in cross-linking, which yield rigid tertiary structures that can sustain wide range of chemical environments. Quaternary structure refers to the structure of a "protein" that is formed between "protein subunits", which is among the most complex forms of a protein. Quaternary structure is highly dynamic and acts as machinery, in most cases where subunits perform synergistically to manifest dynamic functions.

2.2 *Electrochemistry*

2.2.1 Three electrode system for electrochemical analyses

A three-electrode system is the mostly used configuration for electrochemical analyses due to its simplicity for interpreting redox behavior of a system. As the name suggests, there are three electrodes in this configuration, which are the working, counter, and reference electrodes. As illustrated in Figure 2.2, working electrode and counter electrode form the circuit where most redox electrochemistry happens. Working electrode is where the redox electrochemistry of interest happens, and the reference electrode sets a "reference potential" between the working and counter electrodes which in turn accounts for different potential drops at the surfaces near the working and counter electrodes. This configuration allows monitoring of the total amount of redox events happen at the working electrode by monitoring the current while at the same time resolving the potential drop near the working electrode as a proxy for the electrochemical energy required to drive the redox reaction of interest.

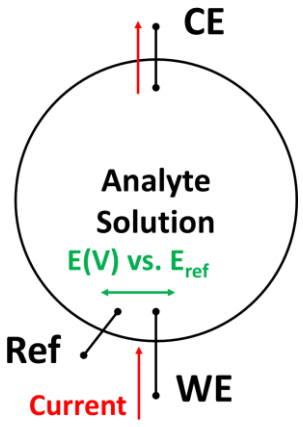

Figure 2.2. Illustration of a three-electrode electrochemical setup and the electrical relation between each circuit component.

2.2.2 Voltammetry

Voltammetry is a powerful technique for investigating the thermodynamics and kinetics of electrochemical systems. In a voltammetry experiment, electrochemical potentials are applied to the system of interest and the electrical current is monitored. Depending on the configuration and the material system, voltammetry can be used to investigate the redox behaviors of interfaces between two materials or dispersed molecules in solution. Depending on the questions of interest, different potential waveform profile can be used to provide resolution and information at various levels. In this work, cyclic voltammetry and differential pulse voltammetry were used to resolve the redox electrochemistry of dissociable protons in biomolecules.

Cyclic voltammetry provides information about the kinetics and thermodynamics of charge transfer and mass transfer processes. As shown in the top panel of Figure 2.3a, a staircase potential profile is applied to the system, and electric current is recorded as a function of the input potential (top panel in Figure 2.3b). Cyclic voltammetry is an especially useful initial analysis technique to understand an electrochemical system. With proper choice of the analytical model, a lot of information can be extracted by varying experimental conditions, such as scan rate, concentration, or solution components[1]. However, measuring the overall current response also results in high background noise, which reduces sensitivity for specific redox reactions of interest, and depending on the reversibility of the process of interest, interpretation of the thermodynamics can sometimes be ambiguous.

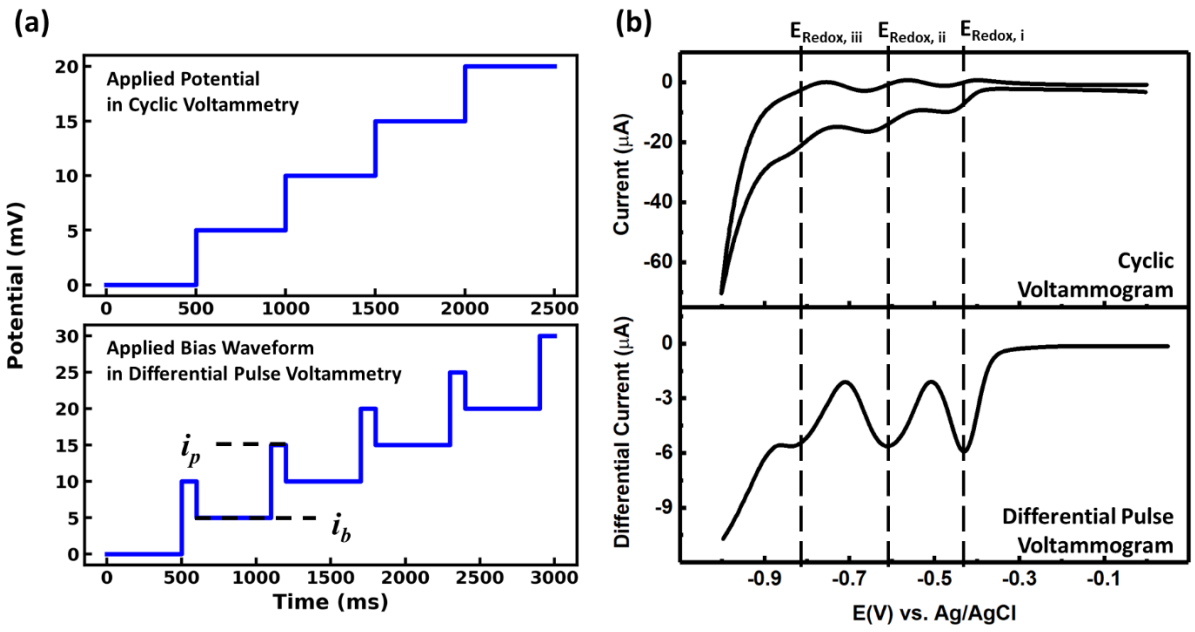

Figure 2.3. (a) The potential waveform for the first 5 steps of cyclic voltammetry (top panel) and differential pulse voltammetry (bottom panel). (b) Illustration of cyclic and differential pulse voltammograms for the same sample.

In contrast to cyclic voltammetry, differential pulse voltammetry probes differential current, where only charge transfer kinetics are monitored. As shown in the bottom panel of Figure 2.3a, the base potential would be held for a period of time, followed by a pulse, and the base current (i_b) and pulse current (i_p) are recorded. Then, the differential current (δi) would be calculated as: $\delta i = i_p - i_b$. Since i_b is the sum of Faradaic and non-Faradaic currents, δi can be treated as the background-subtracted Faradaic current. Since differential current in DPV approximates Faradaic current, in theory, when the redox events between different redox active species are independent, it is possible to express the total differential current as:

$$\delta i_{total} = \delta i_{analyte} + \delta i_{others} \qquad (2.1)$$

where $\delta i_{analyte}$ is the analyte differential current, and δi_{others} is the sum of differential currents from other redox processes that are not of the interest in the measurement. Based on Equation 2.1, deconvolution can be done via subtracting the DPV of a blank solution from the analyte solution. As Figure 2.4 demonstrates, the subtraction of blank DPV (top panel) from analyte DPV (middle panel) results in a deconvolved DPV (bottom panel) that approximates the redox behaviors of the pure analyte. As will be demonstrated repeatedly, this method is extremely powerful in resolving the redox behavior of biomolecules in acidic aqueous environment at platinum electrode, where a non-trivial amount of background and side reactions can happen as a result of platinum catalyzed hydrogen evolution reactions.

The two voltammetry methods introduced here are both powerful techniques for electrochemical analysis, and the choice should be based on the information required and the type of electrochemical system of interest. The focus in this work is mainly the redox potential of molecular moieties, so the more sensitive DPV was chosen for most of the following analyses.

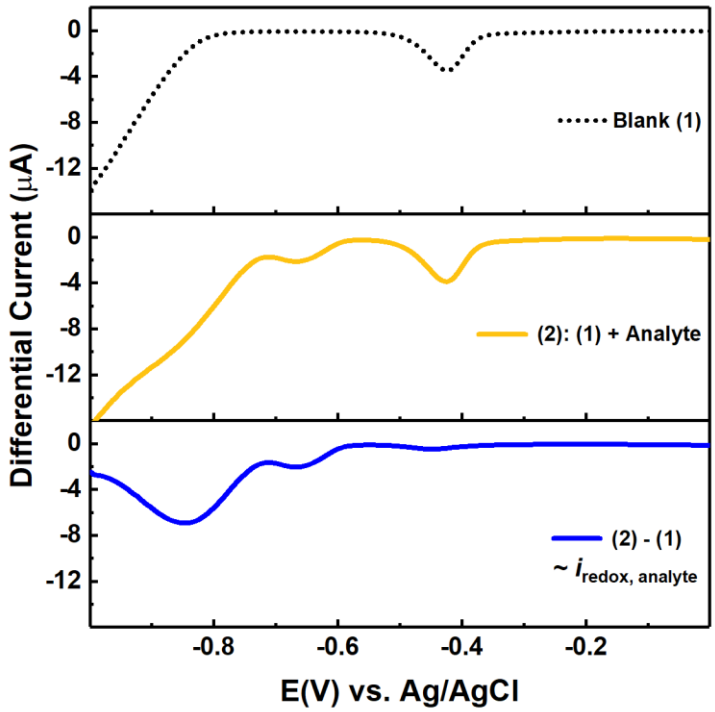

Figure 2.4. A procedural illustration of the deconvolution of a differential pulse voltammogram.

2.3 ***Optical spectroscopy***

Optical spectroscopies use wavelength dependent light-matter interactions to interrogate various physical properties of a molecule. Due to the potential non-invasive nature of these interactions, optical spectroscopies have been combined with various characterization techniques, and can be used for quantitative analysis. In this work, the electrochemically triggered structural transitions of biomolecules were probed via integrating an electrochemical cell with optical measurements to probe structural transitions *in situ*. For intramolecular interactions that induce electronic coupling of peptide bonds, far-UV spectroscopy (absorbance, circular dichroism (CD)) was also used to monitor the shift in structure; for intermolecular interactions that may effect molecular or assembly size, dynamic light scattering (DLS) was used.

2.3.1 Absorbance spectroscopy

Absorbance spectroscopy is based on Beer's law, where the extinction of light scales via a logarithmic relation with transmittance, i.e., the fraction of the light passing through the optical cuvette, which is a function of concentration. Considering the chromophores or molecule of interest to be homogeneously dispersed in space, the intensity of light (I) is attenuated (absorbed) as a function of distance, and this behavior can be describe as:

$$dI \propto -\varepsilon[I(x)c]dx \qquad (2.2)$$

where ε is the molecule-dependent proportionality coefficient (also known as absorptivity or extinction coefficient), representing the probability of photon extinction, and c is the density of chromophores in space. Equation 2.2 can then be rearranged into:

$$\frac{dI}{I(x)} = -\varepsilon \mathrm{c} \mathrm{dx} \qquad \text{Equation 2-2}$$

The integral of Equation 2.2 from x = 0 to x = L is then:

$$-\log\big(I(x)\big)\,|_{x=0}^{x=L} = \varepsilon \mathrm{c}|_{x=0}^{x=L} \quad \Longrightarrow \quad -\log(I(d)/I(0)) = \varepsilon \mathrm{cL} \qquad (2.3)$$

where L is the distance that the probe beam travels within a media. Equation 2.3 is also known as Beer's law, which is widely used in quantitative analysis or the determination of physical properties of a molecule. In common practice, I(d)/I(0) would normally be defined as "transmittance", while – log (Transmittance) would then be defined as "absorbance".

Absorbance spectroscopy is useful for quantitative analysis because absorbance is additive. Assuming the chromophores in a space do not experience interactions that alter their spatial distribution or molecular photophysics, each kind chromophore would then manifest absorbance A_i, and the sum of the absorbances from n species of chromophores is then:

$$\sum_n A_i = \sum_n \varepsilon_i c_i d \qquad (2.4)$$

Equation 2.4 indicates that, with proper calibration, absorbance can be used to quantitatively estimate the evolution of a system over time with equilibrating components with different molar absorptivity values. Such phenomenon has been applied to measure the pH evolution in cellular environment [2], and will be used in the analysis of the structural transitions of biomolecule in later chapters.

2.3.2 Circular Dichroism

Intrinsically chiral biomolecules absorb left- and right-handed, circularly polarized light differently, and this phenomenon is known as circular dichroism (CD, i.e., showing different color based on the circular polarization of the light). For historical reasons, CD is normally reported as ellipticity, which is proportional to the absorbance difference between left- and right-handed circularly polarized light (ΔA). Since CD originates from light absorption, the amount of light being detected significantly influences the signal quality of a CD measurement. For far-UV CD spectroscopy, the material and pathlength of the cuvette, and the solution composition, such as solvent and co-solute, must be taken into consideration. For specific application in this work where salt is required for electrochemistry, common cationic species such as Na^+ and K^+ were found to not affect the measurement of CD down to 190 nm. In contrast, the choice of anionic species greatly impacted the quality of the measurement due to strong absorbances at wavelengths < 200 nm. Perchlorate was found to be an excellent anion that showed no trivial absorbance at 190 nm with concentrations as high as 500 mM, while several milli-molar (mM) of common anions such as OH^- or Cl^-, showed significant absorbance at wavelengths < 200 nm.

Depending on the wavelength, CD can provide information about different hierarchies of biomolecular structure. For biophysical characterization, near-UV (> 250 nm) and far-UV (< 250 nm) are the most commonly monitored regions. Near-UV CD originates from the ΔA of sidechain groups such as tyrosine, phenylalanine, cysteine (also known as disulfide bond), or tryptophan. Since near-UV CD is normally specific to the primary structure of the biomolecule, a spectrum only provides a signature of the tertiary structure. On the other hand, far-UV CD originates from the ΔA of peptide bonds in biomolecules, so structural information is general

for all biomolecules, and it has been widely used to characterize the secondary structure. Furthermore, since the absorbance of peptide bonds is additive, the deconvolution of far-UV CD may also provide quantitative analysis for the secondary structure composition of a biomolecule.

2.3.3 Dynamic Light Scattering

Dynamic light scattering (DLS) analyzes the time-dependent intensity of scattered light to estimate the size distribution of particles in a solution. When a beam of light encounters a particle dispersion, light scatters in all direction due to Rayleigh scattering by particles. The intensity of light scattering fluctuates overtime due to Brownian motion of the particles. By correlating the magnitude of fluctuations with time, the motion of particles can be monitored, and can further be used to infer the mass diffusivity of particles.

For a monodisperse particle solution, a first-order autocorrelation function, g^1, can be generated via surveying the decay rate of scattered light intensity, and can be modeled as[3]:

$$g^1(q,\tau) = \exp[-\Gamma\tau]\,;\; q \equiv \frac{4\pi n}{\lambda} sin\left(\frac{\theta}{2}\right) \; and \; \Gamma \equiv q^2 D_t \qquad (2.5)$$

where λ is the wavelength of light, n is the refractive index of the particle, θ is the angle of light scattering, τ is the delay time of the fluctuation measurement, and D_t is the mass diffusivity of the particles. Since q is a constant given a known set of λ, n, and θ, D_t can be obtained by fitting g^1 with an exponential function of τ. Finally, the size distribution of the particles can be estimated, with D_t given by the Stokes-Einstein relation:

$$D = \frac{k_B T}{6\pi\eta R_h} \qquad (2.6)$$

where k_B is Boltzmann coefficient, T is absolute temperature, η is the viscosity, and R_h is the effective hydrodynamic radius of the particles. For a polydisperse particle solution, a more

sophisticated analytical model based on Equation 2.6 can be used to analyze the autocorrelation of the intensity of light scattering[3]. Based on the introduction thus far, one should be able to perceive that the size distribution obtained from DLS is the 2nd derivative of the result (the pristine result is the autocorrelation function, and the 1st derivative is the mass diffusivity), and careful examination of the assumed parameters (such as refractive index, viscosity, as well as the intrinsic geometry of the particle) is required in order to yield reasonable and physical estimation of size distribution.

Besides size distribution, light scattering intensity in DLS could also a good measure to resolve the sample condition. A DLS measurement of size always includes the measured intensity of scattered light, which can be expressed with the Rayleigh scattering equation[4]:

$$I = I_0 \left(\frac{1+cos^2\theta}{R^2}\right)\left(\frac{n^2-1}{n^2+2}\right)\left(\frac{2\pi}{\lambda}\right)^4\left(\frac{d}{2}\right)^6 \qquad (2.7)$$

where I_0 is the intensity of the incident beam, θ is the scattering angle, n is the refractive index, λ is the wavelength, and d is the diameter of the scatterer. Equation 2.7 shows that light scattering intensity is highly dependent on the sizes of the particle, which means small quantity of bigger particles could have greater influence for the light scattering behavior. For example, when 10 weight % of spherical particles form aggregates of twice the hydrodynamic radius, the signal could increase by a factor of two. Since a degraded or contaminated sample normally appear as polydisperse while a pristine sample normally appear as monodisperse, light scattering intensity can be an additional insurance for quality control of samples besides size distribution.

2.4 *Transmission Electron Microscopy*

Transmission electron microscopy (TEM) utilizes the spatially resolved electron transmission to map the morphology of particles at high resolution (detection limit < 1 nm). As the name suggests, an "electrograph" is taken via transmitting an electron beam through the sample, and an image of intersection between the electron beam and the sample is recorded. For biological samples in this work, sample preparation involves the hydrophilization (via glow discharge surface treatment) of the carbon-coated copper grids that supports the sample, and negative staining to increase the image contrast for the sample. Biomolecules are often stored in solutions containing a significant amount of salt to buffer the pH or control the ionic strength. These salt components may crystalize on the sample and interfere with imaging, so DI water cleaning is often used to eliminate the salt. Due to the water solubility of the sample, glow discharge hydrophilization is often performed on the carbon-coated grids to enhance the adhesion between the grid and the biological samples, so more sample could be retained during rinsing. TEM contrast relies on the difference of electron density between the analyte particle and the carbon-coated grid. Negative staining fills the gaps between particles with a high electron density species such as uranyl acetate, which makes the actual sample area much more transmissive to the electron beam, and thus increases image contrast.

2.5 *pH titration*

pH titration is among the most commonly used methods in wet chemistry, where the macroscopic proton dissociation constants (pKa values) of a molecule can be conveniently determined, often providing information about the thermodynamics and reactivity of a molecule. In a pH titration experiment, the analyte solution is adjusted to a pH that is above or below the protonation states of interest, and the pH will be either increased via adding base or decreased via adding acid to scan through the protonation states. As can be seen in Figure 2.5, the pKa values of a molecule are determined by the locations of the "end points" that indicate the pH where the protonation or deprotonation of certain moiety is complete, so that the change in system pH is no longer buffered by the analyte. Although the measured result is the macroscopic proton dissociation behavior of the whole analyte solution, one can often infer microscopic contributors to proton dissociation behavior via careful control experiments with internal standards, or simply with common chemical sense as demonstrated in Figure 2.5 (carboxyl groups always show lower pKa values than amino groups).

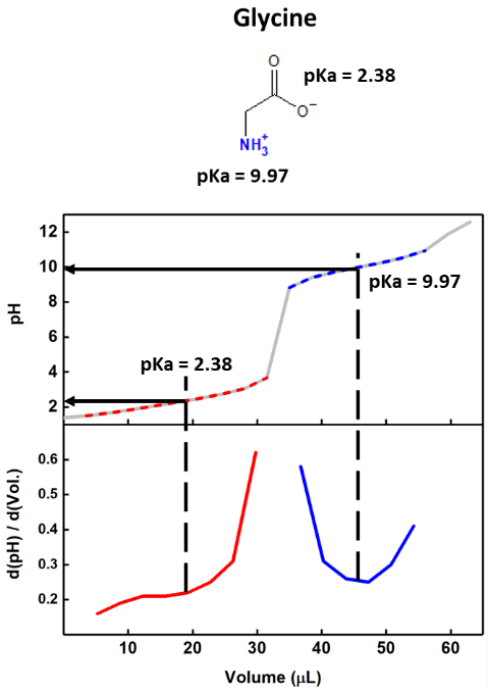

Figure 2.5. The titration curve of glycine.

A main limitation of pH titration in biophysical studies is the requirement of scanning pH. For acid titration, to increase one unit of pH, an order of magnitude of acid would need to be added to the analyte solution, and a similar amount of analyte molecules, on the order of the added acid molecules are needed to provide enough buffering. This characteristic of pH titration limits its resolution near the bookends of the pH scale, where the amount of analyte required often exceeds their solubilities. Moreover, for scarce biomolecules, this method is often limited near neutral pH since probing too high or too low of pH range would require an unreasonable amount of analyte, and the added titrant may greatly alter the chemical environment, and hence the behavior of biomolecules.

2.6 *References*

[1] A. J. Bard, L. R. Faulkner, *Electrochemical Methods: Fundamentals and Applications*, **2008**.

[2] T. A. Trumbo, E. Schultz, M. G. Borland, M. E. Pugh, *Biochem. Mol. Biol. Educ.* **2013**, *41*, 242–250.

[3] J. Stetefeld, S. A. McKenna, T. R. Patel, *Biophys. Rev.* **2016**, *8*, 409–427.

[4] J. H. Seinfeld, S. N. Pandis, *Atmospheric Chemistry and Physics*, John Wiley And Sons, Hoboken, NJ, **2006**.

Chapter 3
Voltammetry of Freely Diffusing Charged Amino Acids and Charged Amino Acid Residues in Peptides

3.1 Overview

This chapter aims to demonstrate electrochemical deprotonation of charged amino acid residues in simple biological molecules as well as their impact for studying the thermodynamics of amino acid residues in more complex peptides. Cyclic voltammetry was first performed on histidine and glycine to demonstrate that dissociable protons in molecular moieties enables electrochemical reduction activities of amino acids, and that the electrochemical reduction of specific molecular moieties in amino acid can be resolved. More sensitive differential pulse voltammetry was performed on charged amino acids, molecular analogues of lysine, and peptides with charged amino acids residues to further resolve the relation between redox potentials and pKa values of molecular moieties in amino acid residues. The redox potentials of different protonatable groups in charged amino acids and peptide residues were found to correlate well with their respective pKa values, as predicted in theory and previous reports [ref]. Moreover, DPV proves to be highly sensitive to the chemical environment surrounding these protonatable molecular moieties and can be effectively used as a proxy for pKa value when pH titration is challenging.

3.2 Introduction and Background

For peptides and proteins, the dynamics associated with function, conformation, and assembly is often controlled by their sequence and/or the charge state of their amino acid residues. The latter is critically influenced by system pH, and how it compares with the pKa values (i.e., proton dissociation equilibrium) of different chemical moieties in these amino acids [1] (e.g., plant aquaporin[2], firefly luciferase[3], viral hemagglutinin[4], and reflectin[5]). Titration of a biomolecule usually requires (1) stability over a wide range of pH values, and (2) that the pKa value of the protonation site of interest be well separated from the isoelectric point (pI) or the pKa values of other protonation sites that can also affect its structure or functions. Alternative methods are therefore needed to study structural dynamics associated with proton dissociation equilibria in peptides and proteins.

Previous work has shown that platinum can catalyze electrochemical reduction of dissociable protons in a variety of molecules[6–8], where the redox potential is correlated to the pKa value of the proton-hosting chemical moiety via [1,8]:

$$\boldsymbol{E^0 = E_{proton\ redox} - \frac{RT}{2.303F} * pKa = E_{proton\ redox} - \left(\frac{59\ mV}{pKa}\right) * pKa\ @\ 298\ K} \quad \textbf{(3.1)}$$

Here, E^0 represents the redox potential of the dissociable proton populates in the amino acid molecular moiety, $E_{proton\ redox}$ represents the redox potential of a hydroium, R is the gas constant, T is the temperature, and F is the Faraday constant; a slope of -59 mV /pKa unit is expected at 298 K for a one electron process. This correlation should be applicable to dissociable protons in freely diffusing charged amino acids, and potentially extendable to charged amino acid residues in peptides and proteins. If indeed the latter is true, electrochemistry would allow one to probe local chemical environments in peptides or

proteins, as well as provide ways to actively trigger protonation-related, dynamic processes in biological molecules[6].

3.3 Methods

3.3.1 Cyclic and Differential Voltammetry

Electrochemical measurements were done in a three-electrode configuration (working electrode: Pt disk; counter electrode: Pt wire; reference electrode: fritted Ag/AgCl in 1M $KCl_{(aq)}$ or saturated calomel electrode (SCE); and an Autolab M204 electrochemical workstation. The Pt disk working electrode (R_{Pt} = 1.5 mm) was polished three times (2 min each) using 1 µm, 0.25 µm, and then 0.05 µm MetaDiTM polycrystalline diamond suspension (Buehler, Lake Bluff, IL, USA) on a microcloth polishing pad. The polished working electrode was then sonicated in water for 2 min. CV measurements were done at a scan rate of 100 mV/s. DPV measurements were done with a potential step size of 5 mV, pulse height of 10 mV, pulse duration of 50 ms, and interval time of 0.5 s.

3.4 Results and Discussion

3.4.1 Protonation Dependent Redox Behavior of Histidine and Glycine

Proton-coupled electron transfer (PCET) is a one proton, one electron process [9,10], hence electrochemical reduction driven by PCET depends on the protonation state of a molecule. The nature of electrochemical reduction of charged amino acids was first demonstrated via cyclic voltammetry (CV) with a Pt electrode performed on freely diffusing histidine (His) and glycine (Gly) in 100 mM KCl supporting electrolyte, in the presence and absence of 10 mM perchloric acid (Figure 3.1). The reason we chose platinum stems from the material's "well-documented" electrocatalytic ability to reduce protons[11]. When no perchloric acid was added, one redox wave appeared between -300 to -900 mV vs. SCE (saturated calomel electrode) in the CVs of both Gly (black) and His (blue) in Figure 3.1a. Under such conditions, the terminal amine[12] (pKa ~ 9 – 10, also see appendix) is the only possible protonated chemical moiety in both His and Gly. Thus, the redox waves between -750 to -900 mV (designated in the light blue region) were assigned to the direct electrochemical deprotonation of the terminal primary amine (NH_3^+). When perchloric acid was mixed with His at a 1:1 molar ratio, two redox waves appeared between -300 to -900 mV (Fig. 1a, red). The dissociated proton from perchloric acid populates the imidazole ring of the His side chain and forms imidazolium (NH^+) due to the ~ 6.5 pKa of His. As such, the redox waves between -500 to -750 mV (light red region) were assigned to direct electrochemical deprotonation of the imidazolium side chain of histidine. Further addition of perchloric acid (2:1 ratio of $HClO_4$:His) produced three redox waves (Figure 3.1a, yellow). Under this condition, both weakly acidic molecular moieties - the terminal amines and the imidazolium of His - are fully protonated. Thus, the redox waves between -300 to -500 mV (yellow region) can be assigned to direct electrochemical reduction

of hydronium (H_3O^+) on the Pt surface[11]. Overall, these voltammograms demonstrate the selective reduction of protons on different chemical moieties in amino acids via electrochemistry. Moreover, the voltammetric approach offers an analytic route to probe and distinguish chemical moieties both with and without titratable side chains.

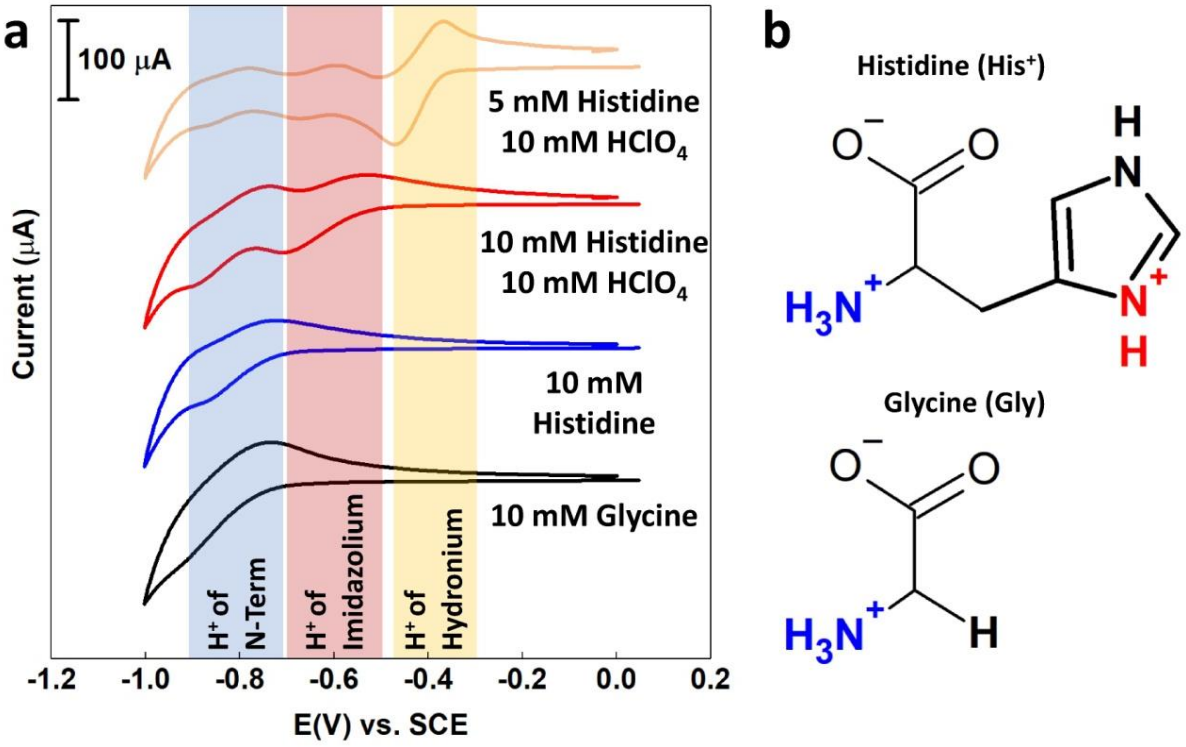

Figure 3.1. Site-specific electrochemical titration of amino acids histidine (His) and glycine (Gly). (a) Cyclic voltammograms of His and Gly in 100 mM KCl as a supporting electrolyte, with and without 10 mM perchloric acid (curves offset for clarity). Negative current peaks seen in the voltammograms between -300 to -900 mV vs. SCE correspond to reduction of hydronium (yellow), the ring imidazolium (NH^+, red), and the terminal amine (NH_3^+, blue), as shown in (b). (b) Molecular structures of His^+ (protonated His under acidic conditions) and Gly, with imidazolium and terminal amine protonation sites colored in red and blue, respectively.

3.4.2 Redox activity of charged amino acids at a Pt Surface

Investigation of direct electrochemical deprotonation on a platinum electrode surface was further extended to all the charged amino acids. Differential pulse voltammetry (DPV) was used as the main voltammetric method onward because it eliminates any irrelevant capacitive features, thus increasing the signal-to-noise ratio from Faradaic processes such as proton reduction. The successful electroreduction of 5 mM freely diffusing amino acids (Gly, Asp, Glu, His, and Lys) in acidic solution (pH 3) is shown in Figure 3.2. Two redox features appear for the blank solution (pH 3, 40 mM NaCl, dotted curves) that are associated with hydronium reduction (-0.42 V vs. Ag/AgCl [11]) and water electrolysis (onset at -0.8 V [11]). For all amino acids measured, the voltammograms reflected additional reduction waves (Figure 3.2, gold traces) that do not exist in the control experiments, indicating the ability to reduce them directly at the Pt electrode surface. The pure voltammetric signal was deconvoluted by subtracting the control experiment from each analyte voltammogram, resulting in baseline subtracted current-voltage plots (blue traces). Without exception, all amine acids show a common redox peak near -0.8 V that is clearly distinguishable from the onset of water electrolysis; using the DPV of glycine as a reference that does not have a charged side chain, our interpretation is that this redox peak represents electro-reduction of the α-amine proton (green arrow and green circles on chemical structures). Other redox features near -0.5 V are seen for Asp and Glu, corresponding to the carboxylic group, which are also distinguishable from hydronium reduction (red arrows and circles on chemical structures). We note here that the pKa values of the carboxylic groups are higher than the solution pH, and a clear trend between shifts in the formal reduction potential and pKa value of the carboxylic group is seen. In the case of His, an additional peak at ~-0.6 V is interpreted as direct reduction of the imidazolium carrying side

chain (purple arrows and circles on chemical structures). Indeed, reported values for the His pKa lie between those of the carboxylic acid and amine groups. Lastly, in the case of Lys, the reduction wave around -0.8 V is broadened and exhibits a negative-tailing peak near -0.85 V, which is further investigated in the next section (blue *).

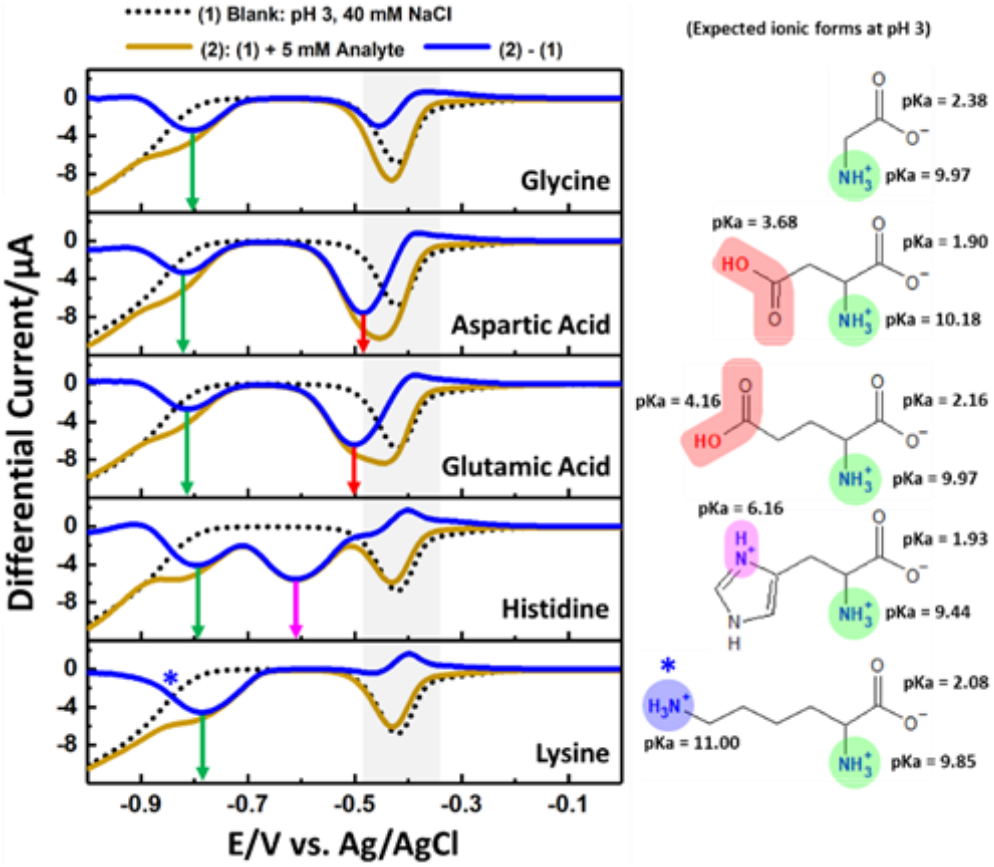

Figure 3.2. Direct, electrochemical reduction of charged amino acids on a platinum electrode demonstrated with distinct redox features of freely diffusing amino acids; differential pulse voltammograms and the corresponding molecular structures of amino acids glycine, aspartic acid, glutamic acid, histidine, and lysine. The blue curve for each amino acid is the deconvoluted voltammogram after subtracting the DPV without analyte (i.e., blank, dotted black) from the DPV with 5 mM of analyte (gold). All experiments were done in 40 mM NaCl aqueous solution at pH 3. Protonated molecular moieties alongside their pKa values are shaded in the same color as the arrows indicating the redox waves assigned to their respective electrochemical deprotonation.

Overall, Figure 3.2 clearly demonstrates that specific proton-containing chemical moieties within different charged amino acids can be reduced at distinct electrochemical potentials and that deconvolution of DPV scans allows one to identify and assign specific redox wave features to specific molecular moieties (e.g., α- and ε-amine, imidazolium, and COOH groups). The outstanding resolution and broad pKa range points to the generality of this method, with arginine being the only exception since the sidechain's pKa of ~ 12.5 causes the potential to shift to such negative values that is masked by the kinetically limited water electrolysis that becomes dominant near – 1 V (**Figure 3.3**). In addition, small differences in redox feature potential for the same molecular moiety can give insight into how the nearby chemical environment modifies the molecular moiety's pKa value (cf. Figure 1 locations of the ε-amino proton).

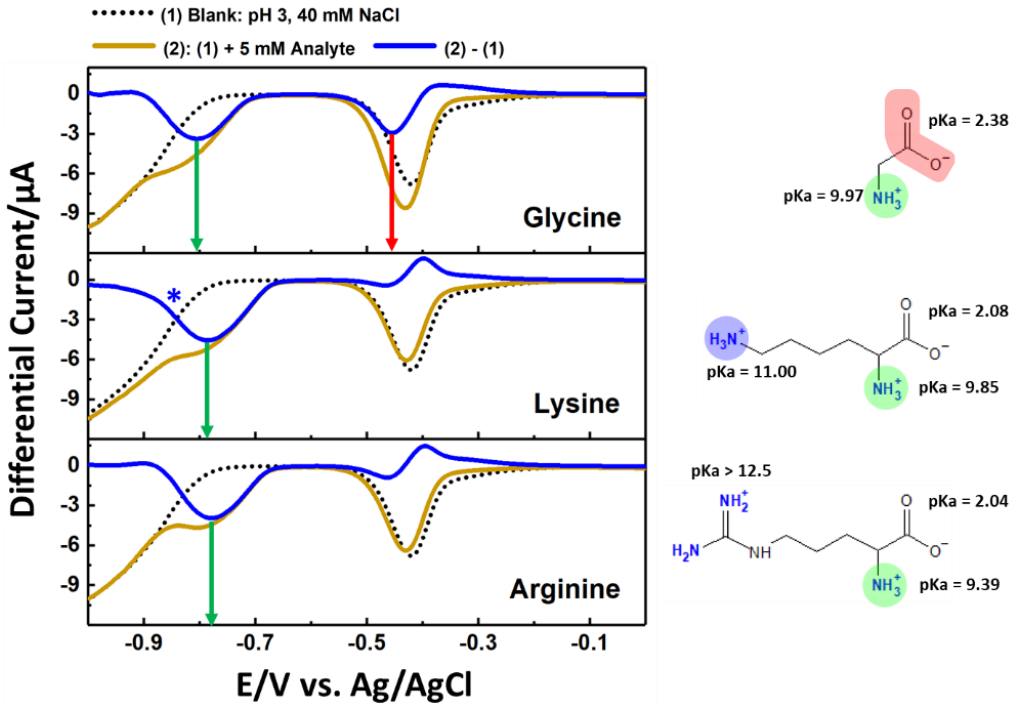

Figure 3.3. Voltammograms demonstrating different redox behaviors of amino acids with redox active sidechain moiety (Lysine) and without redox active (Glycine, Arginine) sidechain moieties.

3.4.3 DPV Study of Lysine and Its Analogues

To demonstrate the utility and generality of electrochemistry to probe proton dissociation equilibria of molecular moieties, DPV was performed on freely diffusing lysine analogs, namely hexylamine and 6-aminocaproic acid, as well as N-acetylated lysine derivatives that encompass the basic amine group (Figure 3.4). Comparing the DPVs of lysine, hexylamine and 6-aminocaproic acid reveals that the -0.85 V tailing feature of lysine (blue *) is due to direct deprotonation of the ε-amine group on all three molecules. This assignment (vs. the feature potentially being due to the a-amine proton) was verified via selective acetylation of lysine at the α- or ε-amino groups. Acetylation will significantly lower the basicity of an amino group[13], and thus should eliminate the redox wave from $-NH_3^+$ deprotonation. Indeed, N-α-acetyl-lysine showed similar redox behavior as 6-aminocaproic acid, which confirmed the validity of using 6-aminocaproic acid and hexylamine as analogs for lysine. In addition, carboxylic acid deprotonation showed the same trend observed before, namely that higher pKa results in more negative formal reduction potential. Comparing ε-acetylated lysine with lysine shows that the redox wave of N-α-acetyl-lysine near -0.8 V is more symmetric, while the redox wave of lysine near –0.8 V was "skewed" toward more negative voltages as a result of additional current from the presence of $\varepsilon\text{-}NH_3^+$. These results indicate that the ε-amino group is redox-active, and the redox events of the two amino groups in lysine are electrochemically separable and can be resolved thermodynamically, even when the amino acids contain relatively high pKa values, as in the case of Lys.

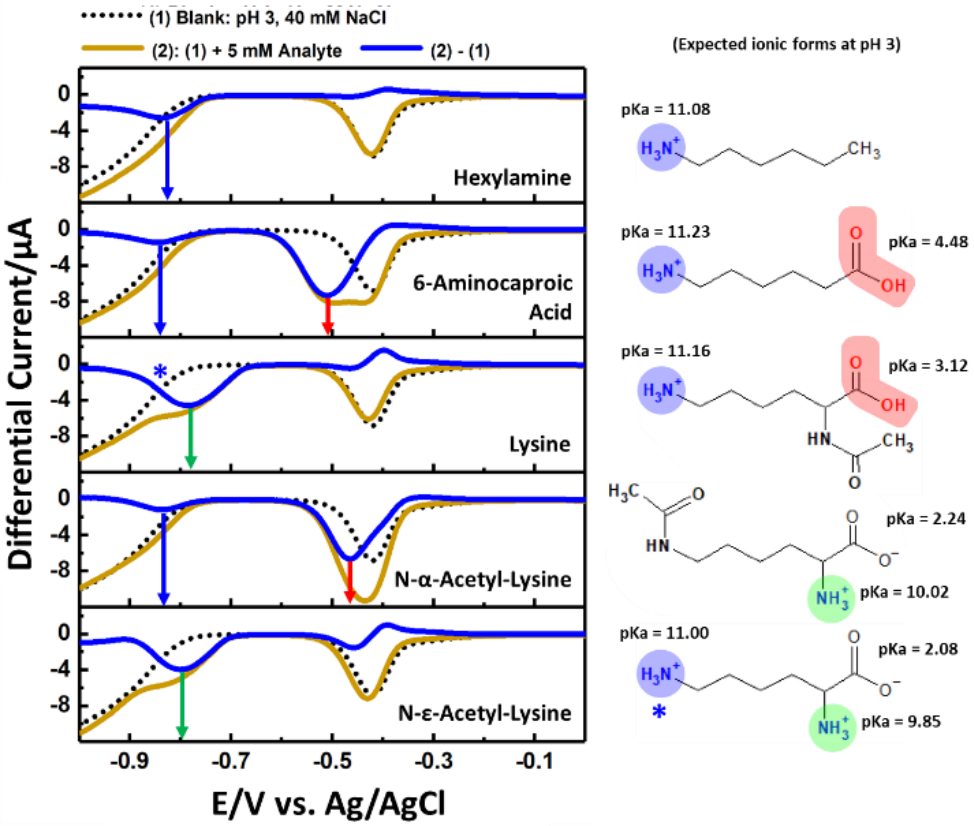

Figure 3.4. Voltammograms and molecular structures of lysine analogs (hexylamine and 6-aminocaproic acid), acetylated lysines, and lysine show that differential pulse electrochemistry can resolve reduction potentials of freely diffusing amino acid residues. The blue curve for each amino acid is the residual signal after subtracting the DPV without analyte (i.e., blank, dotted black) from the DPV with 5 mM of analyte (gold). All experiments were done in 40 mM NaCl aqueous solution at pH 3. Protonated molecular moieties are shaded in the same color as the arrows indicating the redox waves assigned to their respective electrochemical deprotonation.

3.4.4 Correlation of $E_{1/2}$ with pKa value

The aforementioned studies suggest that a correlation between the redox potential for proton electro-reduction and pKa of different molecular groups may exist, and moreover, that the DPV redox potential might be used as a novel analytical predictor of pKa values of amino acids (cf. Eqn. 1). Figure 3.5 indeed shows that this is the case, where all the observed formal redox potentials of various groups (e.g., COOH, α-NH_3^+, ε-NH_3^+, and imidazolium) in different analytes are plotted against their pKa values determined from pH titration (see Supplementary Information). The linear, negative correlation between pKa values and redox potentials in Figure 3.5 is consistent with the prediction of Eqn. 1. Moreover, the experimental slope of – 49.8 ± 0.12 mV / pKa unit is close to the theoretical 59 mV slope predicted from Eqn. 3.1. These values represent an equal amount of electrons and protons transferred to the electrode from the amino acid, and most likely reflect a single proton-single electron reduction in our case. Remarkably, amino acids residues all align on a single curve spanning pKa values of 3-11. Extrapolation of the fitted line to the y-axis produces yields of -310 mV vs Ag/AgCl, which is in line with the standard reduction potential of hydronium on Pt surface[1].

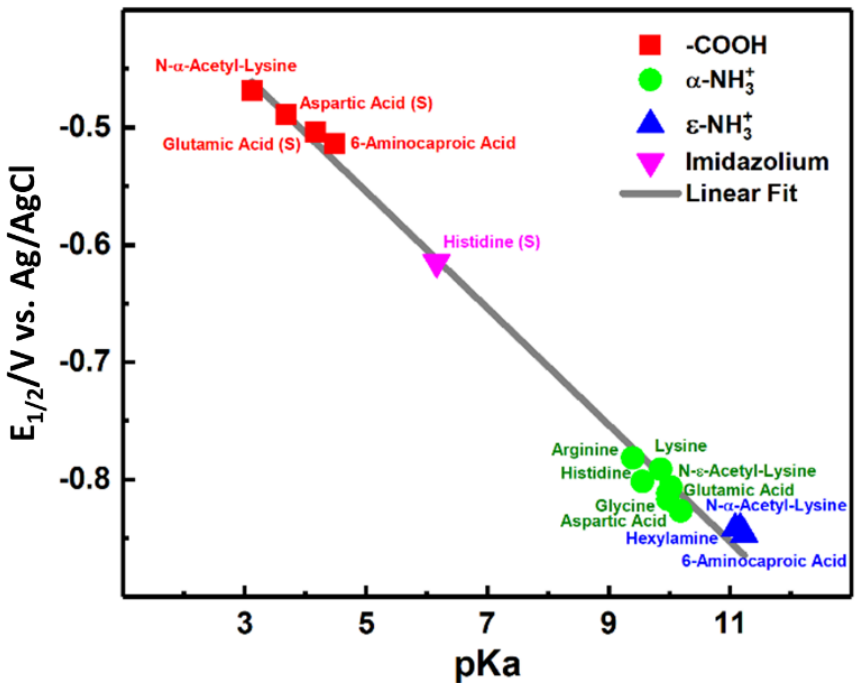

Figure 3.5. Correlation between electrochemically measured $E_{1/2}$ and pKa for a variety of deprotonable groups in different free amino acids. Each data point is labeled with the name of its parent molecule; different colors and shapes refer to their corresponding molecular moieties. Data points of molecular moieties in an amino acid sidechain are denoted with "(S)" in the label. The regression line is $E_{1/2} = -306\ mV - 49.8 \pm 0.12 \left(\frac{mV}{pKa}\right)\ pKa\ @\ 298\ K.$

Next, the biochemical scope was extended to demonstrate that the electrochemical method provided here can be extended to study more complex biomolecules such as peptides. H-Glycine-Glycine-Glycine-OH (Gly-Gly-Gly), H-Glycine-Lysine-Glycine-OH (Gly-Lys-Gly), and H-Glycine-Histidine-Lysine-OH (Gly-His-Lys) tripeptides were measured with differential pulse voltammetry at pH 3, and the peak potentials of the redox waves were compared with the pKa values of their corresponding chemical moieties determined by titration (See appendix). We specifically chose peptides that deviate from one another by a single charged amino acid to examine the sensitivity of our method. The comparison among all

tripeptides is shown in Figure 3.6; colored upward arrows represent where the predicted DPV redox potentials of the different chemical moieties (shaded areas on chemical structures) in the tripeptides should occur using the correlation in Figure 3.5. At pH 3, the Henderson-Hasselbach equation predicts that the amino, imidazolyl, and carboxyl groups can be protonated. For all three tripeptides, the blank subtracted DPV scans show clear redox features that align well with the predicted formal reduction potentials based on pKa values and Fig. 3. Although the redox wave of the amino group of lysine in Gly-Lys-Gly did not show a maximum, a higher potential "shoulder" can be seen, which is consistent with the results in Figure 3.2 and Figure **3.4**. No clear redox feature of the ε-amino group in the lysine residue of Gly-His-Lys was observed at the predicted redox potential, which might be a result of the overlap between the redox waves of the ε-amino and N-term groups, as seen for free Lys (cf. Figure 3.4). The results demonstrate that electrochemistry can provide convenient estimations of pKa values for molecular moieties of charged amino acid residues in tripeptides, and could potentially be expanded to analyze more complex and larger peptides.

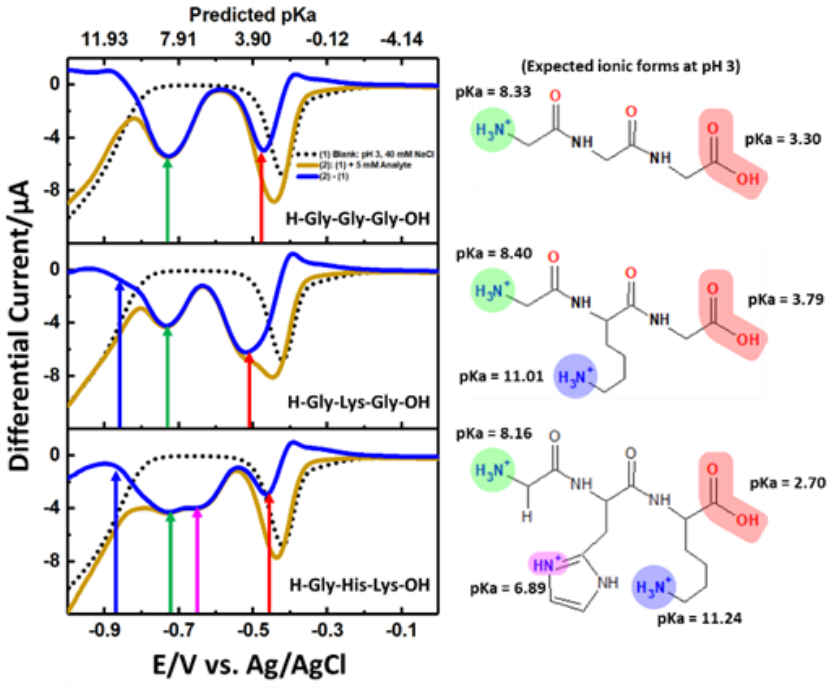

Figure 3.6. DPVs and molecular structures of Gly-Gly-Gly, Gly-Lys-Gly, and Gly-His-Lys tripeptides. Colored arrows in the DPV panel indicate the redox potentials predicted by inserting the pKa values of each molecular moiety (colored shading) into the correlation shown in **Figure 3.5**.

3.4.5 Redox Reactivity of ε-amino Groups in Poly-lysine Decamer

Differential pulse voltammetry was also performed on polylysine decamer (Lys_{10}) to demonstrate the detection and site-selective electroreduction chemical moieties of residues in larger peptides. As shown in **Figure 3.7**, three redox waves appeared in the deconvolved DPV of Lys_{10}. The redox wave near -0.45 V is thus assigned to hydronium reduction, and the redox features between -0.6 and -0.9 V are attibuted to direct electroreduction of molecular moieties in Lys_{10}. The blank subtracted DPV of Lys_{10} shows two separate redox waves (i.e., -0.6 to -0.75 V and -0.65 to -0.9 V) that, according to the correlation in Figure 3.5, lie in the potential

region of amino groups, and correspond to pKa values of 7.3 and 10.0, respectively. This clearly indicated that voltammetry could be used to resolve protonated molecular moieties of identical molecular structures in biological macromolecules just like the case in amino acids (Figure 3.2 and Figure 3.4).

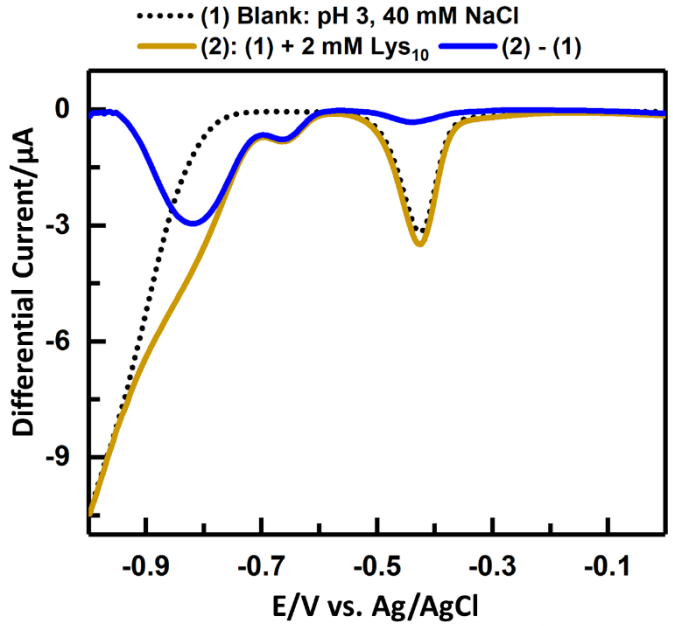

Figure 3.7. Deconvolved DPV of Lys_{10} demonstrating the electrochemical reduction of protons in molecular moieties of Lys_{10} at Pt surface.

Since the electrochemical deprotonation of an amino group is a one electron process, the area ratio of the two redox waves can be used to estimate the average number of amino groups that can be electroreduced when Lys_{10} interacts with the electrode surface. Given this backdrop, the current contribution from individual type of molecular moieties was resolved via fitting the waves with gaussian function (Figure 3.8a). The smaller current, -0.6 to -0.75 V redox wave (green) can be associated with the reduction of the peptide N-terminus, while the larger current, -0.65 to -0.9 V wave is due to the reduction of the more prominent ε-amino

groups in the lysine residues. Although the lysine amino group to peptide N-terminus ratio is 10 in Lys_{10}, the observed current ratio of their electroreduction peaks is ~5. The latter likely indicates that there is a finite electrochemical cross-section between Lys_{10} and the electrode surface that allows only partial deprotonation, and moreover that the partially deprotonated peptide may undergo a structural change, e.g., random coil to α-helix, preventing further electroreduction. The case of Lys_{10} supports our observation in Figure 3.6 that the correlation in Figure 3.5 can be used to quantify pKa values in a complex peptide, and demonstrates that DPV can be used as an alternative for standard chemical titration, where the latter can be problematic or inconclusive when multiple chemical moieties are present and at high pH (see Figure 3.8(b)). In addition, the ability to resolve the relative ratio of charges transferred from different electrochemically titratable groups may provide further insight into the thermodynamics and/or accessibility of charged groups in more complex proteins.

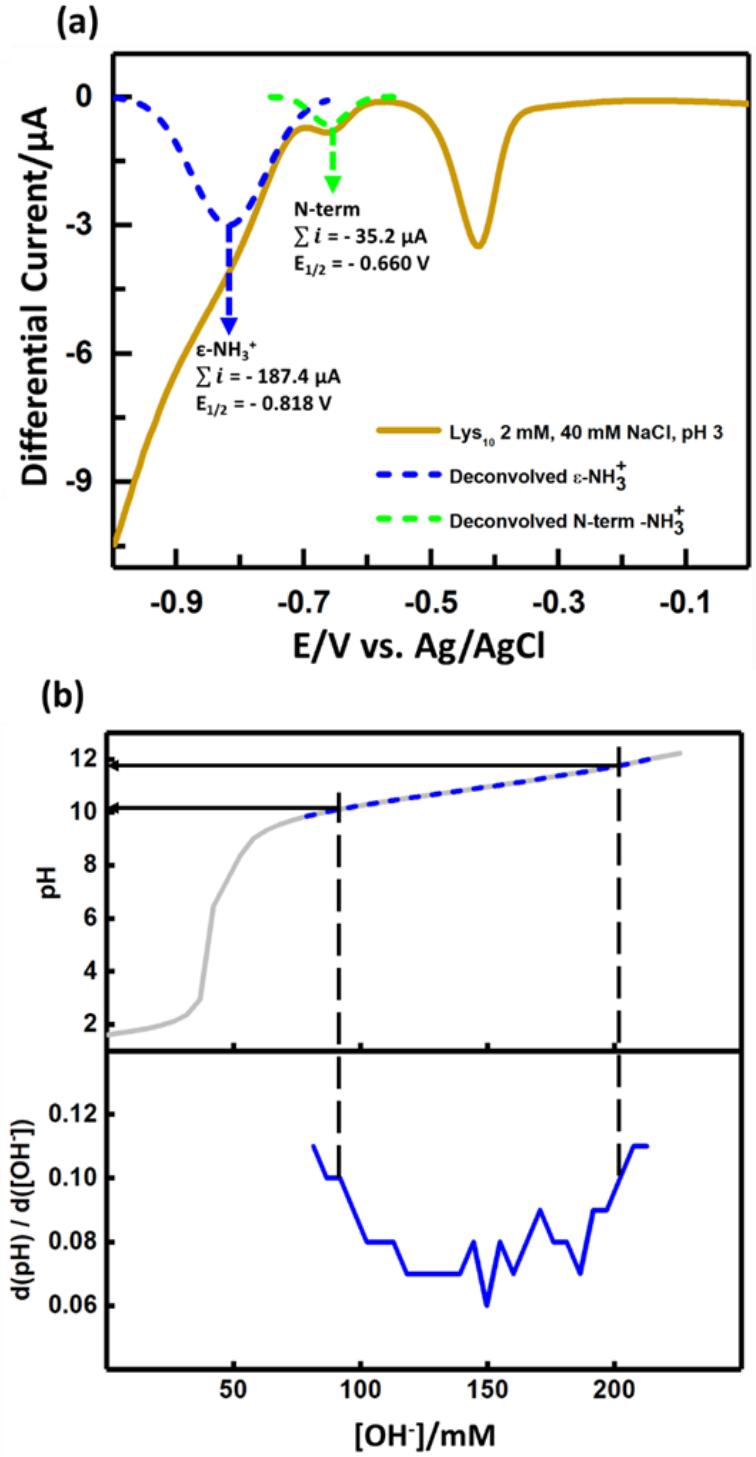

Figure 3.8. (a) DPV of polylysine decamer (Lys_{10}) and the deconvolution of redox features corresponding to the peptide N-terminus or ε-NH_3^+. (b) pH titration for Lys_{10}. Due to the low curvature in the plateau region, the pKa was estimated as the pH value where local minimum of d(pH) / d([OH^-]) appeared.

3.5 ***Summary***

Voltammetric methods clearly demonstrated the possibility of using electrochemistry to differentiate and selectively reduce specific dissociable protons in molecular moieties of simple biomolecules as well as more complex polypeptides such as polylysine. Deconvolution of differential pulse voltammetry was shown to be an effective strategy for isolating electrochemical signals of dissociable protons in molecular moieties of amino acids from the background contributed by platinum catalyzed hydrogen evolution. A linear correlation was found between pKa values and redox potentials of molecular moieties in amino acids as well as amino acid residues in peptides. In the case of polylysine, electrochemistry was able to resolve two types of amino groups: the N-terminus and sidechains bearing exactly the same molecular structure but experiencing different chemical environments. This discovery demonstrated the possibility of using electrochemically determined pKa values of dissociable protons as a proxy for evaluating local chemical environments in biomolecules. Moreover, site-selective, electrochemical reduction of dissociable protons in biomolecules enables the possibility of using electrochemistry to modify protonation level of biomolecules, which in turn could impact the conformation and/or assembly of biomolecules governed by coulombic interactions.

*3.6 **Supplementary Information: Titration of Amino Acids and Tripeptides***

Acid-base titration experiments were done by monitoring pH while gradually adding 2.5 M KOH in 100 mM of pH 1.5 analyte solution. The pH of the analyte solution was adjusted with perchloric acid. pH was monitored with a pH meter (Fisher Scientific, Accumet Basic 150). For consistency, pKa values were determined as the pH value where minimums of the first derivative of a titration curve were shown. The pKa values for some relatively acidic carboxyl groups of the C-terminus were assigned as the onset of the rises in their corresponding parts of titration curves.

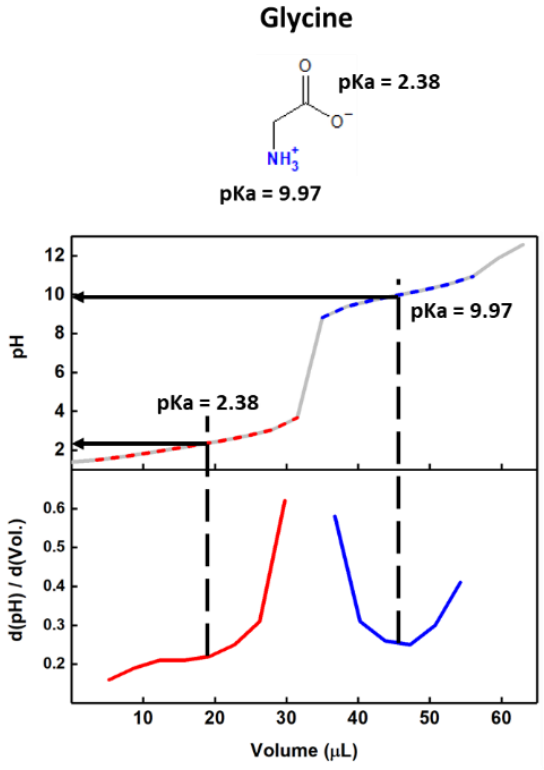

Figure 3.9. Titration curve of glycine.

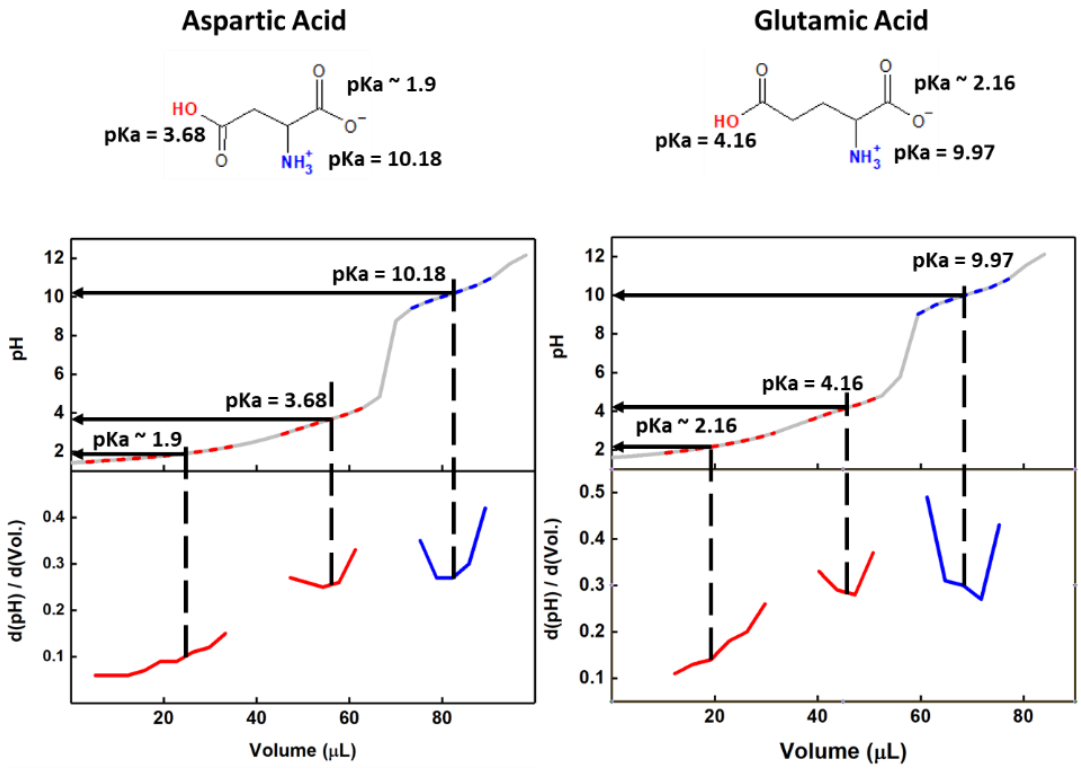

Figure 3.10. Titration curves of aspartic acid and glutamic acid.

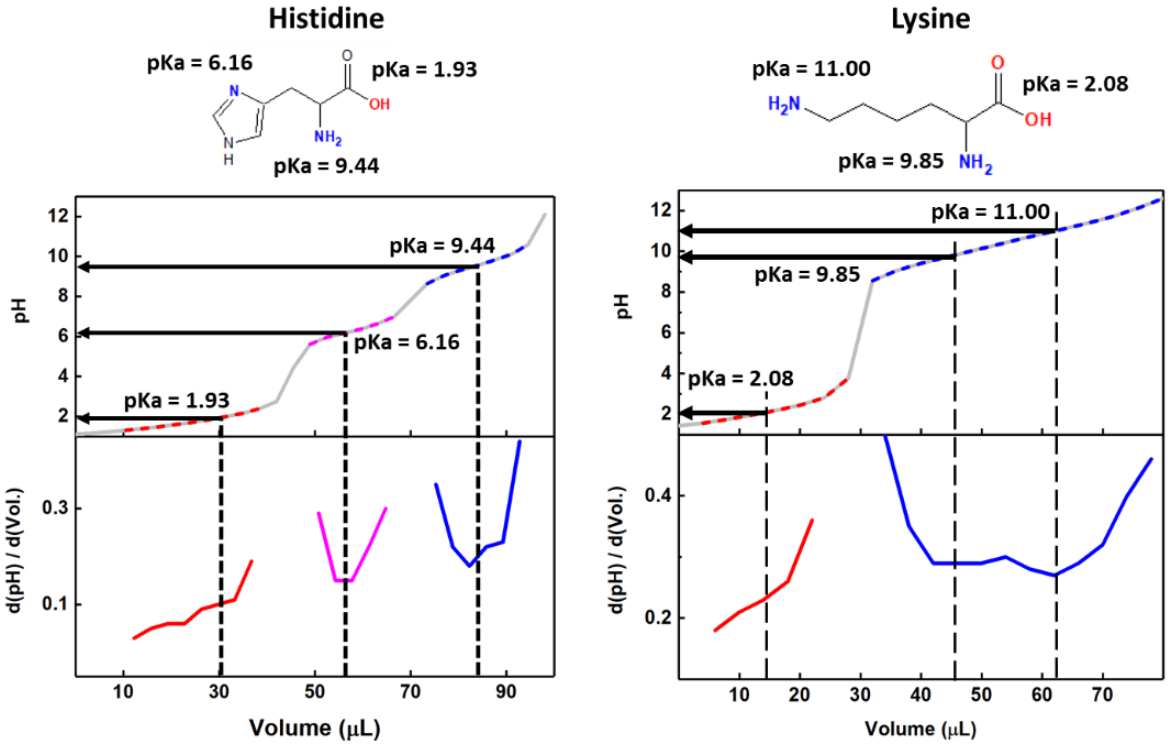

Figure 11. Titration curves of histidine and lysine

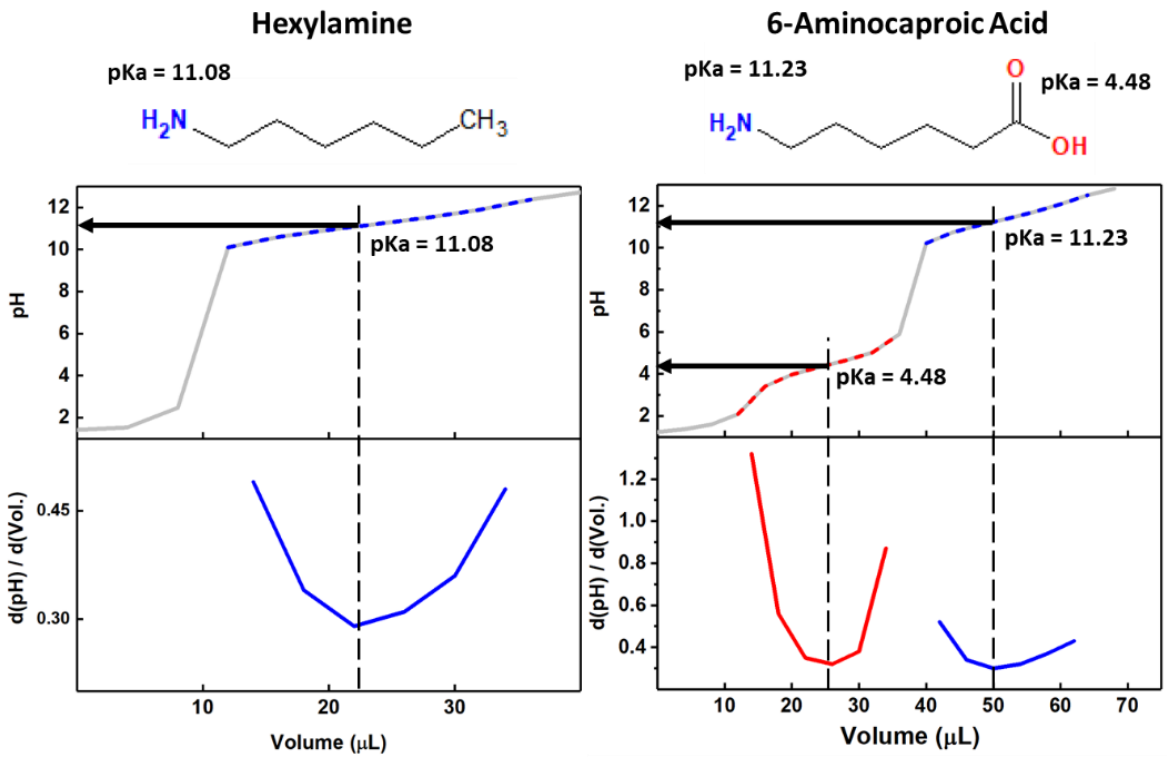

Figure 12. Titration curves of hexylamine and 6-aminocaproic acid.

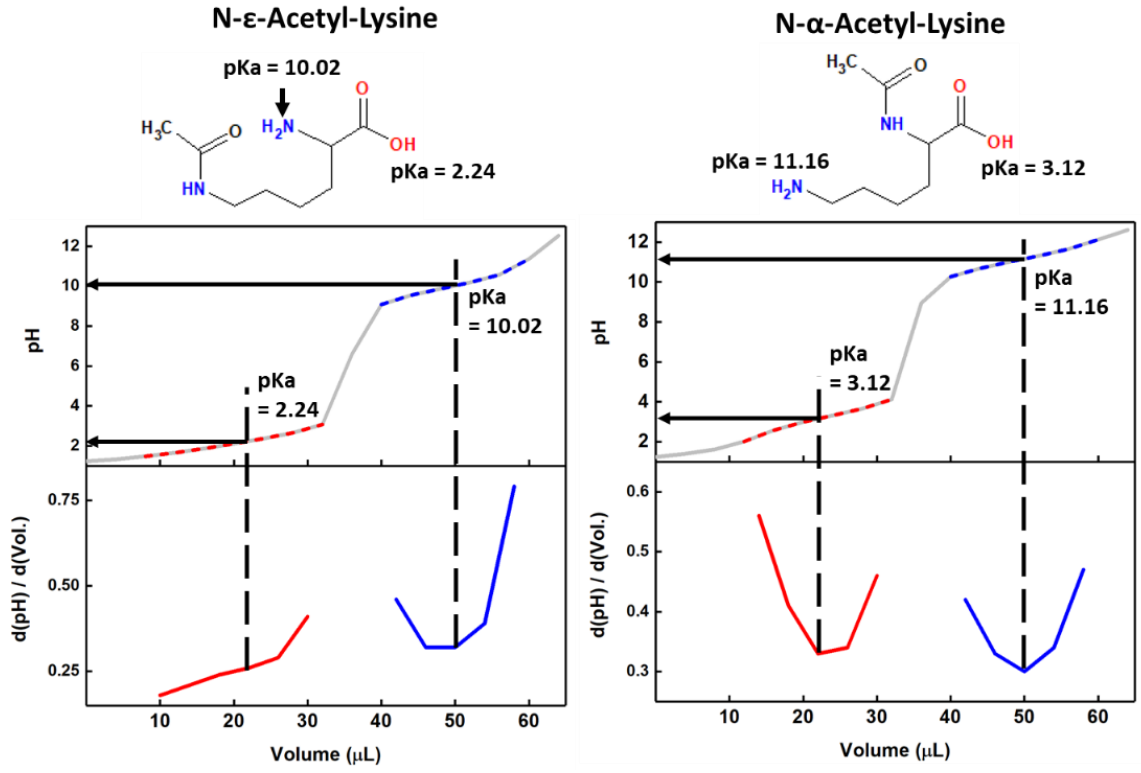

Figure 13. Titration curves of N-ε-acetyl-lysine and N-α-acetyl-lysine.

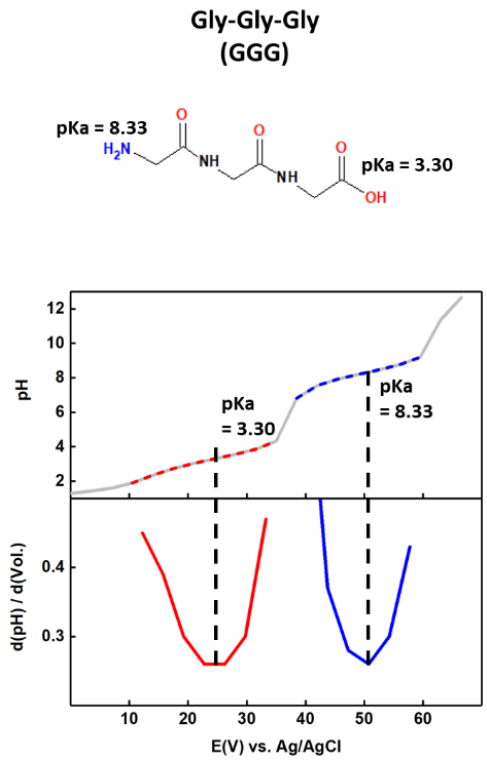

Figure 3.14. Titration curve of Gly-Gly-Gly

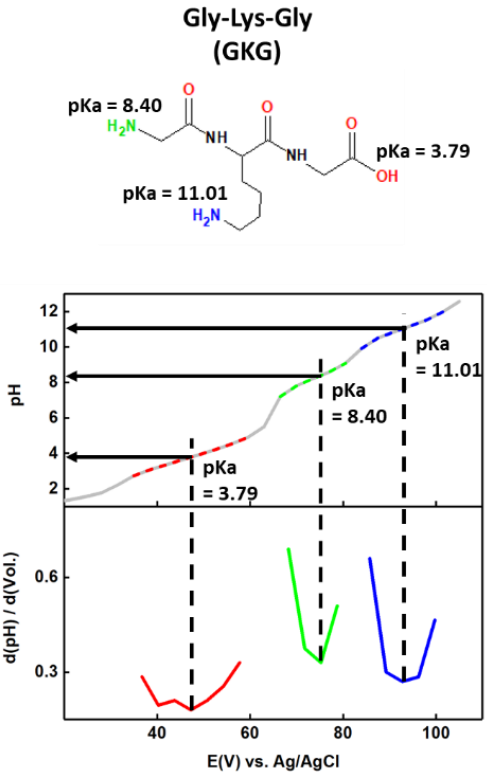

Figure 3.15. pH titration curve of Gly-Lys-Gly

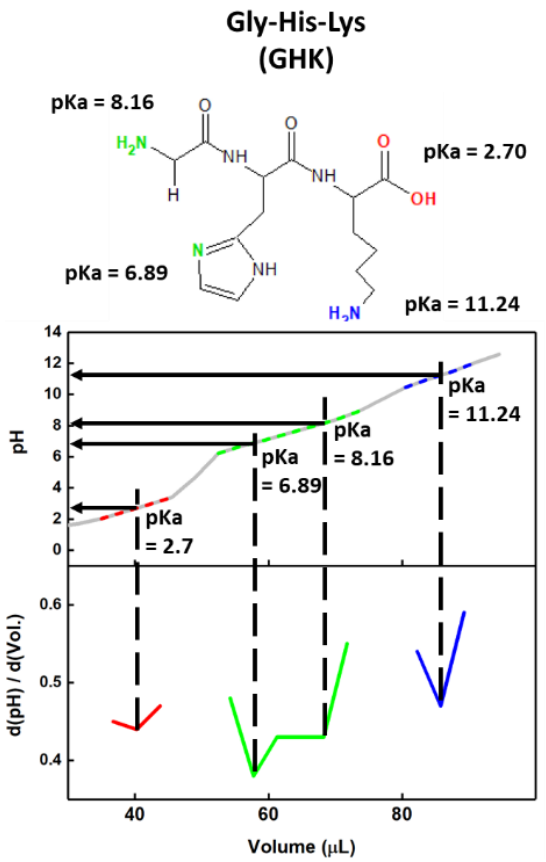

Figure 3.16. Titration curve of Gly-His-Lys

3.7 ***References***

1 G. M. Ullmann and E. Bombarda, pKa values and redox potentials of proteins. What do they mean?, Biol. Chem., 2013, 394, 611–619.

2 S. Törnroth-Horsefield, Y. Wang, K. Hedfalk, U. Johanson, M. Karlsson, E. Tajkhorshid, R. Neutze and P. Kjellbom, Structural mechanism of plant aquaporin gating, Nature, 2006, 439, 688–694.

3 B. R. Branchini, R. A. Magyar, M. H. Murtiashaw, S. M. Anderson and M. Zimmer, Site-directed mutagenesis of histidine 245 in firefly luciferase: A proposed model of the active site, Biochemistry, 1998, 37, 15311–15319.

4 C. M. Mair, T. Meyer, K. Schneider, Q. Huang, M. Veit and A. Herrmann, A Histidine Residue of the Influenza Virus Hemagglutinin Controls the pH Dependence of the Conformational Change Mediating Membrane Fusion, J. Virol., 2014, 88, 13189–13200.

5 R. Levenson, C. Bracken, C. Sharma, J. Santos, C. Arata, B. Malady and D. E. Morse1, Calibration between trigger and color: Neutralization of a genetically encoded coulombic switch and dynamic arrest precisely tune reflectin assembly, J. Biol. Chem., 2019, 294, 16804–16815.

6 S.-P. Liang, R. Levenson, B. Malady, M. J. Gordon, D. E. Morse and L. Sepunaru, Electrochemistry as a surrogate for protein phosphorylation: voltage-controlled assembly of reflectin A1, J. R. Soc. Interface, 2020, 17, 20200774.

7 C. L. Bentley, A. M. Bond, A. F. Hollenkamp, P. J. Mahon and J. Zhang, Electrochemical Proton Reduction and Equilibrium Acidity (p K a) in Aprotic Ionic Liquids: Protonated Amines and Sulfonamide Acids, J. Phys. Chem. C, 2015, 119,

21828–21839.

8 K. Liao, M. Askerka, E. L. Zeitler, A. B. Bocarsly and V. S. Batista, Electrochemical Reduction of Aqueous Imidazolium on Pt(111) by Proton Coupled Electron Transfer, , DOI:10.1007/s11244-014-0340-2.

9 J. L. Dempsey, J. R. Winkler and H. B. Gray, Proton-Coupled Electron Flow in Protein Redox Machines, Chem. Rev., 2010, 110, 7024–7039.

10 S. Y. Reece and D. G. Nocera, Proton-Coupled Electron Transfer in Biology: Results from Synergistic Studies in Natural and Model Systems, Annu. Rev. Biochem., 2009, 78, 673–699.

11 C. Costentin, J. C. Canales, B. Haddou and J. M. Savéant, Electrochemistry of acids on platinum. Application to the reduction of carbon dioxide in the presence of pyridinium ion in water, J. Am. Chem. Soc., 2013, 135, 17671–17674.

12 Chemical Rubber Company, CRC handbook of chemistry and physics, CRC Press, Boca Raton, FL, Electronic.

13 D. L. Nelson and M. M. Cox, Principles of Biochemistry, W. H. Freeman, New York, 4th edn., 2004, vol. 56.

Chapter 4

Electrochemically Driven Coil-to-Helix Transition of Polylysine

4.1 *Overview*

In Chapter 3, various voltammetry results revealed the redox activity of dissociable protons in freely diffusing amino acid and amino acid residues in proteins or peptides, and the linear correlation between the redox potential of dissociable protons and pKa value of the proton-hosting molecular moiety. This discovery shed light on the possibility of using electrochemistry as a universal switching mechanism for protonation of sensitive biomolecular structures, which could greatly expand the design space for biomaterials and allow investigation of intrinsically disordered biomolecular systems that do not possess steady states. In this Chapter, electrochemical investigations were expanded to perform site-selective deprotonation of polylysine sidechains to study the impact of electrochemical proton reduction on the conformation of peptides. In the three parts of the investigation, the redox electrochemistry of dissociable protons in polylysine was first investigated to resolve the correlation between structure and electrochemical reactivity of a biological macromolecule. Then, the conformation transition of electrochemically triggered polylysine was investigated via *in situ* circular dichroism and absorbance. Finally, to further resolve the mechanism of the electrochemically triggered transition of polylysine conformation, a novel, fully deuterated electrochemical system was devised to extend the parameter space beyond that conventionally accessible in aqueous systems.

4.2 *Coil-to-helix Transition of Polylysine*

Proteins or peptides derive amazing complexity and flexibility from a simple architecture constituted by only 21 amino acids. The collection and arrangement of the amino acids form the primary structure, which dictates the inter- or intramolecular interactions of proteins or peptides to manifest various dynamic structures and functions[1]. Though current technologies can readily synthesize peptides or proteins of specific primary structures, the lack of understanding towards the relation between their primary structure and hierarchical assembly prohibits the development of *de novo* proteins or peptides with designed functions[2]. The challenges in resolving the relation between a primary structure and the resulting hierarchical assembly stem from the coupled inter- and intramolecular interactions happening at various length scales, and the dynamic nature of these interactions usually prevent the isolation of structural intermediates[3–9].

Many efforts have focused on studying the relation between primary and secondary structures of simple peptides composed of single or a few distinct amino acids as simplified model systems for complex natural proteins[10–18]. Among the simple peptides, polylysine shows excellent chemical stability across a wide range of pH and salt concentration, which has allowed discovery of several distinct secondary structure states[10,12,15]. As illustrated in Figure 4.1, when the sidechains of polylysine are charged via protonation, the Coulombic repulsion between positive charges in the sidechains promotes the extension of the protein backbone and results in a random coil conformation. When the sidechains of polylysine are neutral, the hydrophobic interaction between the aliphatic sidechains and polar aqueous environment induces the folding into the more compact α-helix conformation, which can further rearrange and assemble into β-sheets when heated to 52 ^{o}C[15]. The existence of states of various solution-

dispersed secondary structures makes polylysine an ideal standard of spectroscopic features for secondary structures of peptides and proteins, which has gained successful quantitative resolution in spectroscopic studies [10,13,15,19–21].

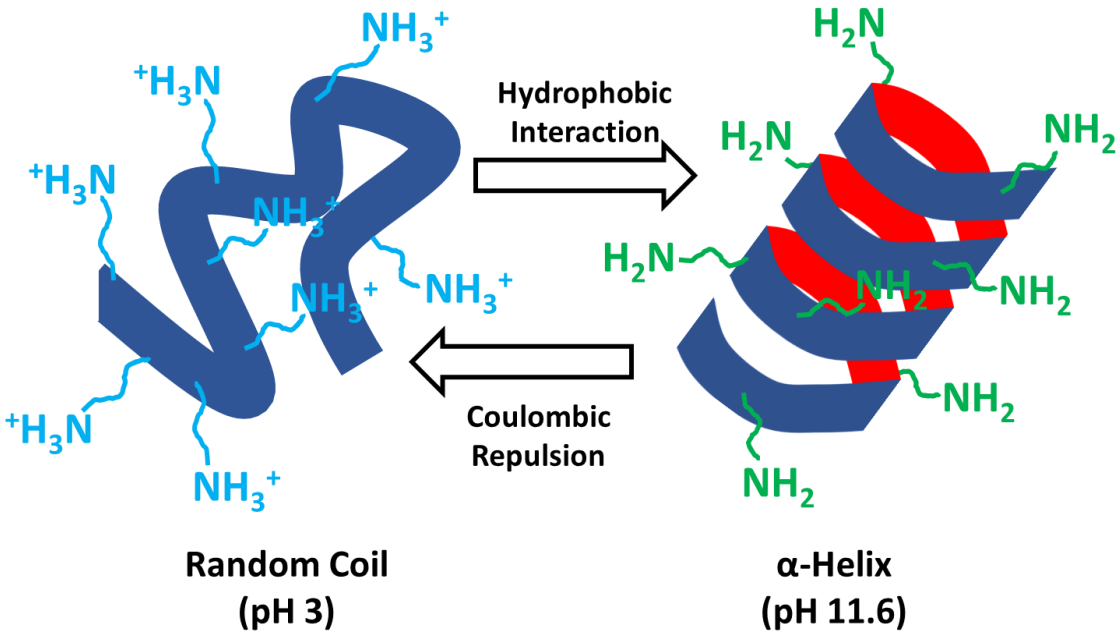

Figure 4.1. Illustration of pH-dependent conformation transition of polylysine from random coil to α-helix.

The work introduced in the following sections sought to resolve the impact of site-selective electrochemical proton reduction on a peptide adopting different protonation-dependent conformations. Polylysine was chosen as the model system in this study due to its unique protonation-sensitive conformation transition, and the high pKa value of the lysine sidechain. As shown in Chapter 3, the higher pKa value of a molecular moiety implies higher electrochemical potential to drive its deprotonation, and hence may be subject to more side reactions coming from the solution environment. If electrochemistry can drive deprotonation of the lysine residues and trigger structural transition in polylysine, other sidechain moieties of

the other charged amino acids or synthetic amino acids residues with lower pKa values may also be electrochemically deprotonated to manifest structural transitions. Novel approaches combining electrochemistry, far-UV spectroscopy, and the deuterium isotope effect were used to characterize the behavior of electrochemically triggered conformation transition of polylysine. This work, detailed in the following sections, demonstrates that unprecedented electrochemical control of biomolecular conformation is possible, which suggests that electrochemistry can be a way to interface electronics and biomolecular systems, as well as activate transitions of biomolecular structures or conformations that cannot be access otherwise.

4.3 *Methods*

4.3.1 Materials and sample preparation

Lysine hydrochloride was purchased from Sigma Aldrich and poly(L-lysine hydrochloride) of different molecular weights (Lys_{10}, MW 3300; Lys_{20}, MW 1600; Lys_{50}, MW 8200) were purchased from Alamanda Polymers. Aqueous solutions of 100 mM $NaClO_4$ (MERCK KGaA, sodium perchlorate anhydrous) were prepared with di-ionized water or deuterated water (D, 99.9% Cambridge Isotope Laboratories, Inc). Perchloric acid (70% Fischer chemicals) was added to adjust the pH/pD of the solutions to 3. KOH and NaOD (Sigma Aldrich, 40 wt%. in D_2O, 99.5 atom % D) were used to adjust the pH/pD of the solutions to 10 and above. Polylysine was solubilized in aqueous solutions and sonicated for 10 minutes before use.

4.3.2 Differential Pulse Voltammetry measurements

Electrochemical measurements were conducted with a three-electrode configuration (working electrode: Pt disk; counter electrode: Pt mesh; reference electrode: fritted Ag/AgCl in 1M $KCl_{(aq)}$) and an Autolab M204 electrochemical workstation. The Pt disk working electrode (R_{Pt} = 1.5 mm) was polished three times (2 minutes each) using 3 μm, 1 μm, 0.25 μm, and 0.05 μm MetaDiTM polycrystalline diamond suspension (Buehler, Lake Bluff, IL, USA) on a microcloth polishing pad. Afterwards, the polished working electrode was sonicated in water for 2 min. The working electrode was polished between each experiment using 0.25 μm, and 0.05 μm polishing pads, followed by 2 minutes of sonication. DPV measurements were performed with a potential step size of 5 mV, pulse height of 10 mV, pulse duration of 200 ms, and interval time of 0.5 s.

4.3.3 in-situ Circular Dichroism (CD) and absorbance measurements

Circular dichroism (CD) spectra were measured using a Jasco J-1500 spectropolarimeter with constant N_2 flushing (Jasco Inc., Easton, MD.) The spectra were measured by using a temperature-controlled (25^{o}C) 0.2 cm path length. The ellipticity, high voltage and absorbance were monitored in parallel.

To perform an *in situ* CD measurement, a Gamry electrochemical workstation was used for chronoamperometry experiments, with absorbance, high voltage, and ellipticity monitored simultaneously. The CD spectra were recorded between 195 nm and 225 nm with a spectral bandwidth of 1 nm. Throughout the whole experiment, the concentrations of the polylysine solutions were 24 μM, 60 μM and 120 μM for Lys_{50}, Lys_{20} and Lys_{10}, respectively.

4.4 ***Result and Discussion***

4.4.1 Voltammetry of Lys_{10}, Lys_{20}, and Lys_{50}

Differential pulse voltammetry was first performed on polylysine having different chain lengths in 100 mM $NaClO_4$ at pH 3 to resolve the redox features of dissociable protons in sidechain amino groups. This solution condition was chosen to ensure full protonation of all molecular moieties in polylysine, sufficient solution conductivity for electrochemistry, and low background absorbance for far-UV spectroscopies. As demonstrated in the previous chapter, differential pulse voltammograms (DPVs) can be further deconvolved via subtracting the blank scan from the analyte scan to eliminate the redox signals of irrelevant redox active species in the solution (Figure 4.2). In Figure 4.2, the blank DPV (black dotted curve) clearly shows the contribution of water electrolysis from – 0.8 V to more negative potentials, and the subtraction of the blank from the DPV of polylysine multimers ($Lys_{10,20,50}$) results in two distinct redox waves. Since amino and carboxyl groups are the only protonatable molecular moieties in polylysine (see structure in Figure 4.2), both redox waves are assigned to NH_3^+ according to the linear correlation found in Chapter 3. As the chain length increases, the relative redox current from dissociable protons in the sidechain amino groups also increases, which suggests that the smaller redox wave between – 0.6 V and – 0.75 V corresponds to NH_3^+ of N-terminus, while the larger redox wave between – 0.7 V and – 0.9 V corresponds to the amino groups in the sidechain of lysine residues.

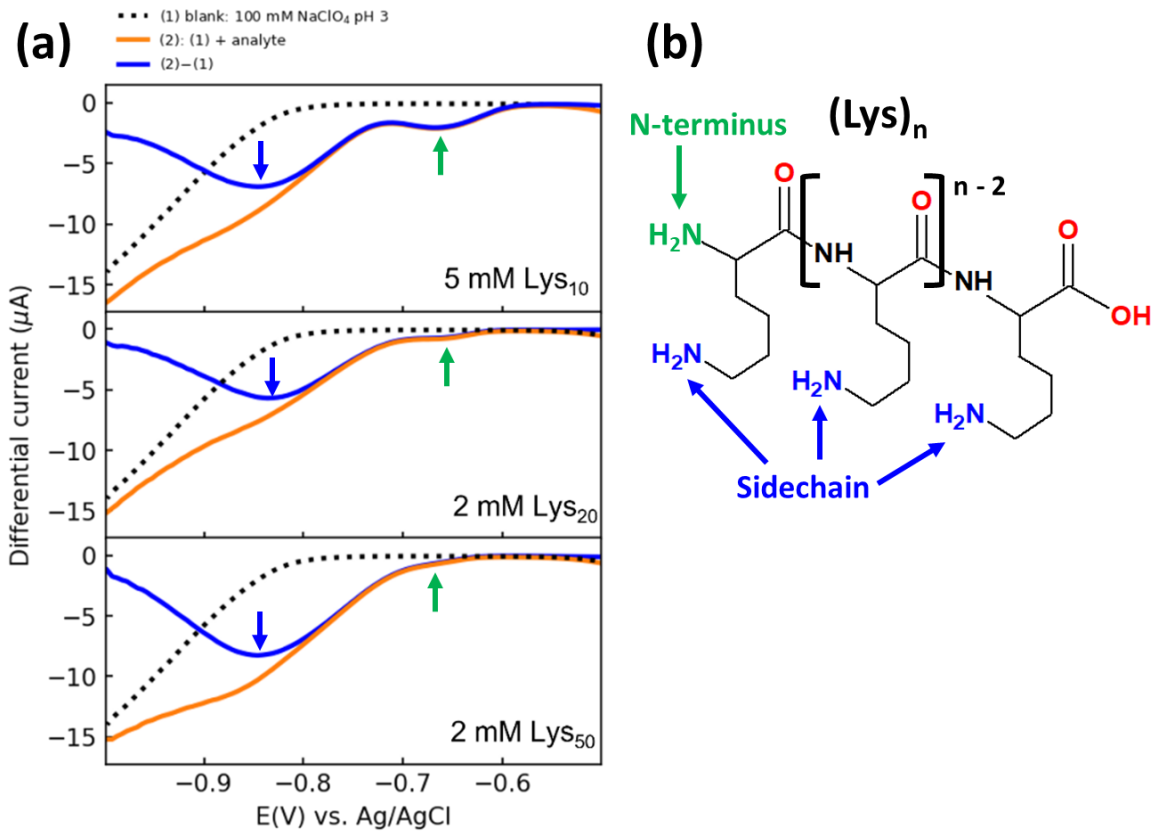

Figure 4.2. (a) Differential pulse voltammograms of 100 mM $NaClO_4$ at pH 3 without (black dotted curve) and with (orange solid curve) 5 mM Lys_{10} (top panel), 2 mM Lys_{20} (middle panel) and 2 mM Lys_{50} (bottom panel). The blue curve was obtained via subtracting the black dotted curve from the orange solid curve. The colored arrows on the figures indicate the corresponding molecular moieties in (b) with the same color code. (b) Molecular structure of polylysine with n repeating units.

Interestingly, unlike the relative differential current showing chain length-dependence, peak potentials and widths of the sidechain redox waves are similar. Since the redox potential of dissociable protons is a proxy of the pKa value of the proton hosting molecular moiety in a peptide (Chapter 3), similar redox potentials indicate comparable pKa values among sidechain moieties within polylysine, regardless of the chain length. Since electrochemical kinetics is a function of potential for a sufficiently fast charge transfer process, this observation suggests

that the dependence of differential current on chain length may likely originate from electrode processes, i.e., interactions between the redox active species and the electrode surface. Moreover, the similar widths show that the distributions of local chemical environments in polylysine are similar, which facilitates the comparison of electrochemically triggered structural transition in polylysine of different chain lengths.

As mentioned in Chapter 3, deprotonation of sidechains in amino acid residues is a one proton, one electron process, so the number of charges transferred in polylysine deprotonation represents the efficiency of sidechain deprotonation per contact between the electrode and the molecule, which can allow further resolution of the electrode process. The deprotonation efficiency was assessed via comparing normalized differential currents of Lys_{10}, Lys_{20}, and Lys_{50}. The peak differential current (δi_{peak}) can be described as [22]:

$$\delta i_{peak} = \frac{nFA\sqrt{D}C^*}{\sqrt{\pi}\sqrt{\tau-\tau'}}\left(\frac{1-\sigma}{1+\sigma}\right) = \left[n\left(\frac{1-\sigma}{1+\sigma}\right)\right]\left[\frac{FA\sqrt{D}C^*}{\sqrt{\pi}\sqrt{\tau-\tau'}}\right] = f(n)\left[\frac{FA\sqrt{D}C^*}{\sqrt{\pi}\sqrt{\tau-\tau'}}\right] \qquad (4.1)$$

where n is the number of charges transferred per unit time, F is the Faraday constant, A is the electrode area, D is the mass diffusivity of the redox active species, C* is the concentration of the redox active species in the bulk, $\tau - \tau'$ is the duration of the pulse of electrochemical potential, $\sigma = exp(\frac{nF}{RT}\frac{\Delta E}{2})$, where ΔE is the pulse height applied in differential pulse voltammetry, and *f*(n) is the deprotonation efficiency function that includes all the terms related to number of charges transferred. Among the three measurements shown in Figure 4.2a, mass diffusivity (D), and concentration (C*) of the polylysines varied. To facilitate comparison, only the ratio of differential current based on Lys_{10} was considered. According to equation 4.1, the ratios of differential currents can be expressed as:

$$\frac{\delta i_{peak,Lys_N}}{\delta i_{peak},Lys_{10}} = \left[\frac{f(n)_{Lys_N}}{f(n)_{Lys_{10}}}\right]\left[\frac{C^*{}_{Lys_N}}{C^*{}_{Lys_{10}}}\right]\left[\frac{D_{Lys_N}}{D_{Lys_{10}}}\right]^{\frac{1}{2}} \qquad (4.2)$$

Equation 4.2 is more convenient than Equation 4.1 because only the relative mass diffusivities of polylysines are required. The relative mass diffusivities of random coil polylysines at pH 3 were estimated via considering the random walk distance of a coiled polymer[23]. The mass diffusivity of a particle relates to its hydrodynamic radius (R_h) via the Stokes-Einstein relation:

$$R_h = \frac{kT}{6\pi\eta_s D} \qquad (4.3)$$

where k is Boltzmann constant, T is temperature, and η_s is viscosity of the solution. Meanwhile, R_h of a coiled polymer such as polylysine at pH 3 is proportional to the random walk distance of the polymer chain, $\langle R^2 \rangle^{1/2}$ [24]:

$$\langle R^2 \rangle^{1/2} = N^{1/2} l = R_h * \text{constant} \qquad (4.4)$$

where N is the number of monomers in a polymer and l is the length of a monomer. By combining Equations 4.3 and 4.4, one can derive a relation between mass diffusivity and chain length of polylysine at constant temperature as:

$$D = \text{constant} * \frac{1}{\sqrt{N}} \qquad (4.5)$$

Since δi is proportional to $\sqrt{D}$, the effect of D can be scaled via multiplying the molar differential current (Figure 4.3 blue) by $\sqrt[4]{N}$, which is shown in Figure 4.3 (yellow). The trend indicates that as chain length increases, the deprotonation efficiency also goes up, which ultimately allowed similar levels of deprotonation in Lys_{10}, Lys_{20}, Lys_{50}, regardless of their chain lengths.

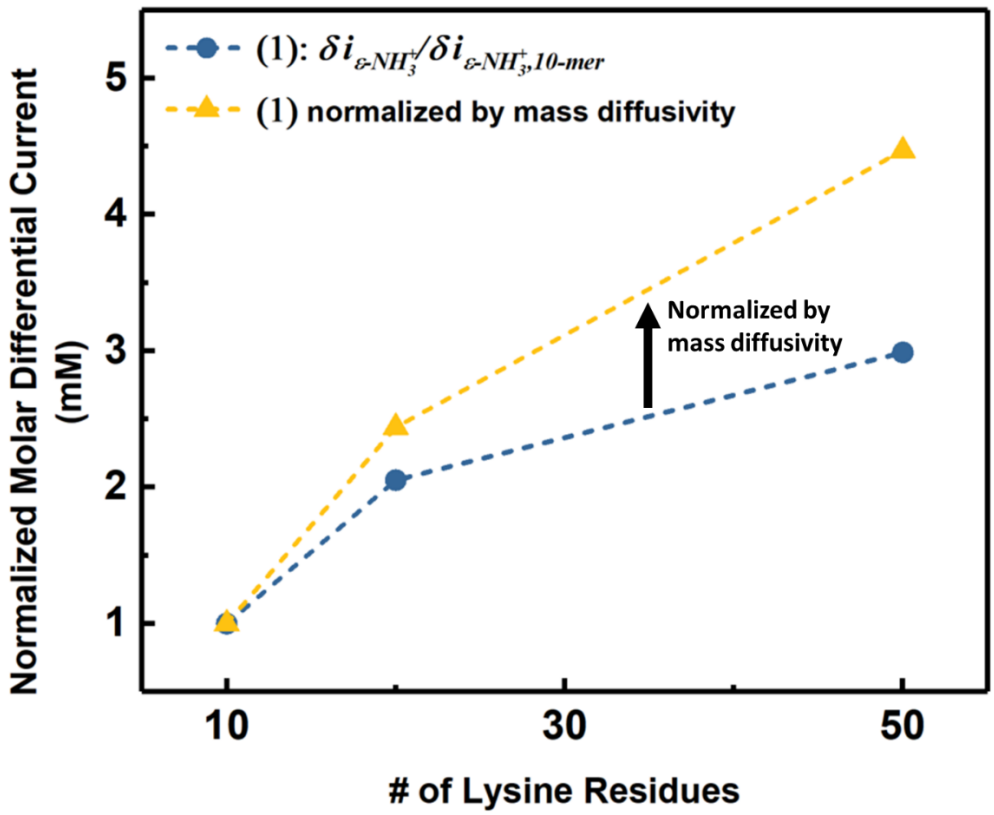

Figure 4.3. The impact of chain length on charge transfer behavior of polylysine. The peak differential current values (v) of ε-NH_3^+ (blue curve) are scaled by molarity and the δi value of ε-NH_3^+ of Lys_{10}. The contribution from the number of charges transferred to δi was further deconvolved via scaling the contribution of mass diffusivity to the data in blue curve (yellow curve) with Equation 4.5.

4.4.2 Conformational Transition of Electrochemically Deprotonated Polylysine

To resolve the conformational transition of electrochemically deprotonated polylysine, *in situ* via circular dichroism (CD) and absorbance spectroscopies of polylysine were carried out under electrochemical biases. As shown in Figure 4.4a and b, a three-electrode system was integrated to an optical cuvette to allow the observation of biomolecular conformation during electrochemical deprotonation of polylysine. As shown in Figure 4.2, the redox wave representing electrochemical deprotonation of polylysine sidechains peaks at around – 850 mV, so – 900 mV was chosen to test the structural conversion of polylysine. A – 900 mV bias successfully triggered structural transitions of Lys_{10}, Lys_{20}, and Lys_{50} (Figure 4.4c), where evolution of both ellipticity and absorbance spectra was observed. The initial CD spectra of the three polylysine molecules at t = 0 min (red traces in Figure 4.4c, top panels) are similar, indicating that all polylysine molecules started in a random coil conformation. As soon as – 900 mV was applied, polylysine reacted to electrochemical deprotonation, and significant shifts in ellipticity could be readily observed after 5 min of bias (green traces in Figure 4.4c, top panels). Comparing the three sizes of polylysines, the CD spectral features of Lys_{50} have clearly evolved from a single band near 200 nm, representing the extended-random coil conformation, to a doublet band between 205 nm an 225 nm, which is characteristic of the α-helix conformation [13].

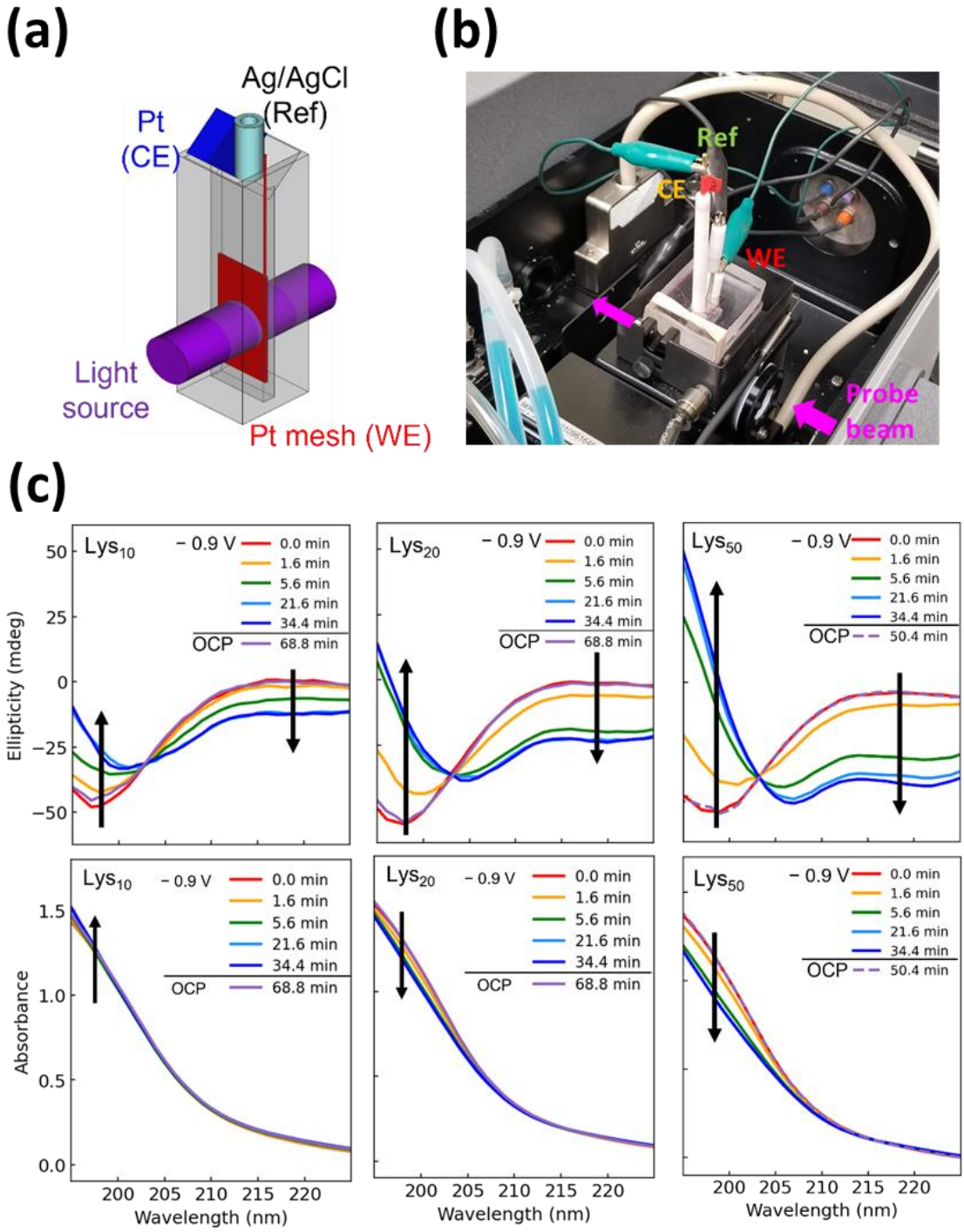

Figure 4.4. (a) Illustration of the electrochemical cuvette and (b) photograph of the *in situ* circular dichroism (CD) and absorbance spectroscopy setup. (c) *in situ* CD spectra of Lys_{10} μM, Lys_{20} μM, and 24 μM Lys_{50} in 100 mM $NaClO_4$ at pH 3. The bias was removed after the 34.4 min in the experiments, i.e., the system was put into an open circuit condition (OCP).

Comparison of CD spectra between electrochemically triggered and pH titrated polylysine revealed that α-helix formation occurs during electrochemical deprotonation. As shown in Figure 4.5, the pH titration indicated that the level conformational transition of Lys_{10} is different from Lys_{20} and Lys_{50}, where only one dip was observed in the CD of Lys_{10} versus two dips for Lys_{20} and Lys_{50}. The CD of helical polylysine between 200-225 nm originates from the coupling between peptide bonds due to the formation of the rigid helical structure, and the deviation between the dip at 190 nm versus 205 nm and 210 nm dictates the strength of coupling between peptide bonds, which can act as a proxy of the rigidity of a helical structure. The less rigid helical conformation of Lys_{10} is expected due to its short chain length. A helix turn requires 3.6 amino acid residues[14], which means there could only be 2 full helix turns in Lys_{10}. Also, secondary structure conformers in a peptide have been known to dynamically equilibrate with each other, where the equilibrium favors random coil at the ends and helix in the middle[7]. The short chain length of Lys_{10} results in a higher volume ratio of terminals and lower volume ratio of helical turns with respect to the volume of a polylysine chain, which in turn yields a less rigid helical conformation for Lys_{10}.

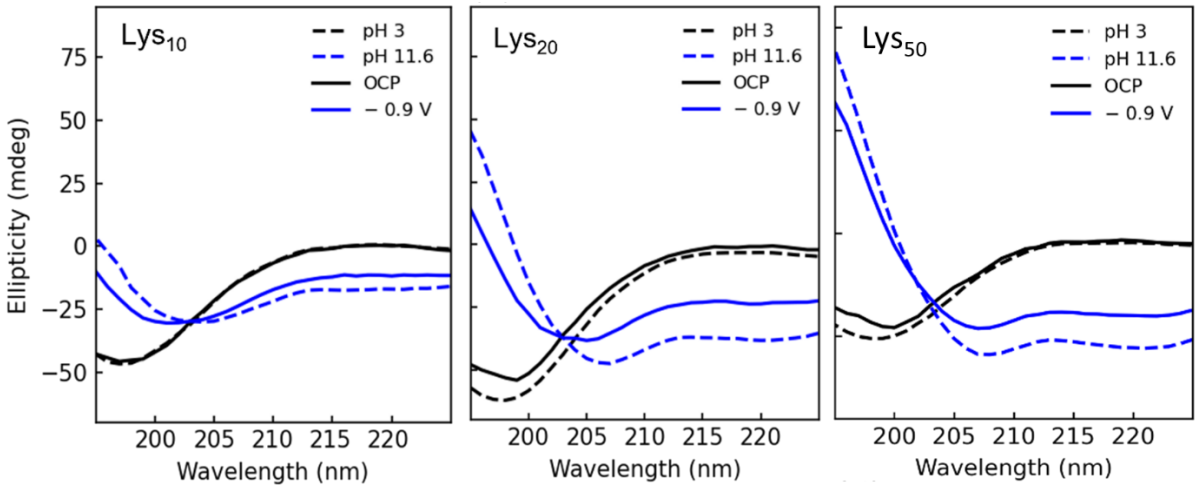

Figure 4.5. Comparison of CD spectra between electrically triggered (solid) and pH triggered (dashed) structural transition of polylysine. The non-triggered polylysine spectra (black) were measured in 100 mM $NaClO_4$ at pH 3. For pH titration, pH was raised to 11.6 to deprotonate the sidechains[15]. For electrochemical deprotonation, the spectrum was measured from polylysine solution after – 0.9 V was applied for more than 35 min. Open circuit potential (OCP) means no bias was applied.

Besides the non-ideal conformational transition of Lys_{10}, differences still exist between electrochemically triggered Lys_{20} and Lys_{50}. For both Lys_{20} and Lys_{50}, pH titration showed sufficient conversion from random coil to α-helix, indicated by the two dips between 200 and 225 nm. However, when – 0.9 V was applied, only Lys_{50} showed enough shift where the wavelength of dips in the electrochemically triggered CD spectrum overlapped the dips in the pH titration case. The different levels of electrochemical conversion between Lys_{20} and Lys_{50} may come from the accessibility of solvent molecules to the helical structure in polylysine. As shown in Figure 4.4c, the initial (red) and post-electrochemical triggered (lavender) CD spectra of polylysine overlap, which indicates that the electrochemical transition of polylysine is fully reversible. The reverse process should involve a protonation step where solvent exposure of

the sidechains is pivotal. As has been discussed in Section 4.4.1, a polymer chain can be described as a random walk of a polymer with many rigid domains. Since these rigid domains can be an amino acid or a helical segment in a peptide[25], the observation in Figure 4.5 suggests that Lys_{50} may be long enough that the interchain interaction between helical domains creates a kinetic barrier for backward helix-to-coil transition, which has been reported in a theoretical study[26].

4.4.3 Time-resolved Multivariate Analysis for Dynamic Structural Evolution of Polylysine

The *in situ* CD in Figure 4.4c clearly demonstrated that electrochemistry can trigger the structural transition of polylysine and provide a way to probe intermediate conformations of a peptide. To better resolve the time dependence of polylysine ellipticity, the ellipticity of Lys_{50} at 220 nm under three biases, i.e. – 0.9 V, – 0.85 V, and – 0.8 V, were measured as functions of time (Figure 4.6). Ellipticity was monitored at 220 nm to maximize the sensitivity of detection. Also, the shift in ellipticity (Δ|Ellipticity|) was used in the following analyses to facilitate comparison between results at different electrochemical potentials.

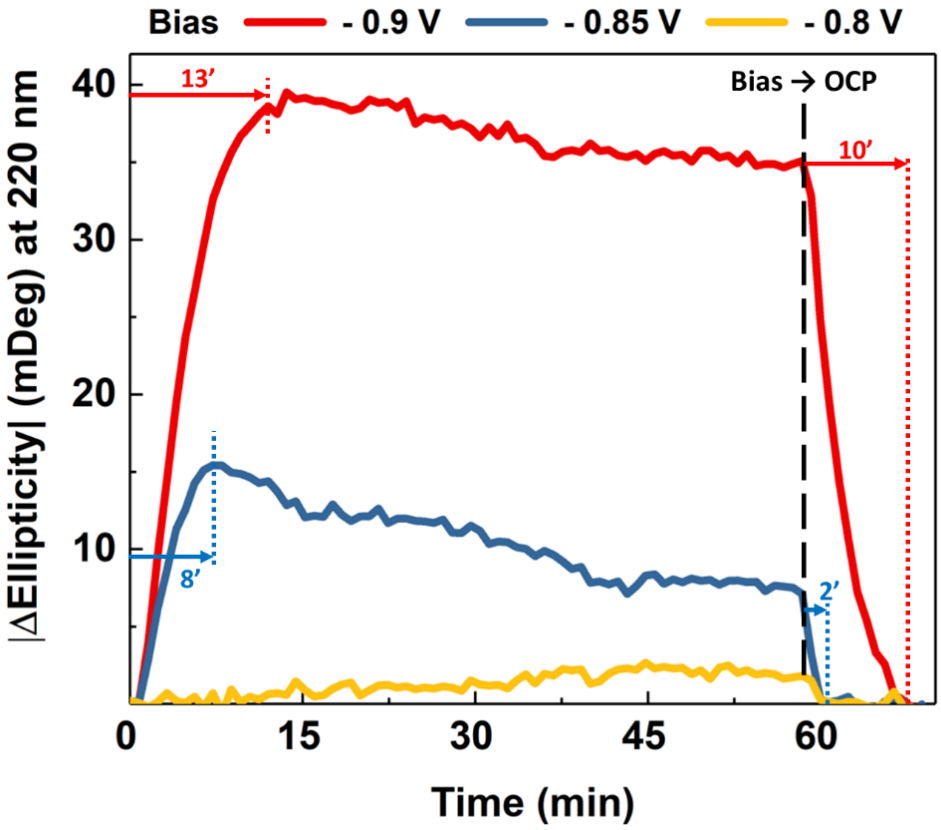

Figure 4.6. Dynamic evolution of ellipticity (220 nm) of 24 μM Lys50 in 100 mM $NaClO_4$ at pH 3, triggered by – 0.9 V (red), - 0.85 V (blue), and – 0.8 V (yellow).

As shown in Figure 4.6, electrochemically triggered Lys_{50} shows different CD trends with bias. DPV of Lys_{50} (Figure 4.2) showed that the differential current of dissociable proton reduction in polylysine sidechains increases as the applied electrochemical potential increases, which implies that applying higher potential increases the formation of α-helical structures in polylysine. When the bias was increased from – 0.8 V to – 0.9 V, the increasing rate and level of conversion conforms with the observation in DPV. Notably, polylysine triggered by - 0.85 V and – 0.9 V showed similar kinetic behaviors where Δ|Ellipticity| increased drastically and was followed by a slow decay; whereas, polylysine triggered by – 0.8 V showed a slow rise before reaching a plateau at 45 min. The cut-off bias for electrochemically triggering polylysine was further investigated via comparing Δ|Ellipticity| of Lys_{50} triggered by – 0.8 V and – 0.75 V at 200 nm, where shifts in Δ|Ellipticity| are more sensitive (than 220 nm) in the beginning of the conformational transition and allows better resolution of subtle conformational shifts. As shown in Figure 4.7, - 0.75 V did not trigger a distinguishable conformational transition of Lys_{50}, which indicates that the conformational transition in Figure 4.6 may be driven by the pH gradient generated from water electrolysis, since the onset of water electrolysis is around – 0.8 V for the solution condition used in this series of experiments (black dotted curves in Figure 4.2a).

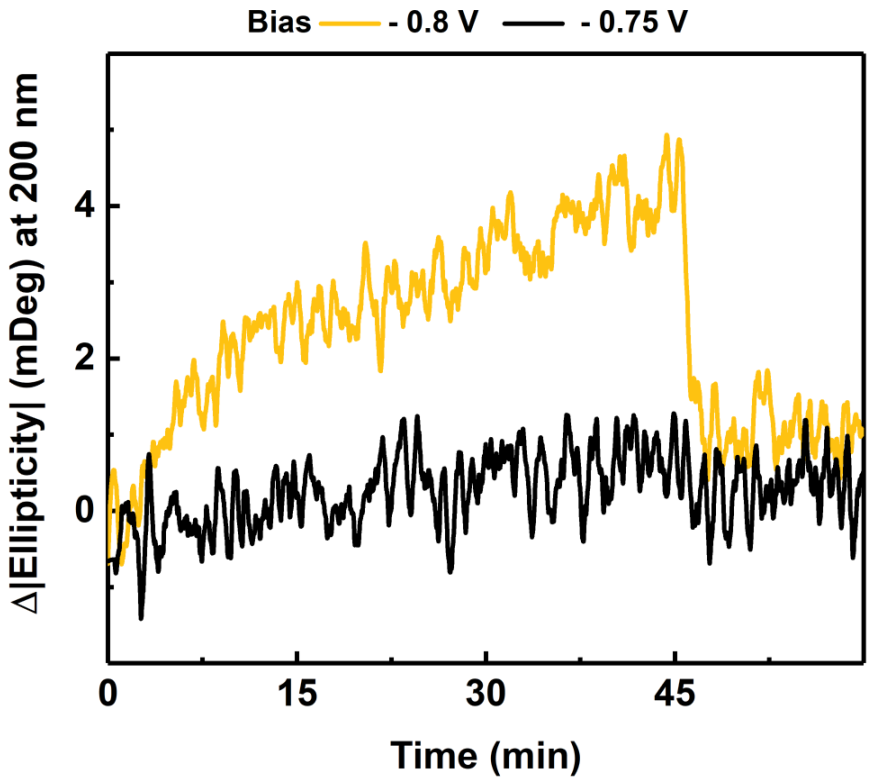

Figure 4.7. Dynamic evolution of ellipticity (220 nm) of 24 μM Lys_{50} in 100 mM $NaClO_4$ at pH 3, triggered by – 0.8 V (yellow) and – 0.75 V (black).

4.4.4 Isotope Effect in Electrochemical Triggering of Deuterated Polylysine

In the previous section, the electrochemical onset potential to trigger the Lys_{50} conformational transition was shown to overlap with the onset potential for water electrolysis, indicating that the sidechain deprotonation of Lys_{50} may originate from OH^- produced in water electrolysis. To unequivocally resolve the contribution of direct electrochemical deprotonation of Lys_{50} causing conformational transition, *in situ* CD was performed with Lys_{50} in a fully deuterated environment to expand the solvent window. Deuterium oxide (D_2O) has been reported to have a wider solvent window than water (H_2O) due to higher activation energy for breaking the O-D bond, larger solvation barrier in D_2O, and lower ion product[27]. As shown in Figure 4.8, the onset of electrolysis for D_2O is 40 mV more negative than H_2O, which indicates that a deuterated system may help isolate the electrochemically triggered coil-to-helix transition of Lys_{50} from electrolysis of solvent.

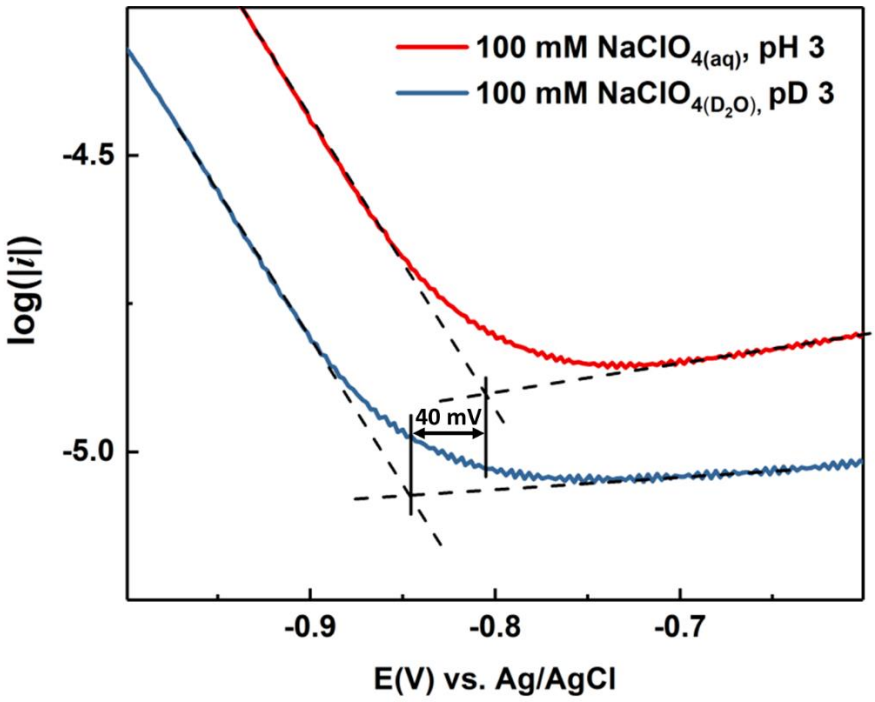

Figure 4.8. Tafel plot for electrochemical splitting of water at pH 3 and deuterium oxide (D_2O) at pD 3. Both solutions were supported by 100 mM $NaClO_4$, and measured by the three electrode system specified in the Methods section.

Figure 4.9 shows the deconvoluted DPVs of Lys_{50} in 100 mM $NaClO_4$, H_2O solution at pH 3 or D_2O solution at pD 3. The D_3O^+ redox wave (Figure 4.9, bottom panel) appeared at the same potentials as H_3O^+ in H_2O (Figure 4.9, top panel), and the peak differential current of D_3O^+ is lower than that of H_3O^+ by a factor of 1.6, which indicates that the choice of solvent may impact the kinetics of H^+ or D^+ reduction, without impacting the charge transfer thermodynamics. Similar explanation may be applied to the similar onset potentials of the redox waves of deuterated and protonated Lys_{50} sidechain moieties, where the shifts were less than the expected 40 mV for the different solvent environment, as shown in Figure 4.8. However, the redox wave corresponding to deuterated Lys_{50} sidechains became wider and shifted to higher peak potential. Since D^+ and H^+ shares similar electrochemical

thermodynamics, the different redox potential of deuterated Lys_{50} sidechains may originate from the larger solvation barrier of D_2O [27,28], which may further influence the electrochemical transition of Lys_{50} conformation. Most importantly, the more negative onset redox potential of D_2O electrolysis in Figure 4.9 clearly showed that it is possible to isolate the redox events of Lys_{50} sidechain and trigger Lys_{50} conversion, while keeping D_2O electrolysis at a minimum level.

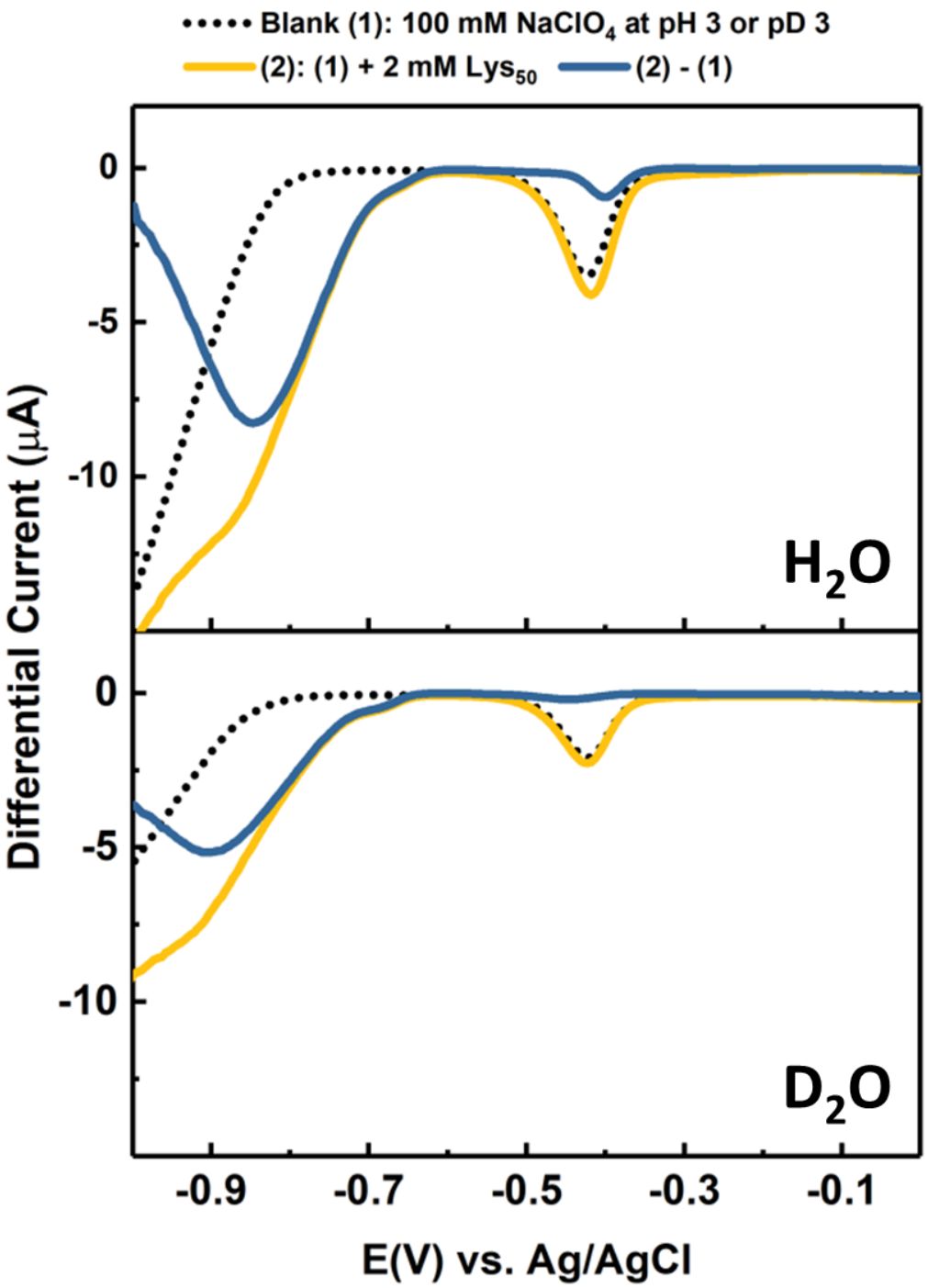

Figure 4.9. DPV of 100 mM $NaClO_4$, H_2O solution at pH 3 (top panel) or D_2O solution at pD 3 (bottom panel) without (black dotted) and with (yellow solid) 2 mM Lys_{50}. The blue solid curve was obtained via subtracting the black dotted curve from the yellow curve.

in situ CD was performed on Lys_{50} in D_2O at – 0.9 V, - 0.85 V, and – 0.8 V, and Δ|Ellipticity| at 220 nm was monitored (Figure 4.10) to investigate the role of direct electroreduction in the conformation transition of polylysine. In contrast to Lys_{50} in H_2O, where – 0.8 V barely triggered any conversion over 1 hour, deuterated Lys_{50} showed a distinctive rise of Δ|Ellipticity| at – 0.8 V within minutes, and the rise of Δ|Ellipticity| is comparable to the one of Lys_{50} in water at – 0.85 V. Since solvent electrolysis is less pronounced at – 0.8 V in D_2O (Figure 4.9), the ability to trigger greater conformation transition of Lys_{50} at – 0.8 V in D_2O clearly shows that a direct electrode process may be the main contributor to the conformation transition of Lys_{50}.

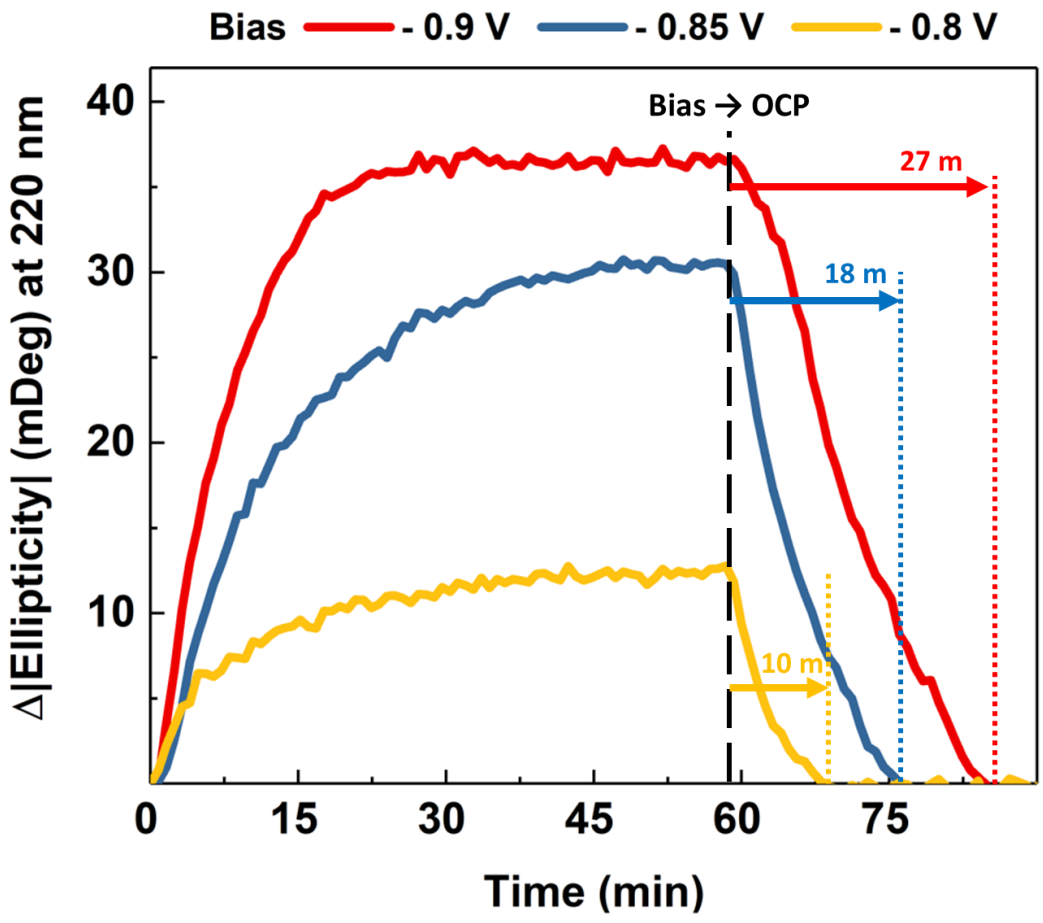

Figure 4.10. Dynamic evolution of ellipticity (220 nm) of 24 μM Lys_{50} in 100 mM $NaClO_4$ in D_2O at pD 3 triggered by – 0.9 V (red), - 0.85 V (blue), and – 0.8 V (yellow).

The more pronounced conformational transition of deuterated Lys_{50} was attributed to the slower reaction that back converts α-helix to random coil. Due to the lower differential current observed of deuterated Lys_{50} sidechains in DPV, the rate of electrochemical deprotonation of Lys_{50} sidechains is expected to be slower. Thus, the observed higher level of α-helix transition likely originates from a slower reverse reaction, which could be confirmed by the post-bias recovery rate being slower than the rate observed in H_2O (see Figure 4.6). In addition, the absorbance of Lys_{50} at 200 nm shows a greater decrease in D_2O than in H_2O (Figure 4.11). The absorbance of proteins and peptides near 200 nm corresponds to the π-π* electronic transition of peptide bonds, and hypochromicity (i.e., a decrease in molar absorptivity of a molecule) could be observed when the formation of rigid conformation (such as α-helix) promotes the dipole-dipole interactions between peptide bonds[14,17,29]. Using hypochromicity as a proxy of the rigidity of an α-helical structure, Figure 4.11 suggests that D_2O stabilizes the formation of α-helices in Lys_{50} more than H_2O. As has been reported in previous research [30,31], deuterium allows stronger "heavy" hydrogen bonds with greater bonding enthalpy, which induces the formation of more rigid α-helices via fortifying the intramolecular hydrogen bonding between the amide nitrogen and amide carbonyl. Since the exposure time of polylysine to D_2O before voltammetry and spectroscopy experiments is considered long enough for hydrogen-deuterium exchange in polylysine to be complete at pD 3[1], these observations are coherent with the reported isotope effect on proteins, namely, enhanced stability due to stronger deuterated bonds formed in the helical structure, coupled with an increase in solvation enthalpy.

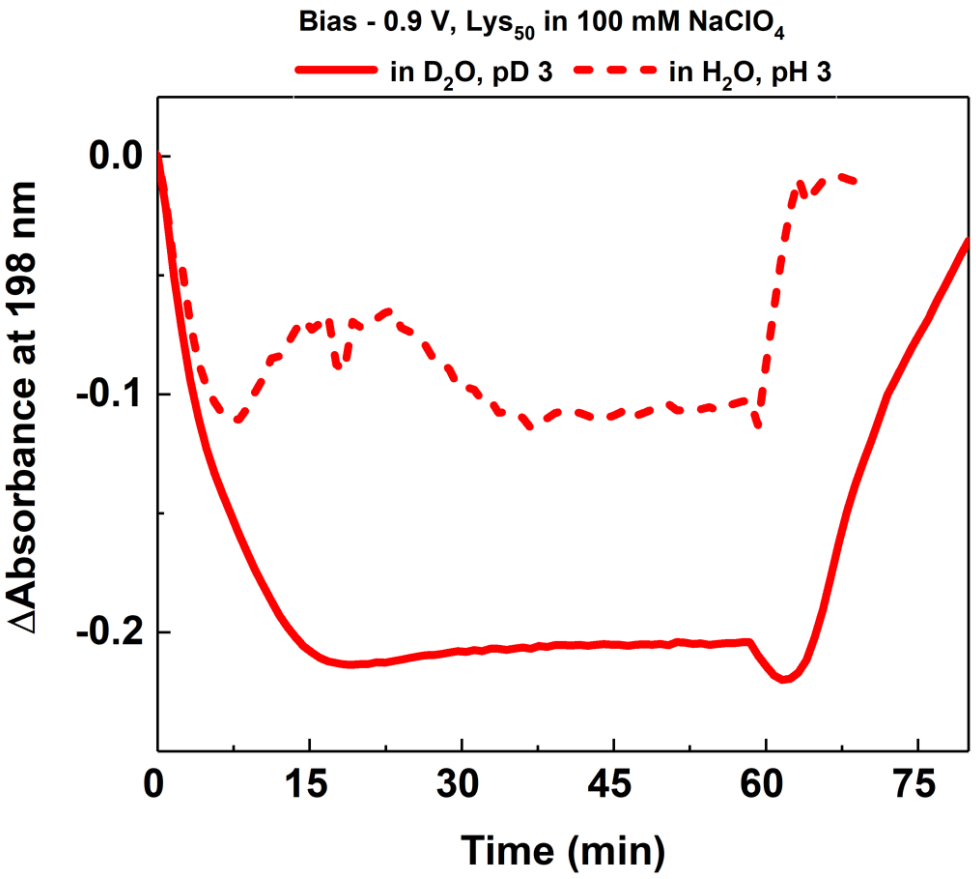

Figure 4.11. Dynamic evolution of ellipticity (220 nm) of 24 μM Lys_{50} in 100 mM $NaClO_4$ in D_2O at pD 3 (solid) or H_2O at pH 3 (dashed) triggered by – 0.9 V.

4.5 *Summary*

In this chapter, protonated polylysine was demonstrated to undergo structural transition when site-selective electrochemical deprotonation depletes positive charges in amino acid sidechain moieties. Differential pulse voltammetry was successfully extended to investigate the redox electrochemistry of dissociable protons in polylysine, and hinted that the mechanism is a complex electrode process. With the resolved voltammetry of molecular moieties in polylysine, *in situ* optical spectroscopy of electrochemically triggered polylysine in both water and D_2O demonstrated the successful triggering of conformation transition. The dynamic transition triggered by electrochemical deprotonation of polylysine sidechains serves as a valuable case for conformation transition of peptides triggered by electrochemistry. Polylysine sidechain NH_3^+ has the highest pKa value among all sidechain moieties in charged amino acids, and hence the most energetically unfavorable redox electrochemistry. Being able to trigger conformation conversion associated with polylysine implies the possibility of generalized site-selective electrochemistry to other protonation-sensitive biomolecular systems where the active protonated moiety has a pKa value lower than lysine amino groups.

Moreover, *in situ* optical spectroscopy was shown to be useful to resolve the dynamic structural conversion of peptides or even proteins. Given that site-selective deprotonation electrochemistry may be used to trigger structural transitions governed by the protonation of charged amino acid residues, the combination of electrochemistry and *in situ* optical spectroscopies may allow the investigation of dynamic intermediates of macromolecular systems, where the lack of distinct steady states limits the investigation of these systems via traditional approaches.

4.6 *References*

[1] A. J. Percy, M. Rey, K. M. Burns, D. C. Schriemer, *Anal. Chim. Acta* **2012**, *721*, 7–21.

[2] A. Thomas, S. Deshayes, M. Decaffmeyer, M. H. Van Eyck, B. Charloteaux, R. Brasseur, *Proteins Struct. Funct. Bioinforma.* **2006**, *65*, 889–897.

[3] H. E. Stanger, F. A. Syud, J. F. Espinosa, I. Giriat, T. Muir, S. H. Gellman, *Proc. Natl. Acad. Sci.* **2001**, *98*, 12015–12020.

[4] R. Levenson, C. Bracken, N. Bush, D. E. Morse, *J. Biol. Chem.* **2016**, *291*, 4058–4068.

[5] R. Levenson, C. Bracken, C. Sharma, J. Santos, C. Arata, B. Malady, D. E. Morse1, *J. Biol. Chem.* **2019**, *294*, 16804–16815.

[6] S.-P. Liang, R. Levenson, B. Malady, M. J. Gordon, D. E. Morse, L. Sepunaru, *J. R. Soc. Interface* **2020**, *17*, 20200774.

[7] B. Fierz, A. Reiner, T. Kiefhaber, *Proc. Natl. Acad. Sci.* **2009**, *106*, 1057–1062.

[8] B. Fierz, T. Kiefhaber, *J. Am. Chem. Soc.* **2007**, *129*, 672–679.

[9] F. Eker, K. Griebenow, R. Schweitzer-Stenner, *J. Am. Chem. Soc.* **2003**, *125*, 8178–8185.

[10] W. L. Mattice, W. H. Harrison, *Biopolymers* **1975**, *14*, 2025–2033.

[11] Y. Bai, J. S. Milne, L. Mayne, S. W. Englander, *Proteins Struct. Funct. Genet.* **1993**, *17*, 75–86.

[12] R. Townend, T. F. Kumosinski, S. N. Timasheff, G. D. Fasman, B. Davidson, *Biochem. Biophys. Res. Commun.* **1966**, *23*, 163–169.

[13] N. J. Greenfield, G. D. Fasman, *Biochemistry* **1969**, *8*, 4108–4116.

[14] W. Moffitt, *Proc. Natl. Acad. Sci.* **1956**, *42*, 736–746.

[15] P. K. Sarkar, P. Doty, *Proc. Natl. Acad. Sci.* **1966**, *55*, 981–989.

[16] S. Polling, A. R. Ormsby, R. J. Wood, K. Lee, C. Shoubridge, J. N. Hughes, P. Q. Thomas, M. D. W. Griffin, A. F. Hill, Q. Bowden, T. Böcking, D. M. Hatters, *Nat. Struct. Mol. Biol.* **2015**, *22*, 1008–1015.

[17] K. Rosenheck, P. Doty, *Proc. Natl. Acad. Sci.* **1961**, *47*, 1775–1785.

[18] A. Mirtič, J. Grdadolnik, *Biophys. Chem.* **2013**, *175–176*, 47–53.

[19] W. Dzwolak, R. Ravindra, C. Nicolini, R. Jansen, R. Winter, *J. Am. Chem. Soc.* **2004**, *126*, 3762–3768.

[20] W. Dzwolak, V. Smirnovas, *Biophys. Chem.* **2005**, *115*, 49–54.

[21] P. C. Painter, J. L. Koenig, *Biopolymers* **1976**, *15*, 229–240.

[22] Allen J. Bard, L. R. Faulkner, *Electrochemical Methods: Fundamentals and Applications*, Wiley, New York, **2000**.

[23] R. O. Ebewele, *Polymer Science and Technology*, CRC Press, **2000**.

[24] K. Haydukivska, V. Blavatska, J. Paturej, *Sci. Rep.* **2020**, *10*, 14127.

[25] S. Y. Lau, A. K. Taneja, R. S. Hodges, *J. Biol. Chem.* **1984**, *259*, 13253–13261.

[26] C. Park, W. A. Goddard, *J. Phys. Chem. B* **2000**, *104*, 7784–7789.

[27] S. Cai, T. Bai, H. Chen, W. Fang, Z. Xu, H. Lai, T. Huang, H. Xu, X. Chu, J. Ling, C. Gao, *J. Phys. Chem. Lett.* **2020**, *11*, 303–310.

[28] S. S. Stadmiller, G. J. Pielak, *Protein Sci.* **2018**, *27*, 1710–1716.

[29] W. T. Simpson, D. L. Peterson, *J. Chem. Phys.* **1957**, *26*, 588–593.

[30] A. R. Ubbelohde, K. J. Gallagher, *Acta Crystallogr.* **1955**, *8*, 71–83.

[31] M. Calvin, J. Hermans, H. A. Scheraga, *J. Am. Chem. Soc.* **1959**, *81*, 5048–5050.

Chapter 5

Dynamics of Electrochemically Triggered Reflectin Assembly

Adapter from: S.-P. Liang, R. Levenson, B. Malady, M. J. Gordon, D. E. Morse, L. Sepunaru, *J. R. Soc. Interface* **2020**, *17*, 20200774.[1]

5.1 *Overview*

In this chapter, site-selective electrochemical deprotonation was applied to reflectin protein to explore the possibility of using electrochemistry to trigger protein assembly. As will be detailed in the following section, reflectin can dynamically assemble into various sizes in response to the protonation state of its histidine residues. This characteristic was exploited to demonstrate how electrochemistry can resolve the redox potential of dissociable protons in a natural protein, and further trigger protein assembly. The work here follows the protocol developed in Chapter 4 where voltammetry was first used to resolve the redox behavior of reflectin, and *in situ* spectroscopies were then used to determine the outcome of site-selective electrochemical deprotonation. A novel approach, namely, droplet electrochemistry, was specifically developed to utilize less material without immobilizing them on an electrode surface, which may influence their behavior. In addition to *in situ* circular dichroism introduced in the last chapter, *in situ* dynamic light scattering was also developed to analyze reflectin assembly, since light scattering is extremely sensitive to particle size, and thus an excellent matric to observe reflectin assembly during site-selective electrochemical deprotonation.

5.2 *Tuning Coulombic Interactions in Reflectin in vitro via Charge-neutralization*

Enzymatically catalyzed phosphorylation is one of the most ancient and universally distributed mechanisms of biological signal transduction, regulating the structure, hierarchical assembly and function of proteins in response to a wide range of neuronal, hormonal and environmental triggers [2,3]. While several molecular mechanisms may govern this regulation, the phosphorylation of cationic protein domains most commonly acts via charge neutralization. This effect can be mimicked by pH-titration or genetic engineering, as seen in the case of the complex protein reflectin A1[4,5]. This cationic, intrinsically disordered block-copolymer-like protein mediates the neuronally controlled fine-tuning of color reflected from the intracellular Bragg lamellae in squid skin for camouflage and communication[5–7]. *In vivo*, progressive charge-neutralization by neuronally activated phosphorylation overcomes Coulombic repulsion of reflectin's cationic domains, driving condensation, folding, and hierarchical assembly, resulting in osmotic dehydration of the reflectin-containing Bragg lamellae. This reversible dehydration, in turn, modifies the lamellar spacing and effective refractive indices, leading to a change in reflected color[8,9]. *In vitro*, neutralization of charges in the protein's histidine residues by pH titration or salt titration act as a surrogates for the charge-neutralization by phosphorylation *in vivo,* driving reflectin assembly [4,5]. As can be seen in

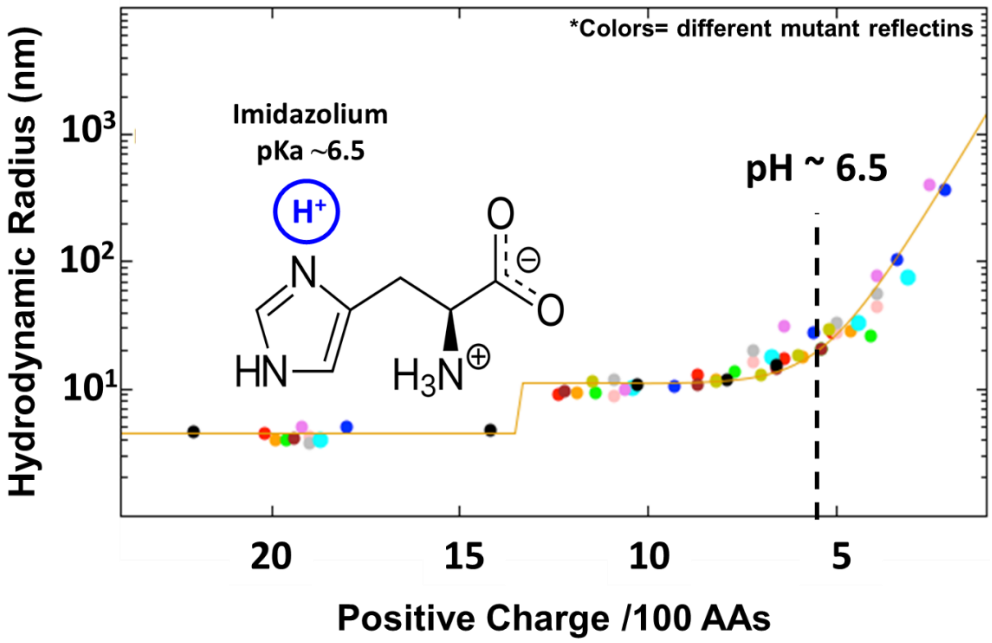

Figure 5.1. pH titration curve of hydrodynamic radius of reflectin measured by dynamic light scattering showing the pH dependent, size-tunable reflectin assembly (reproduced from Levenson et al., **2019** [5]). The colors represent different mutants of reflectin. All the curves are normalized to the estimated number of positive charges on reflectin to facilitate comparison.

Unique among the cationic amino acids in proteins, the pKa of histidine's imidazolium sidechain lies in the physiological range of pH, enabling its tunable ionization to control the structures, interactions and activities of many proteins.[10] Examples include the catalytic triads of hydrolases[11], other enzymatic proton shuttles,[12] and conformational changes and/or assembly (e.g., in firefly luciferase[13], viral hemagglutinin[14] and reflectin[5]). In Chapter 3, the imidazolium of histidine in the monomeric state, and in oligopeptides in solution were shown to be directly deprotonated under acidic conditions on a platinum electrode at a formal reduction potential that was clearly distinguishable from those of hydronium and the terminal primary amine. In the following sections, voltammetry was used to further demonstrate that, in the case of the histidine-rich reflectin protein, transitory contact of freely diffusing reflectin

with an appropriately biased platinum electrode is shown to reduce the protonated imidazolium sidechains of histidine residues in the protein, driving its assembly as an *in vitro* surrogate for the protein's charge-neutralization by phosphorylation *in vivo.*

5.3 ***Methods***

5.3.1 Reflectin A1 expression and purification

Recombinant Doryteuthis opalescens reflectin A1 was synthesized from a recombinant DNA construct and purified by methods described previously [4,5]. Briefly, Rosetta 2 (DE3) E.coli cells were grown in liquid cultures from freshly plated transformants in the presence of 50 mg ml^{-1} kanamycin to maintain selection of the recombinant DNA plasmid. Expression was induced in the logarithmic growth phase by addition of 1 mM isopropylthioglactoside. Expression proceeded for approximately 6 h, after which cells were centrifuged and frozen at − 80 °C. Reflectin A1 inclusion bodies then were purified from thawed cell pellets with BugBuster medium (Novagen, Inc., Madison, WI, USA), as directed by the manufacturer. Inclusion bodies were solubilized in 5% acetic acid/8 M urea. Reflectin was purified initially by ion exchange over a HiTrap XL (GE Healthcare) cation exchange column eluted with a gradient of 5% acetic acid/6 M guanidinium chloride. Fractions containing reflectin were collected and diluted in 5% acetic acid/8 M urea, concentrated by centrifugal filtration and loaded onto a HPLC reverse-phase C10 column equilibrated with 0.1% aqueous trifluoracetic acid and eluted with a gradient of 95% acetonitrile/0.1% TFA. The resulting purified protein was lyophilized and stored at −80 °C until solubilization for use. Purity was confirmed by SDS-PAGE on 10% tris-acetate SDS-PAGE gels (Life Sciences, Carlsbad, CA, USA).

5.3.2 Protein solubilization and sample preparation

Lyophilized reflectin A1 was solubilized by the addition of 0.22 μm-filtered 25 mM sodium acetate, pH 4.5 buffer. Concentration was determined by measuring absorbance (A280) using a calculated extinction coefficient of 120,685 l mol^{-1} cm^{-1} [15]. For electrochemical measurements in buffered solution, the protein was dialysed 1000-fold three times against buffer solution (with pH and chemical composition as described) to remove unwanted counter ions from protein purification. For measurements in unbuffered solutions, samples were initially dialysed into 25 mM sodium acetate, pH 4.5 as above, and then further dialysed 1000-fold three times into an unbuffered solution, with final pH adjusted with perchloric acid. Final pH after dialysis was confirmed in all cases with a pH meter. Protein was stored at 4°C and filtered through a 0.1 μm syringe filter shortly before use. DLS and TEM were used to confirm the monomeric state of the protein at the start of all experiments[4,5].

5.3.3 Cyclic voltammetry measurements

Electrochemical measurements using Autolab M204 electrochemical workstation were done in a three-electrode configuration (working electrode: Pt disk; counter electrode: Pt wire; reference electrode: fritted Ag/AgCl in 1 M $KCl_{(aq)}$ or SCE. The potential difference between SCE and AgCl (in 1 M $KCl_{(aq)}$) was experimentally determined to be +7.0 mV. The Pt disc working electrode (R_{Pt} = 1.5 mm) was polished three times (2 min each) using 1 μm, 0.25 μm and then 0.05 μm MetaDiTM polycrystalline diamond suspension (Buehler, Lake Bluff, IL, USA) on a microcloth polishing pad. The polished working electrode was then sonicated in water for 2 min. CV measurements were done at a scan rate of 100 mV s^{-1}.

5.3.4 Differential pulse voltammetry measurements

All DPV measurements were done in a miniaturized three-electrode configuration with the Pt electrode prepared via an identical polishing protocol as described above. In this series of experiments, the electrochemical 'cell' was a 10 µl droplet of analyte solution on the Pt disc electrode pointed upward. A Pt wire counter electrode was inserted between the working and reference electrode. DPV measurements were done with a potential step size of 5 mV, pulse height of 10 mV, pulse duration of 50 ms and interval time of 0.5 s.

5.3.5 Constant potential electrochemistry with in situ dynamic light scattering

Constant potential electrochemical measurements were carried out in a three-electrode configuration (working electrode: Pt coil; counter electrode: Pt wire; reference electrode: Ag/AgCl) with an Autolab M204 electrochemical workstation (Metrohm). The three electrodes were assembled in a DLS compatible optical cuvette and sealed with parafilm to prevent dust from the surroundings. DLS was performed with a Malvern Zetasizer Nano ZS (Worcestershire). The samples were probed with a 632.8 nm HeNe gas laser with a beam diameter of 0.63 mm ($1/e^2$) and detected by an Avalanche photodiode (Q.E. greater than 50% at 633 nm) in a back-scattering configuration at 7° from normal. The measurements were done with 2 ml sample volumes at 25°C (see main text for the applied potentials). All samples were measured at OCP for at least 30 min to ensure signal stability over time.

5.3.6 Transmission electron microscopy

Electrochemically driven reflectin A1 assemblies and their parallel controls were collected straight from the DLS cuvette (before and after applying −750 mV for 30 min) in the vicinity of the working electrode with micropipette and directly applied to 400-mesh carbon-coated grids (Electron Microscopy Services, Hatfield PA). Prior to sample application, grids were treated by glow discharge for 20 s. Five microlitres of freshly prepared sample was applied for 2 min before wicking away excess solution with filter paper. Samples were then negatively stained by application of 20 µl freshly filtered 1.5% uranyl acetate three times, with wicking in between each application. Samples were examined in a 200 kV ThermoFisher Talos G2 TEM in bright field mode.

5.3.7 Titrations

Titration experiments were done by monitoring pH while gradually adding 2.5 M NaOH in 100 mM of pH 2 analyte solution. The pH of the analyte solution was adjusted with perchloric acid. pH was monitored with a pH meter (Fisher Scientific, Accumet Basic 150).

5.4 *Results and Discussion*

5.4.1 Electrochemistry in a Droplet

Sensing electrochemical signal of aqueous biomolecules at catalytic platinum surface can be challenging due to the intrinsic high background noise from electrochemical characteristics, and the low signal from material characteristics and availability. Platinum (Pt) is catalytic for hydrogen evolution reactions, which involve the electrochemical reduction of hydronium (H_3O^+) and water (H_2O). As showed in Figure 5.2, differential pulse voltammetry at a Pt surface in an acidic aqueous environment has high background noise on the order of 100 pA, which sets the qualitative detection limit of this system to be 300 pA when a signal-to-noise-ratio of 3 is considered. On the other hand, the electrochemical redox current (i) often follows the relation:

$$i \propto n\sqrt{D}c \qquad (5.1)$$

where "n" is the number of charges transferred, "D" is the mass diffusivity of the redox active species, and "c" is the concentration of analytes. Reflectin has mass diffusivity of ~ 3 x 10^{-12} m^2/sec (measured by dynamic light scattering) and 30 protonated histidine residues. Using histidine amino acid as a reference[16], one can estimate the redox current from reflectin to be around 50 nA/mM of reflectin per proton transferred. In an ideal case where all the 30 protons participate in the electrochemical reaction, the minimum amount of reflectin required for a single electrochemical analysis would equal to at least all the reflectin available for one week of synthesis (5-10 mg). Considering the minimum amount of reflectin required for an analysis, only low signal could be obtained in a conventional small electrochemical cell that requires more than 2.5 mL of solution.

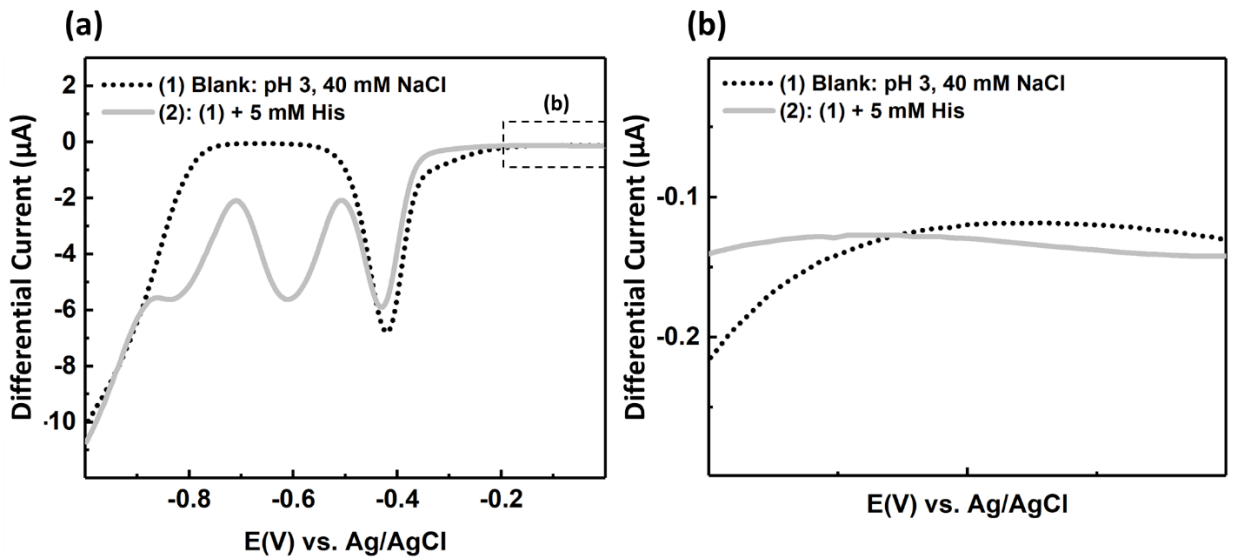

Figure 5.2. A demonstration of the magnitude of background current via (a) differential pulse voltammograms of pH 3, 40 mM NaCl with and without 5 mM of Histidine, and (b) a zoom-in view of the non-faradaic region.

A droplet electrochemistry configuration was developed to realize economical and reliable electrochemical analysis of biomolecules. As has been stated in the previous paragraph, concentration is the only variable to tune the redox signal in voltammetry of reflectin and is limited by the yield of reflectin synthesis. Reducing the volume of electrochemical analysis with a limited amount of available reflectin became necessary to enrich reflectin concentration. As showed in Figure 5.3, a Pt disk electrode is reversed to serve as both the sample substrate and the working electrode, and the reference electrode and platinum wire counter electrode are arranged around the droplet to complete the circuit. To retain the integrity of a voltammetry experiment, diffusion layers at the cathode and the anode need to be separated to prevent shorting of the circuit, which sets the minimum size of a voltammetry experiment to be the sum of cathodic and anodic diffusion layer thickness. The upper limit diffusion layer thickness can be estimated with the following equation [17]:

$$\delta < 6\sqrt{Dt} \qquad (5.2)$$

where D is the mass diffusivity of the redox active species and t is the total amount time the redox overpotential is applied. Since a proton has the highest mass diffusivity (9 x 10^{-8} m^2/s [18]) among all species in an aqueous environment, by considering the voltammetry time scale of around 100 sec, the diffusion layer thickness of all species should be contained within 500 μm from the electrode surface, which indicates that in theory a voltammetry can be performed as long as the counter and working electrodes are 1 mm apart. The droplet electrochemistry reduces the experiment size by more than 100 folds, which enables enriching the concentration of biological sample by more than 100 times.

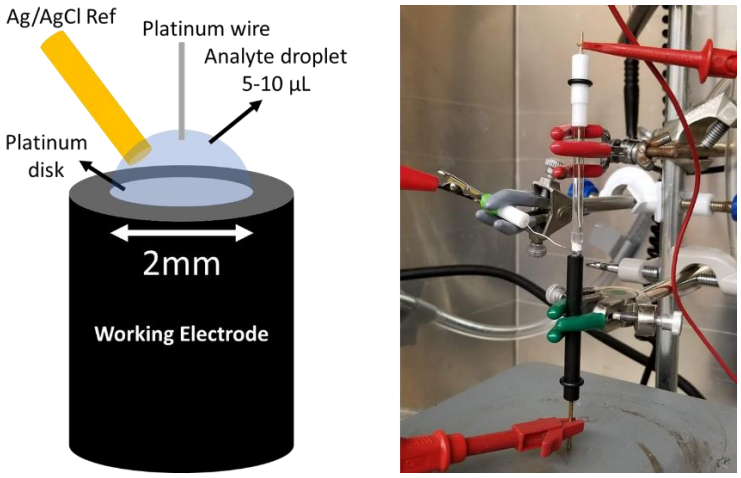

Figure 5.3. Illustration and photograph of electrode configuration for droplet electrochemistry.

5.4.2 Direct Electrochemical Deprotonation of Reflectin

Direct electrochemical deprotonation of reflectin was verified via performing the approach introduced in Chapter 3 to analyze amino acids in the microdroplet. All the samples were adjusted to pH 3 in 40 mM NaCl to ensure a dominant population of imidazolium, while maintaining electrolyte support. The resulting DPV of His shows three clear reduction waves (Figure 5.4a). As have been shown in Chapter 3, the reduction wave peaking at -450 mV corresponds to the aqueous solvent's hydronium proton reduction. Because we confirmed that the reduction potentials of the protonated amino acid moieties are correlated with their pKa values (Chapter 3), we can assign the reduction wave peaking at -600 mV to the deprotonation of imidazolium, and the shoulder near -770 mV to deprotonation of the terminal amine. In Gly-Gly-Gly, investigated as a control tripeptide with non-titratable side chains (cf. Figure 5.4b), the reduction wave peaking at -450 mV reflects hydronium reduction, while the reduction wave peaking at -720 mV corresponds to deprotonation of the terminal amine, as illustrated in Chapter 3 (Figure 3.1). Similar to Gly-Gly-Gly, Gly-Gly-His also shows two waves: the hydronium reduction wave peak at -450 mV and a broad wave between -600 and -800 mV. Comparison of the molecular structures of the tripeptides (Figure 5.4b) indicates that Gly-Gly-His at pH 3 will have an extra protonated imidazolium moiety in addition to the protonated terminal amine. We thus attribute the broad peak of Gly-Gly-His to the overlap of two redox waves, namely the terminal amine and the imidazolium. Shifts in the reduction potentials of protons on the Gly and His residues in the two tripeptides are associated with shifts in local pKa values due to the chemical environment in the tripeptide, an effect that has been documented[19–23] and seen in other pH titration experiments (See Appendix in Section 3.6).

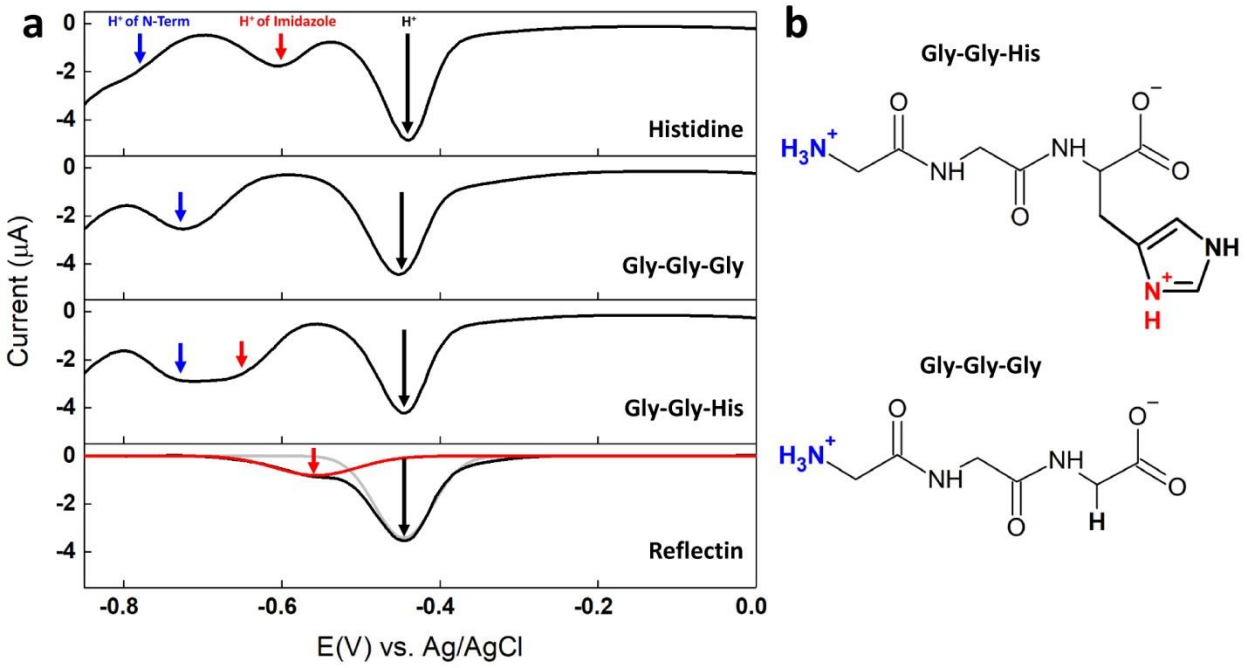

Figure 5.4. (a) Differential pulse voltammograms (DPVs in 40 mM NaCl at pH 3, measured vs. Ag/AgCl) for 1 mM histidine, 2 mM tripeptide H-glycine-glycine-glycine-OH (Gly-Gly-Gly), 2 mM tripeptide H-glycine-glycine-histidine-OH (Gly-Gly-His), and 25μM reflectin protein. The reflectin DPV was baseline subtracted for peak deconvolution (red = imidazolium; grey = hydronium). Arrows show the evolution of DPV peak potential for the designated electrochemically active imidazolium NH^+ (red) and terminal amine (NH_3^+, blue), as represented in (b). (b) Molecular structures of Gly-Gly-His and Gly-Gly-Gly tripeptides, with imidazolium and terminal amine protonation sites colored in red and blue, respectively.

The aforementioned experiments demonstrate that the imidazolium of histidine, in freely diffusing form or in a peptide, can be electrochemically deprotonated; as such, we next sought to see if this phenomenon could be extended to histidines contained within a macromolecular protein. We successfully demonstrated this effect with reflectin, the histidine-rich (31 His / 350 AAs) protein that functions as a sensitive transducer of neuronal signals governing the dynamic changes in skin color for camouflage and communication in squids[7]. Reflectin was

chosen for this test because recently it was shown that its biological activity is mediated by charge neutralization-driven assembly to form large multimers, and that pH-titration of its histidine residues can be used as an *in vitro* surrogate for the neurotransmitter-mediated phosphorylation that triggers this assembly *in vivo* [4,5]. This assembly effect thus provides a sensitive measure of histidine deprotonation within the protein. Additionally, reflectin monomers at low pH are known to be intrinsically disordered[5], indicating that many of its amino acids are likely exposed to the solvent, and therefore accessible for direct electrochemical reduction with a Pt electrode.

The DPV of reflectin (Figure 5.4) exhibits a large reduction wave at ca. -450 mV (vs. Ag/AgCl) corresponding to hydronium reduction (for the solvent at pH 3), with a pronounced shoulder at -550 to -650 mV that becomes more apparent upon deconvolution (red curve). This shoulder and its resolved peak clearly occur in the range of imidazolium reduction (-500 to -700 mV) as seen in the previous data in Figure 5.1 and 5.Figure 5.2, with the observed variation in reduction wave width for reflectin being attributable to differences in pKa for multiple histidine residues in the protein that depend on the local sequence environment. The presence of this reduction wave for reflectin, and its corresponding thermodynamic equivalency with the freely diffusing histidine, indicates that direct charge exchange occurs between the imidazolium sidechains in reflectin and the Pt electrode. This observation of selective electrochemical reduction of cationic histidine residues in the protein is mechanistically distinct from earlier reflectin thin film work demonstrating that anionic amino acids in the native sequence of wild-type reflectin in the solid state can act as a conducting proton ‘shuttle’ under high humidity (> 70% relative humidity) conditions[24].

5.3.3 in situ Dynamic Light Scattering for Electrochemistry-driven Reflectin Assembly

The hypothesis of direct charge exchange mechanism involving imidazolium sidechains was further confirmed via monitoring reflectin sizes *in situ* with dynamic light scattering (DLS, Figure 5.5) and *ex situ* with transmission electron microscope (TEM) (Figure 5.6). By combining electrochemistry with DLS to measure the apparent size-distributions of reflectins within the domain of a Pt coil electrode (Figure 5.5b), we observed no change in the size of reflectin monomers under open circuit potential (OCP), as well as after 20 min application of -475 mV (vs. Ag/AgCl), a potential sufficient to reduce only the hydronium ion (Figure 5.5c, d). At this low potential, only free hydronium would be reduced, gradually changing the solution pH near the electrode surface; apparently, the limitation of this effect by diffusion makes it ineffective in driving assembly. In marked contrast, dramatic, time-dependent assembly of reflectin is triggered by application of -700 mV, which was shown above (cf. Figure 5.4) to be sufficient to reduce the imidazolium of histidine in various states.

Since the intensity of Rayleigh scattering scales with particle radius[25], the back-scattered photon count rate from the DLS photodetector was used to directly measure reflectin assembly (particle formation) as time progressed (Figure 5.5c). Decay of the autocorrelation function of the scattering allows determination of particle diffusivity [26], and from this, via the Stokes-Einstein relation, the size-distribution of the particles' effective hydrodynamic diameters (Figure 5.5d). To gain deeper insight into the electro-assembly process, the reflectin particle size distributions were analyzed at six time points (Figure 5.5c, d). At time (i), analyses at all potentials show similar count rates, with size distributions of particles in all samples showing the approximate diameter of the reflectin monomer (ca. 10 nm). At time (ii), the -700 mV (green curve) sample exhibited a bimodal size distribution, while all other samples remained

as monomers. With progressively longer times, the size distributions of particles in the - 700 mV sample increased steadily until reaching a plateau (~ 70 nm) after ca. 10-15 min.

The results shown in Figures 3c and d are especially interesting because they appear to differ from those obtained when reflectin assembly is driven by a pH jump, change in ionic strength or genetic engineering[4,5,27]. All methods trigger assembly by charge-neutralization or screening, but unlike the bulk process seen conventionally, electrochemical reduction inherently requires mass transport of reflectin to and from the electrode, as well as multiple $His^+ \rightarrow$ His turnovers, resulting in more gradual and controllable change in assembly size. The latter may therefore offer a unique possibility using electrochemistry to isolate early and potentially never-before-analyzed intermediates in the assembly of proteins.

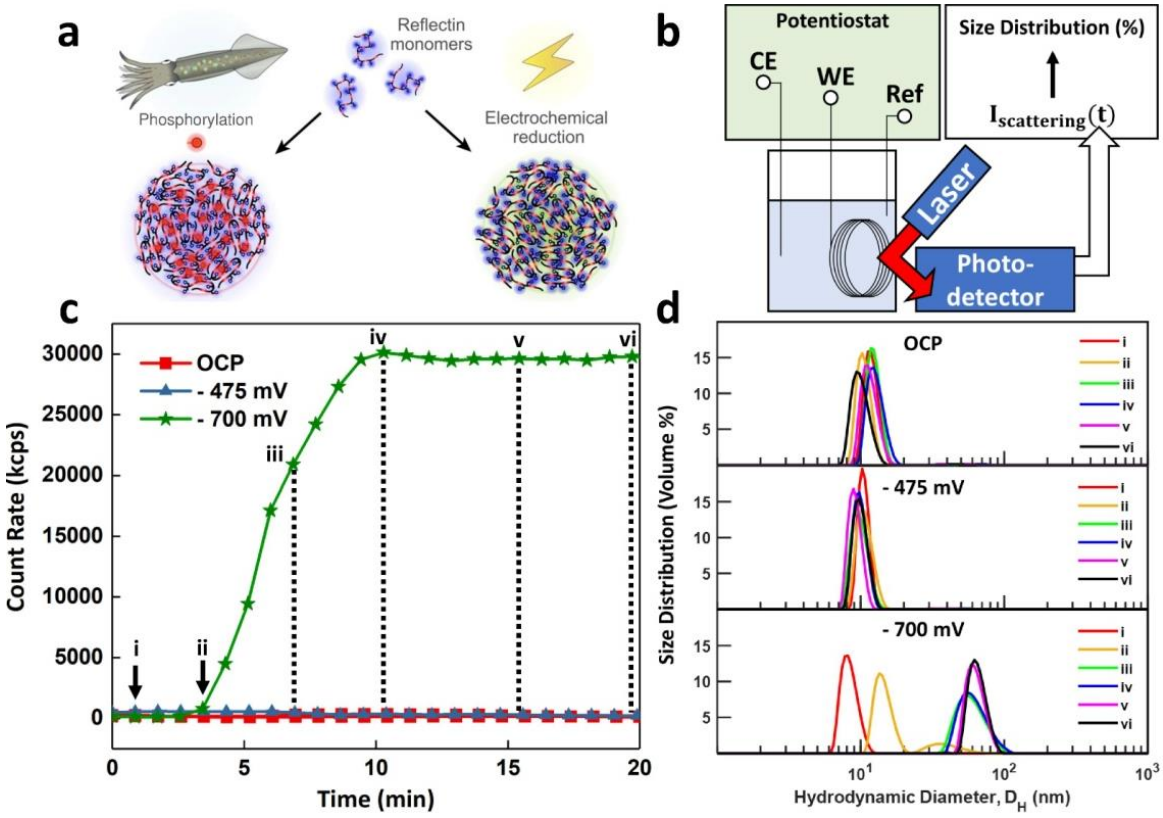

Figure 5.5. Electrochemical assembly of reflectin protein. (a) In the squid, a neurotransmitter triggers enzymatic phosphorylation, neutralizing reflectin and driving its condensation, folding and assembly[6]. In vitro, electrochemical reduction of histidine imidazolium postulated to act analogously to pH-titration, neutralizing the protein and driving assembly. (b) Experimental setup to electrochemically trigger reflectin assembly with in situ DLS. (c) Reflectin DLS intensity (count rate) for open circuit potential (OCP, red), -475 mV (blue), and -700 mV (green) conditions with respect to Ag/AgCl. (d) Reflectin particle size distributions (volume %) measured by DLS at times (i-vi) indicated in (c). Reflectin monomer D_H = 8-12 nm.

Results of the DPV and DLS analyses of reflectin were further confirmed by TEM (Figure 5.6). In the sample analyzed under OCP conditions, only reflectin monomers (D < 15 nm) were seen, whereas the sample exposed to -700 mV for 30 min contained significantly larger particles (D = 40-70 nm), further supporting our electrochemical spectroscopy results.

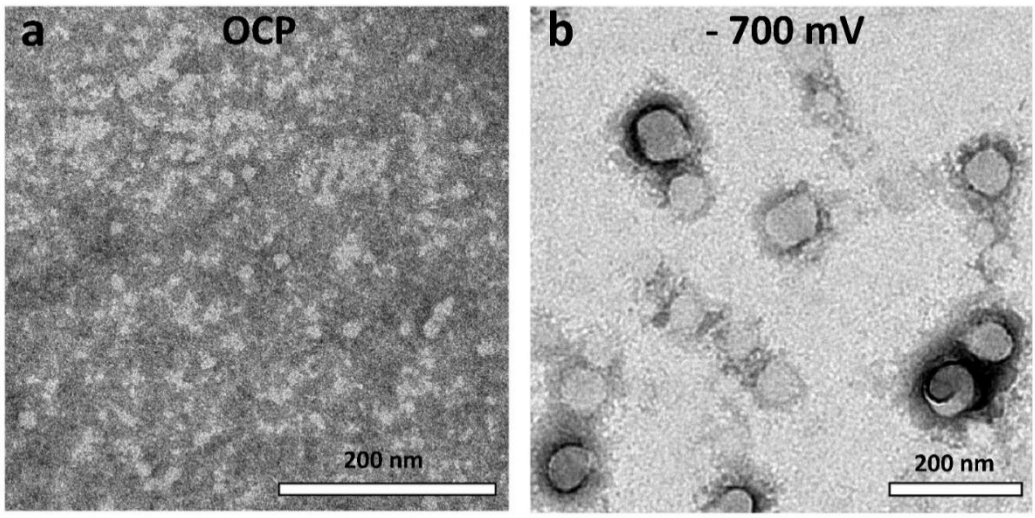

Figure 5.6. Transmission electron microscopy (TEM) images of aliquots of reflectin (pH 3, 40 mM NaCl): (a) before any bias was applied (OCP, open circuit potential); (b) after -700 mV vs. Ag/AgCl had been applied for 30 min. Samples were collected from the center of the DLS/Pt coil as shown in Figure 5.3b.

5.3.5 in situ Circular Dichroism for Electrochemically triggered Pre-assembly Reflectin

One main question associated with the mechanism of reflectin assembly is the existence of intermediate, pre-assembly states where reflectin monomers were oriented into a specific conformation prior assembly. The investigation of this question is especially challenging due to the dynamic nature of reflectin assembly, making isolation of pre-assembly reflectin impossible with traditional approaches such as pH titration. The combination of site-selective electrochemistry and chemical environment provides a plausible approach to investigate pre-assembly intermediates. As shown in Figure 5.7, although the redox potential of imidazolium

in histidine in reflectin in 10 mM NaCl at pH 3 stays the same as reflectin in 40 mM NaCl at pH 3 (Figure 5.7a), reflectin assembly did not occur when site-selective electrochemical deprotonation happened. From the work done by Levenson et al., reflectin assembly is known to be sensitive to both acidity and salinity of the environment, which was then found in the *in situ* DLS experiments to suppress (Figure 5.7) or promote (Figure 5.5) electrochemically triggered reflectin assembly. While the environment suppresses the assembly formation due to either low pH or low salt, electrochemically deprotonated reflectin is hypothesized to be kinetically "trapped" in the pre-assembly state, where the reflectin bears enough chemical pressure to assemble, but fast re-protonation prohibits reflectin from assemble. Leveraging this phenomenon with *in situ* CD, the otherwise challenging secondary structure transition of reflectin from monomeric to pre-assembly state could be probed.

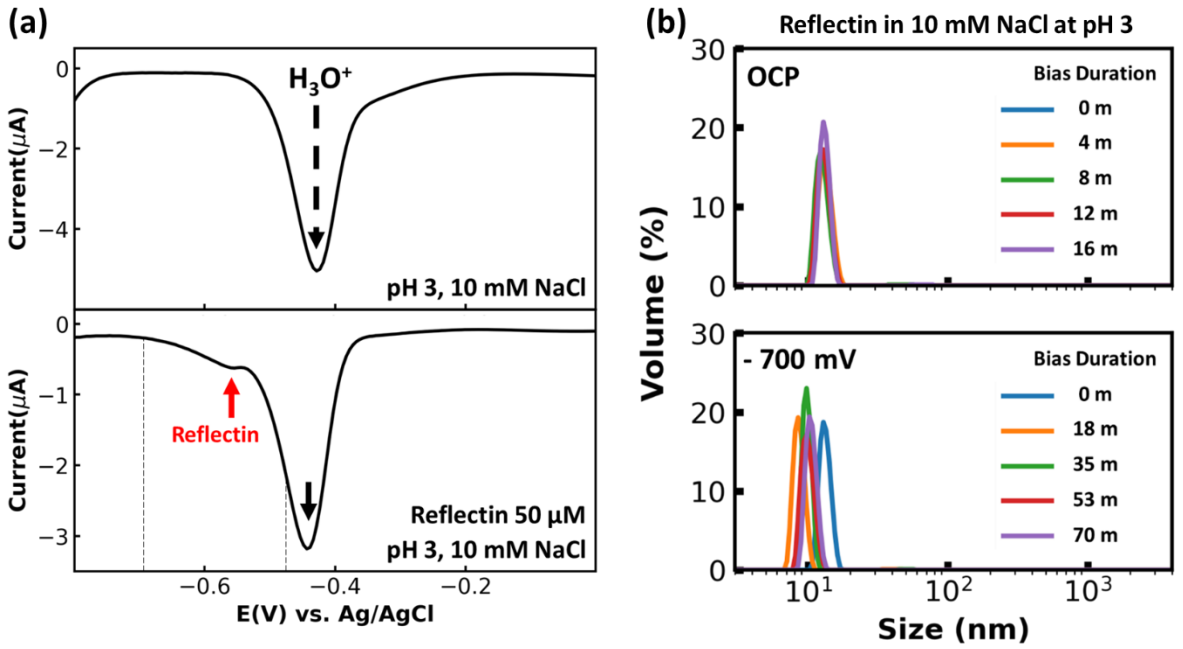

Figure 5.7. (a) DPV of 10 mM NaCl at pH 3 without (top panel) and with (bottom panel) reflectin. (b) *in situ* DLS experiments on reflectin 2 μM in 10 mM NaCl at pH 3 at OCP (top panel) and – 700 mV (bottom panel) demonstrating suppression of electrochemically tirggered reflectin assembly under salt concentration lower than threshold 40 mM NaCl. The dashed lines on the bottom of (a) highlights – 475 mV and – 700 mV.

To probe the pre-assembly, secondary structure transition of reflectin, reflectin in 10 mM NaCl at pH 3 was monitored via *in situ* CD at similar biases applied in *in situ* DLS experiments. 10 mM NaCl was chosen to stay away from the threshold 40 mM NaCl that promotes electrochemically triggered reflectin assembly, and maintain solution conductivity. As shown in Figure 5.8b, DPV was performed on reflectin in 10 mM NaCl at pH 3, and the voltammogram was similar to the one shown in Figure 5.4, indicating sufficient ionic strength with 10 mM NaCl. *in situ* CD performed at open circuit potential and – 475 mV shown similar spectra over the course of 20 mins (Figure 5.8c), indicating no secondary structure transition of reflectin. However, when – 700 mV was applied, a clear shift in the spectrum between 200 and 210 nm was observed over 20 mins, indicating the development of secondary structure without assembly. Also, when compared the CD spectrum of pH titrated refelctin (Figure 5.8b, re-produced from Levenson et al., **2019** [5]) electrochemically triggered reflectin clearly shows different ellipticity trends between random coil-like monomer and helix-like multimer, indicating that the observed optical behavior may be from an electrochemically trapped intermediate, namely, some form of pre-assembled reflectin.

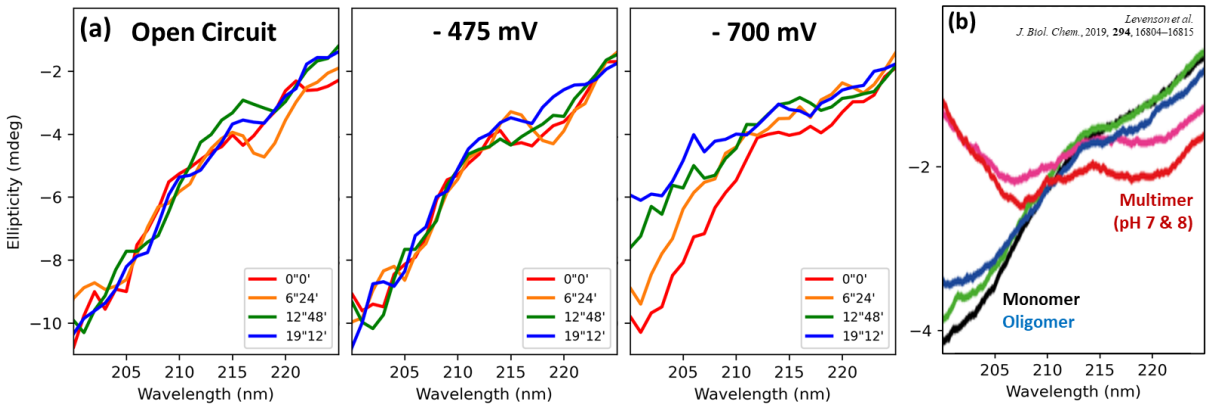

Figure 5.8. Electrochemically triggered reflectin in 10 mM NaCl at pH 3 shows evidence of pre-assembly secondary structure. (a) *in situ* CD of reflectin at open circuit potential, - 475 mV, and – 700 mV over 20 mins (times noted). (b) CD spectra of reflectin at various pH titration (reproduced with permission[5]).

The simultaneously collected *in situ* absorbance confirmed hypochromicity of pre-assembly reflectin (Figure 5.9), which further indicates the structure of pre-assembly reflectin. When – 700 mV was applied to the blank solution, no significant absorbance change was observed, indicating the amount of hydrogen evolution reaction would not generate light scattering H_2 bubbles over a span of 20 mins. No absorbance change occurred when – 475 mV was applied to the reflectin sample in 10 mM NaCl at pH 3 (Figure 5.9b, left panel), indicating no change in reflectin optical behavior at a bias lower than deprotonation potentials. However, when – 700 mV was applied, absorbance decreased by 0.25 unit (Figure 5.9b, right panel). The decreasing absorbance indicated increasingly stronger coupling between amide bonds [28–30], which further implies the formation of a rigid, helix-like structure when site-selective electrochemical deprotonation occurs. Furthermore, decreasing absorbance supports the hypothesis that the observed optical behavior is from trapped pre-assembly reflectin

monomers, because reflectin assemblies would lead to more scattering, which should increase absorbance.

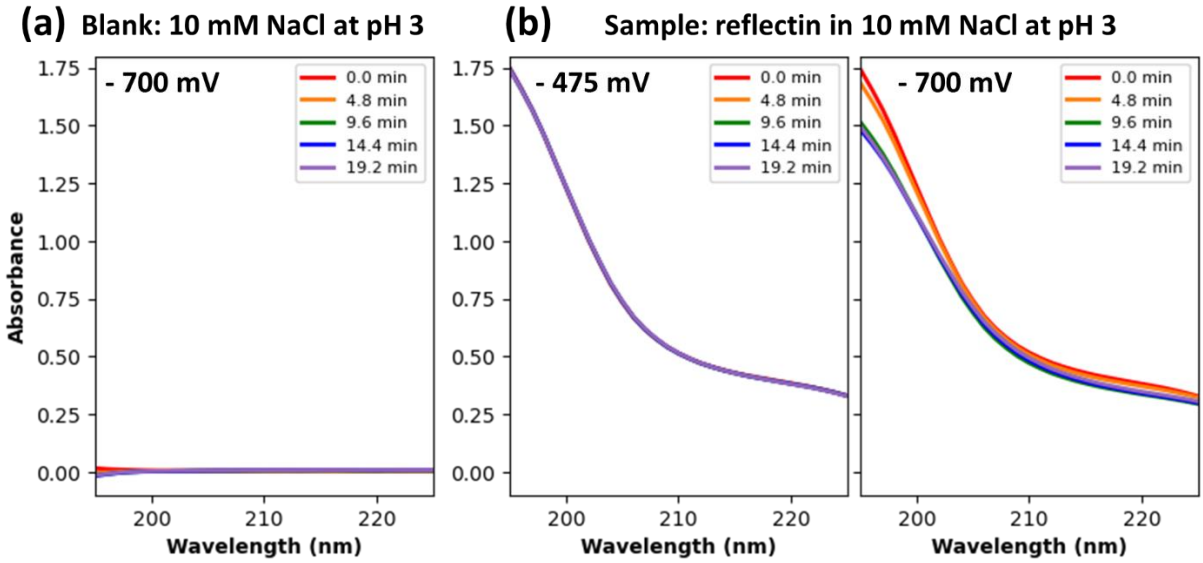

Figure 5.9. *in situ* absorbance of 10 mM NaCl at pH 3 (a) without reflectin at – 700 mV as well as (b) with reflectin at – 475 mV (b, left panel) and at – 700 mV (b, right panel).

The dynamic changes in ellipticity and absorbance at 202 nm of electrochemically triggered reflectin were also studied as shown in Figure 5.10. Absorbance at 202 nm versus the more common 195 nm was chosen due to lower fluctuations in ellipticity. Again, when – 475 mV was applied, no significant shift in ellipticity nor absorbance were observed. However, when – 700 mV was applied, continuous shifts in both ellipticity and absorbance indicated that the dynamic structural transition of pre-assembly reflectin occurs in roughly three stages. In stage 1 (0-5 min), no transition was observed. However, in stage 2 (5-10 min), the ellipticity and absorbance both change dramatically, followed by saturation (or slow change) in stage 3 (10-20 min), but only when the bias was – 700 mV (above the deprotonation threshold). Though further investigation is needed, the surprisingly consistent time horizons between *in*

situ DLS (Figure 5.5c), *in situ* CD, and *in situ* absorbance (Figure 5.10) have suggested the possibility of progressive structural transitions of reflectin at different hierarchical structures.

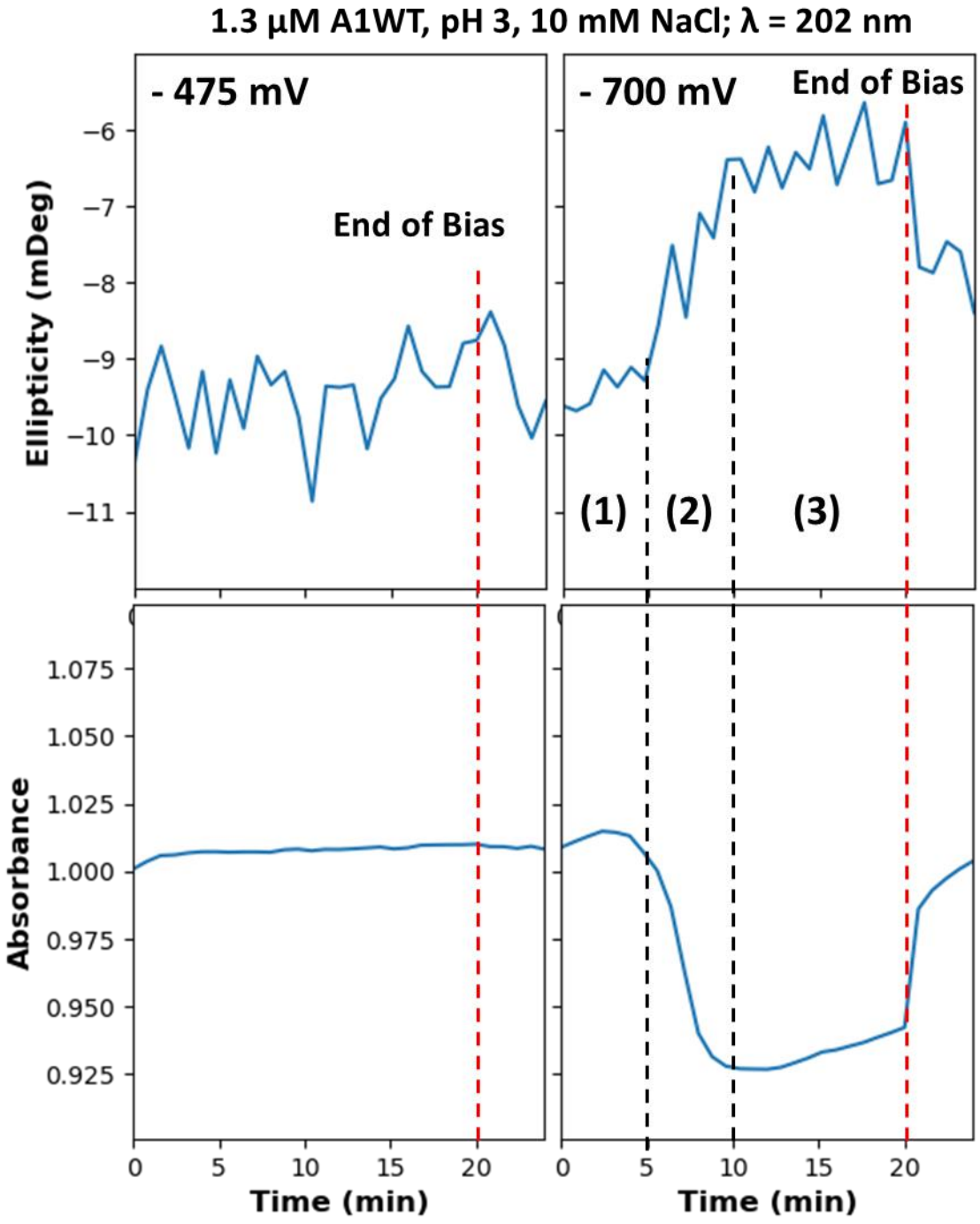

Figure 5.10. Time dependence of ellipticity (top panels) and absorbance (bottom panels) of reflectin in 10 mM NaCl, pH 3 monitored at 202 nm under – 475 mV (left panels) and -700

mV (right panels). At – 700 mV (right panels), the black dashed line highlights the boundary between the three stages. The red dashed lines on the plots for both biases indicates the end of bias (t = 20 min).

5.5 *Summary*

Bentley et al.[31] reported that the protons of acidic amines can be directly reduced at platinum electrodes with reduction potentials correlated with their pKa values. This observation suggests that electrochemistry can be used to selectively target the deprotonation of specific amino acid residues within proteins. Histidine residues are ideal targets for this because their sidechain has the lowest pKa of all positively charged AAs. Accordingly, we have shown that the imidazolium of histidine in the monomeric state, in oligopeptides and in proteins in solution can be directly deprotonated under acidic conditions on a platinum electrode, at a formal reduction potential that is clearly distinguishable from those of the hydronium cation and terminal primary amine. Cyclic and differential pulse voltammetry clearly showed that the formal reduction potentials of these protonated moieties correlated well with their respective pKa values. The relatively low electrochemical reduction potentials observed make this method especially useful for the biophysical analysis of proteins. Specific electroreduction of imidazolium moieties in the His-rich protein, reflectin, revealed variations in pKa sensitive to local environments in the protein, and led to the unprecedented discovery that assembly could be manipulated electrochemically by charge neutralization of amino acid side chains.

These findings demonstrate that electrochemistry can be used to probe protein thermodynamics and manipulate protein net charge, opening a new approach to unravel the mechanisms governing protein assembly as well as control the assembly processes that are of fundamental importance in normal physiology and degenerative diseases. For example, the direct, site specific electroreduction of reflectin presented herein acts as a surrogate for its physiological phosphorylation. Moreover, the possibility to isolate early intermediates in

protein assembly using electrochemistry suggests that it may be useful in analyzing never-before-seen early intermediates in charge-mediated regulation of protein structure and function, including, for example, the phosphorylation-driven assembly of amyloid proteins associated with Alzheimer's and Parkinson's diseases[2,32]).

5.6 *References*

[1] S.-P. Liang, R. Levenson, B. Malady, M. J. Gordon, D. E. Morse, L. Sepunaru, *J. R. Soc. Interface* **2020**, *17*, 20200774.

[2] F.-X. Theillet, A. Binolfi, T. Frembgen-Kesner, K. Hingorani, M. Sarkar, C. Kyne, C. Li, P. B. Crowley, L. Gierasch, G. J. Pielak, A. H. Elcock, A. Gershenson, P. Selenko, *Chem. Rev.* **2014**, *114*, 6661–6714.

[3] H. Nishi, A. Shaytan, A. R. Panchenko, *Front. Genet.* **2014**, *5*, 270.

[4] R. Levenson, C. Bracken, N. Bush, D. E. Morse, *J. Biol. Chem.* **2016**, *291*, 4058–4068.

[5] R. Levenson, C. Bracken, C. Sharma, J. Santos, C. Arata, B. Malady, D. E. Morse1, *J. Biol. Chem.* **2019**, *294*, 16804–16815.

[6] M. Izumi, A. M. Sweeney, D. DeMartini, J. C. Weaver, M. L. Powers, A. Tao, T. V. Silvas, R. M. Kramer, W. J. Crookes-Goodson, L. M. Mäthger, R. R. Naik, R. T. Hanlon, D. E. Morse, *J. R. Soc. Interface* **2010**, *7*, 549–560.

[7] L. M. Mäthger, E. J. Denton, N. J. Marshall, R. T. Hanlon, *J. R. Soc. Interface* **2009**, *6*, S149–S163.

[8] D. G. DeMartini, D. V. Krogstad, D. E. Morse, *Proc. Natl. Acad. Sci.* **2013**, *110*, 2552–2556.

[9] A. Ghoshal, D. G. DeMartini, E. Eck, D. E. Morse, *J. R. Soc. Interface* **2013**, *10*, 20130386.

[10] S. M. Liao, Q. S. Du, J. Z. Meng, Z. W. Pang, R. B. Huang, *Chem. Cent. J.* **2013**, *7*, 44.

[11] G. Dodson, *Trends Biochem. Sci.* **1998**, *23*, 347–352.

[12] W. W. Bachovchin, J. D. Roberts, *J. Am. Chem. Soc.* **1978**, *100*, 8041–8047.

[13] B. R. Branchini, R. A. Magyar, M. H. Murtiashaw, S. M. Anderson, M. Zimmer,

Biochemistry **1998**, *37*, 15311–15319.

[14] C. M. Mair, T. Meyer, K. Schneider, Q. Huang, M. Veit, A. Herrmann, *J. Virol.* **2014**, *88*, 13189–13200.

[15] M. R. Wilkins, E. Gasteiger, A. Bairoch, J. C. Sanchez, K. L. Williams, R. D. Appel, D. F. Hochstrasser, *Methods Mol. Biol.* **1999**, *112*, 531–552.

[16] L. G. Longsworth, *J. Am. Chem. Soc.* **1953**, *75*, 5705–5709.

[17] A. J. Bard, L. R. Faulkner, *Electrochemical Methods: Fundamentals and Applications*, **2008**.

[18] S. A. Fischer, B. I. Dunlap, D. Gunlycke, *Chem. Sci.* **2018**, *9*, 7126–7132.

[19] D. Kohda, T. Sawada, F. Inagaki, *Biochemistry* **1991**, *30*, 4896–4900.

[20] S. Kuramitsu, K. Hamaguchi, *J. Biochem.* **1980**, *87*, 1215–1219.

[21] J. D. Forman-Kay, G. M. Clore, A. M. Gronenborn, *Biochemistry* **1992**, *31*, 3442–3452.

[22] P. R. Gooley, M. A. Keniry, R. A. Dimitrov, D. E. Marsh, D. W. Keizer, K. R. Gayler, B. R. Grant, *J. Biomol. NMR* **1998**, *12*, 523–534.

[23] S. Pahari, L. Sun, E. Alexov, *Database (Oxford).* **2019**, *2019*, DOI 10.1093/database/baz024.

[24] D. D. Ordinario, L. Phan, W. G. Walkup IV, J.-M. Jocson, E. Karshalev, N. Hüsken, A. A. Gorodetsky, *Nat. Chem.* **2014**, *6*, 596–602.

[25] J. H. Seinfeld, S. N. Pandis, *Atmospheric Chemistry and Physics*, John Wiley And Sons, Hoboken, NJ, **2006**.

[26] W. I. Goldburg, *Am. J. Phys.* **1999**, *67*, 1152–1160.

[27] A. R. Tao, D. G. DeMartini, M. Izumi, A. M. Sweeney, A. L. Holt, D. E. Morse, *Biomaterials* **2010**, *31*, 793–801.

[28] W. Moffitt, *Proc. Natl. Acad. Sci.* **1956**, *42*, 736–746.

[29] K. Rosenheck, P. Doty, *Proc. Natl. Acad. Sci.* **1961**, *47*, 1775–1785.

[30] W. T. Simpson, D. L. Peterson, *J. Chem. Phys.* **1957**, *26*, 588–593.

[31] C. L. Bentley, A. M. Bond, A. F. Hollenkamp, P. J. Mahon, J. Zhang, *J. Phys. Chem. C* **2015**, *119*, 21828–21839.

[32] S. Tenreiro, K. Eckermann, T. F. Outeiro, *Front. Mol. Neurosci.* **2014**, *7*, 42.

Chapter 6
Summary and Outlook

6.1 Recapitulation

In this thesis, the site-selective reduction electrochemistry of dissociable protons in charged amino acids in biomolecules was successfully resolved, and applied to polylysine and reflectin to trigger their structural transition. In Chapter 3, a deconvolution method was developed to resolve the redox electrochemistry of dissociable protons in molecular moieties while hydrogen evolution occurs at the electrochemical potential of interest. The combination of the deconvolution method for voltammetry and pH titration enabled the discovery of the linear relation between redox potentials of dissociable protons and pKa values of proton-hosting molecular moieties in amino acids and amino acid residues in peptides. These discoveries suggest that electrochemistry can be used to analyze the proton dissociation thermodynamics of biomolecules, and deprotonate sidechain moieties, which may activate structural transitions or functions associated with protein structure. Furthermore, the protocol, i.e., the conditions, methods, and procedure developed for analysis in this work can be generalized to analyze biomolecules beyond the scope of this work.

Two model systems, namely, polylysine and reflectin, were triggered with deprotonation electrochemistry and clearly showed structural transitions. In Chapter 4, electrochemically triggered coil-to-helix transition of polylysine was successfully demonstrated via combining voltammetry, *in situ* circular dichroism (CD) and absorbance, as well as pH titration. Deconvoluted differential pulse voltammograms (DPV) showed that the site-selective electrochemical deprotonation of lysine sidechains is effective, even for polylysine with 50 residues. Additionally *in situ* CD and absorbance showed that the level of polylysine

conversion depends on chain length and electrochemical potential applied. This electrochemically triggered conformation transition was further investigated in a deuterated system to leverage the deuterium isotope effect, such as higher solvent electrolysis potential and higher hydration enthalpy. The result indicated that the site-selective electrochemical deprotonation alone is sufficient to trigger the high pKa lysine sidechain moiety and trigger structural conversion, which implies the potential applicability of site-selective electrochemical deprotonation in other protein or peptide systems with different protonation-sensitive amino acid residues.

In Chapter 5, electrochemical deprotonation was demonstrated to trigger reflectin assembly via *in situ* dynamic light scattering (DLS). To analyze scarce biomolecular samples, a droplet electrochemistry method was developed and shown to reduce the sample size by 100 fold. The deprotonation electrochemistry of reflectin was successfully resolved. A salt concentration threshold for electrochemical triggering of reflectin was found, and was leveraged to create a state to test if reflectin structural transition could happen when assembly does not. *in situ* CD of reflectin in 10 mM NaCl (< threshold ~ 40 mM NaCl) was tested and indicated a shift in secondary structure. Though further investigation is needed, the evidence found in electrochemistry-coupled *in situ* spectroscopies has shown potentials to resolve the dynamic hierarchical structure of proteins and other biomolecules.

6.2 Implications

The investigations of polylysine and reflectin in this thesis suggest that the resolved site-selective deprotonation electrochemistry method may be used to studying more biomolecular systems. In the case of polylysine, the lysine residues were the redox active species, and, in the case of reflectin, the histidine residues were the redox active species. The successful electrochemical triggering of structural conversion with these two amino acid residues clearly shows that these positively charged amino acid moieties can act as effective targets to trigger structural transition. Meanwhile, in the case of reflectin, structural transitions were found at multiple levels via both *in situ* CD, absorbance, and DLS spectroscopies. All the evidence demonstrated here suggests that site-selective electrochemistry is an effective method for switching the structures of a biomolecule on demand, which can be especially helpful for biomolecules that do only adopt transient structures under specific chemical environments or subject to aggregation.

Meanwhile, optical spectroscopies were shown to be highly compatible with site-selective electrochemical deprotonation in determining the level of structural transition of biomolecules. Even though there were only two spectroscopy techniques used in this thesis, more optical spectroscopies could be included to further expand the utility of electrochemistry-coupled *in situ* spectroscopies for investigating biomolecular systems. The work in this thesis only focused on the far-UV absorbance-type spectroscopies. However, far-UV is not the only spectral window that can provide structural information for biomolecules. For example, via chemical modifications with fluorescence labels or charge transferring chromophores, biomolecules could show structure-dependent optical behaviors in the visible region, which,

with sophisticated design of experiments, may even be more informative than far-UV measurements.

Lastly, there are still many electrochemical techniques remaining to be explored to further expand the utility of site-selective electrochemical deprotonation of biomolecules. All electrochemical analyses performed in this work are DC techniques. DC electrochemistry is easier to interpret, so is suitable for the pioneering investigation done in this work. However, as has been shown in the *in situ* spectroscopies, interesting time dependences of biomolecular structural evolution have been observed. To resolve time dependent electrode processes, AC techniques such as electrochemical impedance spectroscopy can be useful. Furthermore, adding AC perturbations to the DC bias applied to trigger site-selective electrochemical deprotonation may allow the resolution and deconvolution of dynamics or kinetics occurring at different time scales.

6.3 Outlook

The core innovation of this work is the resolution of the platinum-catalyzed proton-coupled electron transfer in biomolecules, and the discovery of its utility in manipulating biomolecular structures at different length scales (i.e., secondary structure or assembly). Although the characterizations in this work were all optical, site-selective electrochemical deprotonation does not need to be limited by optical methods. For example, electron or atomic force microscopies have been used in characterizing the morphologies of protein or peptide assemblies. The integration of site-selective deprotonation electrochemistry may allow the observation of early onsets of protein assemblies that normally cannot be observed or isolated, such as the intrinsically disorder proteins (IDPs) that are commonly seen in neurodegenerative diseases such as Tau in Alzheimers disease. Also, electrochemical manipulation of biomolecular structure may be leveraged to enable new material design or inspire novel biomaterial applications. With the knowledge of lysine and histidine being switchable with site-selective electrochemical deprotonation, *de novo* peptide-based materials with bio-inspired dynamic function may be designed and synthesize to create novel applications.